https://ntrs.nasa.gov/search.jsp?R=19740024134 2020-03-11T19:07:34+00:00Z

UNH-

Analysis of the 0.511 MeV Radiation at the OSO-7 Satellite

by

Philip P. Dunphy
B.S., Seton Hall University, 1965

(NASA-CR-139585) ANALYSIS OF THE 0.511 MeV RADIATION AT THE OSO-7 SATELLITE Ph.D. Thesis (New Hampshire Univ.) 139 p HC $10.00 CSCL 03B G3/29 N74-32247 Unclas 46876

Department of Physics
UNIVERSITY OF NEW HAMPSHIRE
Durham

ANALYSIS OF THE 0.511 MeV RADIATION AT THE OSO-7 SATELLITE

by

PHILIP P. DUNPHY

B. S., SETON HALL UNIVERSITY, 1965

A THESIS

Submitted to the University of New Hampshire

In Partial Fulfillment of

The Requirements for the Degree of

Doctor of Philosophy

Graduate School

Department of Physics

March, 1974

This thesis has been examined and approved.

Edward L. Chupp, Thesis director, Professor of Physics

Richard L. Kaufmann, Professor of Physics

William R. Webber, Professor of Physics

David G. Clark, Associate Professor of Physics

Harvey K. Shepard, Associate Professor of Physics

Date

DEDICATION

To my parents

ACKNOWLEDGEMENTS

The author wishes to thank Professor Edward L. Chupp for initiating the work which led to this thesis as well as for his continuing advice and encouragement. Special thanks are also due to Dr. David J. Forrest for his numerous and enlightening discussions. Helpful comments were also given by Dr. Amar N. Suri, Dr. Claus Reppin and Mr. Chung-jen Tsai.

The work of Dr. Paul R. Higbie, Miss Susan J. Croteau and Mr. Stephen Foss in developing and carrying out the computer programming for the UNH-OSO project has been invaluable. The plotting and data handling done by Mrs. Dipika Patel, Mr. Indulis Gleske, and Mr. Ronald Adams was also very helpful.

The task of typing initial drafts was graciously done by Mrs. Patricia Ferguson and that of the final manuscript by Mrs. Gail Mumme. The job of producing the drawings and graphs in this work was capably handled by Mr. Daniel Gats and Miss Janet Varney.

This research was supported by the National Aeronautics and Space Administration under Grant NGL-30-002-018 and Contract NAS5-11054

TABLE OF CONTENTS

LIST OF TABLES

LIST OF FIGURES

ABSTRACT

ANALYSIS OF THE 0.511 MeV RADIATION AT THE OSO-7 SATELLITE

by

PHILIP P. DUNPHY

Observations of the 0.511 MeV positron-annihilation gamma-ray by the UNH detector on the OSO-7 satellite are presented along with a description of the detector itself. Variables which affect the counting rate for this line are discussed. Local production is shown to be important and a contribution from the Earth is found to be in agreement with that measured by balloon-borne detectors. An upper limit flux of 7.6×10^{-3} photons $cm^{-2}sec^{-1}$ is obtained for the quiet Sun and a positive solar flux of 6.3×10^{-2} ($\pm$ 2.0 $\times 10^{-2}$) photons $cm^{-2}sec^{-1}$ is obtained for the 3B flare of August 4, 1972. The width of this annihilation line gives an upper limit temperature for the annihilation region of $\lesssim 6 \times 10^{6}$ °K. An analysis of the line width and position also shows that the contribution to the line from positronium annihilation is less than 100% at the 99% confidence level. An upper limit is also found for an isotropic cosmic flux. This is 8×10^{-3} cm^{-2} $sec^{-1}sr^{-1}$.

I. INTRODUCTION

A. Astrophysical Significance of the 0.511 MeV Radiation

The gamma-ray line at 0.511 MeV is the characteristic radiation emitted as the result of the annihilation of a positron and a free electron at rest (see Appendix I). Astrophysically, this radiation is related to positrons in the same way that gamma rays are related to energetic charged particles in general--they travel virtually directly from the point of origin of the particle reactions without the intermediate magnetic field interactions and energy loss mechanisms of charged particles. Because the production of gamma rays is a complicated process, in practice many parameters of the interactions must be known or hypothesized (fluxes, energy spectra, ambient densities, etc.). Therefore, gamma ray measurements do not replace cosmic ray measurements but complement them in the same way that measurements in other regions of the electromagnetic spectrum do.

A gamma ray line at 0.51 MeV has long been observed in detectors flown beneath high altitude balloons. This has generally been attributed to positron production in cosmic ray interactions in the atmosphere with subsequent annihilation. This source has also been seen at satellite altitudes. The following section reviews these experiments in some detail.

Of greater astrophysical interest are possible fluxes from the Sun, from other discrete sources, and from our galaxy as a whole. The quiet Sun emits a negligible amount of 0.511 MeV radiation

(Appendix I). Upper limits for this flux have been tabulated by Chupp (1971) for experiments performed prior to 1969. The lowest upper limit was measured by Haymes et al. (1968) and was 8.4×10^{-4} photons $cm^{-2}sec^{-1}$; furthermore, there was no evidence of any radiation of nuclear origin from the Sun at that time.

Present theoretical calculations (Cheng, 1972) show that measurable fluxes of annihilation radiation from the Sun can only be expected during solar flare activity. Several workers have calculated positron production and annihilation rates for flares as discussed in Appendix I. Different models can predict vastly different time characteristics (Chupp, 1971). The intensity and time dependence of the flux depends on the initial proton energy spectrum and the ambient particle density and composition. The time dependence can also be affected by the magnetic field in the positron deceleration region. The width of the 0.511 MeV line can reveal the thermal velocities of positrons and electrons in the annihilation region and the formation of the positron-electron bound state (positronium). Such measurements combined with measurements in other regions of the electromagnetic spectrum and the detection of the flare-related charge particles and neutrons can give valuable knowledge about the flare environment.

Other extraterresterial discrete sources for which upper limits have been given include the Crab Nebula, the Cygnus and Virgo regions, and Centaurus A (Chupp, 1971). A limit on an isotropic flux which could presumably be produced in our galaxy has been

published by Metzger et al. (1964). This measurement by the Ranger 3 spacecraft gives a limit of 1.4×10^{-2} photons $cm^{-2}sec^{-1}$.

The hypothetical annihilation flux produced within our galaxy and its significance has been discussed by Stecker (1969) and Ramaty, Stecker and Misra (1970). Ramaty and Lingenfelter (1966) have treated cosmic ray interactions in the galaxy which yield positrons by the $\pi^+ \rightarrow \mu^+ \rightarrow e^+$ scheme. These positrons have initial energies greater than 10 MeV, and their escape from the galaxy is an important consideration in estimating the equilibrium positron flux. In addition, the production and decay of positron-emitting nuclei may be an important source of galatic positrons in the range 0.1 to 10 MeV (Verma, 1969). The intensity of the associated annihilation radiation depends on parameters similar to those involved in solar flare events. Positron production is a function of the primary cosmic ray intensity and the density and composition of the interstellar gas. The equilibrium positron intensity also depends on the energy loss rate of the positrons (since they annihilate near rest) and their survival time against annihilation and leakage from the galaxy. The resultant annihilation radiation from the given direction can then be calculated, knowing the amount of matter in the direction of observation. Positive measurements of, or limits on, such a flux would add to knowledge of the galactic cosmic ray flux and to the distribution of matter in the galaxy.

B. History of Observations of Atmospheric and Cosmic Annihilation Radiation

1. Balloon Observations

The measurement of low-energy atmospheric gamma rays began two decades ago as a result of attempts to detect radiation from extraterresterial sources. Experiments by Rest, Reiffel and Stone (1951) and Perlow and Kissinger (1951) involved using Geiger-Muller tubes in anticoincidence to detect gamma rays of energies < 4 MeV and < 15 MeV, respectively. Subsequent balloon flights by K. A. Anderson (1961) and J. I. Vette (1962) gained energy spectrum information between 25 and 1060 keV using unshielded NaI scintillation detectors. The data of Anderson extrapolated above 300 keV agreed well with rocket data gathered by Northrop and Hostetler (1961).

Improved spectral data was obtained by F. C. Jones (1961) using a balloon-borne CsI(Tl) phoswitch detector surrounded by a 4-cm thick passive lead collimator and a 3-cm thick lead shutter. The energy loss spectrum in this detector was divided into 31 bins between ≈ 0.1 to 2.4 MeV. No evidence of 0.511 MeV radiation was detected; however, the presence of a large amount of unshielded lead and the small opening angle of the collimator made detection of the atmospheric spectrum difficult.

Numerous experiments have been made with balloon-borne inorganic scintillators with charged-particle rejection and a minimum of massive material in the vicinity of the detector. A

gamma ray line at 0.5 MeV attributed to positron annihilation was first found with such a detector by L.E. Peterson (1963). Details of the measurement, as well as others of a similar nature, have been summarized by Kasturirangan et al. (1972). Peterson's detector consisted of a 5.1 cm dia. x 5.7 cm long NaI(Tl) - phoswich arrangement flown in 1961 at 55° N geomagnetic latitude and an atmospheric depth of 6.0 g cm^{-2}. The published intensity of the 0.51 MeV line was 0.31 $\pm$ 0.03 photons $cm^{-2}sec^{-1}$ at ceiling altitude. This was later revised to 0.62 $\pm$ 0.06. In 1962 an experiment was flown by Frost et al. (1966) at the same latitude to a depth of 3.5 g cm^{-2}. The detector was a 3.4 cm x 5.4 cm NaI(Tl) scintillator with a CsI(Tl) collimator. The intensity at altitude was 0.60 photons $cm^{-2}sec^{-1}$.

Data at 47° N has been obtained by Rocchia et al. (1965) during three flights in 1963-1964 to a ceiling of 5.0 g cm^{-2}. The detector was an unshielded 4.4 cm x 5.1 cm NaI(Tl) scintillator and the measured intensity varied between 0.34 and 0.40 photons $cm^{-2}sec^{-1}$. A series of measurements have been made by Chupp et al. (1970) at 42° N with a variety of inorganic scintillators and shield configurations from 1966 to 1968. A mean intensity of 0.18 photons $cm^{-2}sec^{-1}$ was observed. Haymes et al. (1969) have flown a 10.1 cm x 5.1 cm NaI(Tl) detector surrounded by a thick (7.0 cm) NaI(Tl) active collimator. These investigators give an upper limit to the 0.511 MeV intensity of 0.2 photons $cm^{-2}sec^{-1}$ at 42° N and 3.9 g cm^{-2} in 1967.

An intermediate latitude measurement (27°N) was made by Nakagawa et al. (1971) in 1970 using an unshielded 15 cm^3 Ge(Li)

detector. The result was an intensity of 0.12 ± 0.03 photons $cm^{-2}sec^{-1}$ at 7.0 g cm^{-2}. Finally, a series of balloon flights was done by Kasturirangan et al. (1972) near the equator (7.6° N) with plastic shielded NaI(Tl) detectors. These flights gave a rate of 0.08 ± 0.01 photons $cm^{-2}sec^{-1}$ at 6.0 g cm^{-2} residual atmosphere. All of the above results have been normalized to a common atmospheric depth (6.0 g cm^{-2}) by Kasturirangan et al. and plotted to give the dependence of the 0.51 MeV intensity on magnetic latitude.

The present experiment as well as other satellite experiments, which are summarized below, eliminate the uncertainties involved in correcting for atmospheric depth and in comparing the results from detectors with different sensitivities and angular responses. These difficulties are explained in the papers of Chupp and Forrest (1970) and Haymes et al. (1970).

2. Satellite Observations

Gamma ray measurements made on the Ranger 3 and Ranger 5 spacecraft (Metzger et al., 1964) have given an indication of the gamma ray environment in cislunar space. The detector consisted of a 2.75 inch x 2.75 in. CsI(Tl) scintillator-phoswitch combination calibrated in flight with Co^{57} and Hg^{203} sources and pulse-height analyzed with a 32-channel analyzer with two gain modes. The detector was capable of being extended from the spacecraft on a 6-foot boom, with data taken in both the stowed and extended position. This permitted evaluation of local production in the spacecraft. The energy range covered was 70 keV to 4.4 MeV.

A small peak at 0.51 MeV was found in the stowed spectra of both detectors and was attributed to secondary production. No peak was observed in the extended position, giving an upper limit for an isotropic flux of 0.014 photons $cm^{-2}sec^{-1}$. These measurements were made a distance of 7×10^4 km to 4×10^5 km from the Earth, making contributions from this source negligible.

Measurements in the 0.3 to 3.7 MeV range were made on the Cosmos 135 and Cosmos 163 satellite during 1966 and 1967. The Earth orbits had 600 km apogee and 250 km perigee with an inclination of 49°. These experiments used 64-channel analyzers to sort the output of a 4.0 cm x 4.0 cm NaI(Tl) scintillator-phoswitch arrangement. Data in the 0.5 MeV region has been described by Konstantinov, et al. (1970), giving positive evidence of annihilation radiation attributed to the Earth's atmosphere. The quoted flux varies with rigidity between 0.05 photons $cm^{-2}sec^{-1}$ and 0.2 photons $cm^{-2}sec^{-1}$ for rigidities between 14 and 1 GV. No fluxes are quoted for other sources although Golenetskii et al. (1971) give upper limit values for the gamma ray intensities in interplanetary space of 4.0×10^{-2} and 7.7×10^{-2} photons $cm^{-2}sec^{-1}$ MeV^{-1} sr^{-1} in the range 0.45 to 0.65 MeV for two different fits to the data.

An experiment similar to the Ranger series was placed on the Apollo 15 and 16 space vehicles. The detectors consisted of 7.0 cm dia. x 7.0 cm long NaI(Tl) scintillators with plastic active charged-particle shields. A boom was used to extend the detectors up to 7.6 m from the edge of the spacecraft. After correction for spacecraft production and local absorption, there was a weak positive flux

at 0.51 MeV of $3.0 \pm 1.5 \times 10^{-2}$ photons $cm^{-2}sec^{-1}$ (Trombka et al. 1973; Peterson and Trombka, 1973). This corresponds to an isotropic flux of $2.4 \pm 1.2 \times 10^{-3}$ photons $cm^{-2}sec^{-1}sr^{-1}$. This measurement seems inconsistent with the Ranger upper limit and may be due to locally produced positrons or low energy positrons of solar or cosmic origin that annihilate near the detector (Peterson and Trombka, 1973).

II. DESCRIPTION OF DETECTOR

A. Physical Description

The University of New Hampshire gamma-ray monitor on the OSO-7 satellite has been described in the literature (Higbie et al., 1972). The following will summarize the characteristics which are important in the accumulation and analysis of data at 0.5 MeV. The basic detector is a 7.6 cm diameter by 7.6 cm high cylindrical NaI(Tl) crystal hermetically sealed in a thin stainless steel housing and mounted directly on an RCA C31012 photomultiplier.

This assembly is shielded in the forward direction by a 0.5 cm thick CsI(Na) slab and in all other directions by a CsI(Na) cup of 2.8 cm average thickness and 3.8 cm thickness near the detector (Figure II-1). Charged-particle interactions in the shield above a nominal threshold of 100 keV veto coincident interactions in the detector. The shield also serves to supress the recording of Compton scattering in the detector by detecting the scattered photon. Events entailing a 0.511 MeV escape gamma ray which interacts in the shield are similarly supressed. The thickness of the shield is sufficient to significantly attenuate gamma rays other than those entering the forward aperture. A small X-ray detector covering the range 7.5 to 120 keV is included in the compartment for the purpose of monitoring solar activity.

The detector is located in a segment of the rotating wheel section of the OSO-7 spacecraft. The detector faces radially outward with crystal and cup axes in line. The spin axis of the satellite is

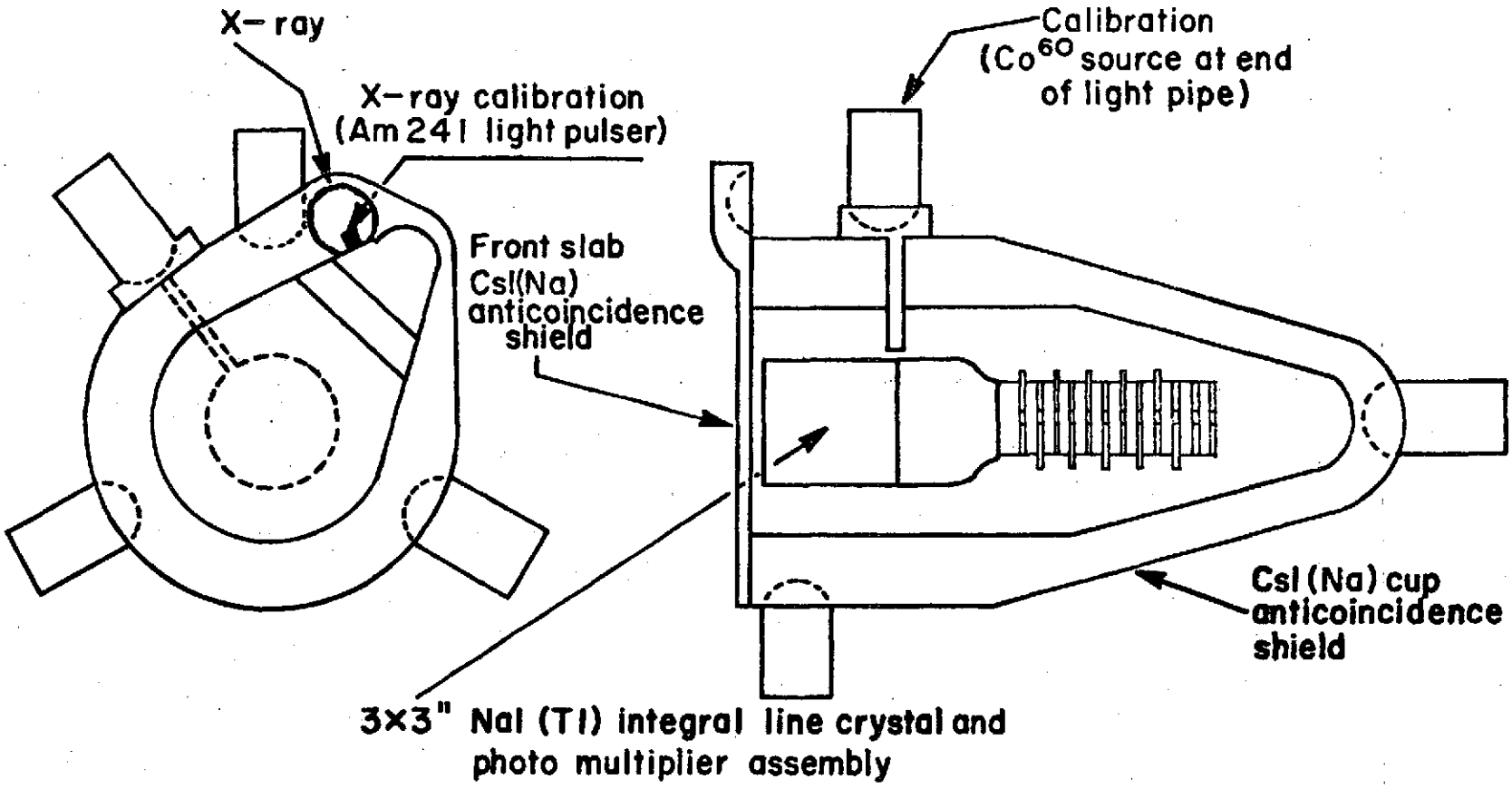

Figure II-1. Schematic diagram of the gamma-ray monitor showing the main detector, charged-particle shield, X-ray detector, and calibration sources.

normal to the plane of the wheel. Thus the field of view of the detector sweeps around a great circle in the celestial sphere containing the wheel plane with a period of about 2 seconds.

B. Detector Characteristics

1. Energy range and resolution

The energy range of the monitor is 0.3 to 9.1 MeV. The output of the central detector is pulse-height analyzed by means of a Quadratic Analog to Digital Converter (Burtis et al., 1972). The channel n into which the pulse is directed is not related to the energy loss E in the crystal in a linear way but by the function

$$E = c(n+n_0)^2,$$

where c and n_0 are constants. Since the energy resolution of the detector (or the full width at half maximum of a spectrum peak due to a gamma ray line) is proportional to $\sqrt{E}$ (or FWHMα[$n+n_0$]),

and $$\Delta E = 2c(n+n_0)\Delta n,$$

if ΔE is taken to be the FWHM of a peak, its width in channels n is independent of energy. The quadratic analysis optimizes telemetry and pulse height analyzer usage by giving equal widths to peaks throughout the energy range. The pulse height analysis covers 377 channels and the FWHM for peaks was chosen to be approximately 5 channels. The nominal energy range is 0.3 to 9.1 MeV but the gain can be adjusted by command over a 6:1 range. The detector was designed to give an energy resolution of approximately

$$\Delta E/E = 7.5\%$$

at E = .662 MeV where ΔE is the FWHM.

2. Photopeak sensitivity

The total interaction rate R in a detector due to a parallel flux F incident on the sensitive area A is given by

$$R = F \varepsilon A = FS_T$$

where ε is the total efficiency and S_T is the total sensitivity. When a gamma-ray photon interacts in a detector it does not necessarily lose all of its energy. Compton scattering with subsequent escape of the scattered photon or pair production with subsequent escape of one or both 0.511 MeV annihilation photons deposits only part of the original photon energy in the detector. The ratio of the interactions leading to total energy loss to the total number of interactions is called the photofraction f.

When the flux of a gamma-ray line causes a peak in the detected spectrum, the counting rate in the peak is given by

$$R_p = Ff\varepsilon A = FS_p$$

where S_p is the photopeak sensitivity. Values for the total sensitivity, photopeak sensitivity, efficiency, and photofraction for a 7.6 cm by 7.6 cm NaI(Tl) crystal are given in Table II-1 for a parallel beam of 0.511 MeV incident energy (Heath, 1964; Neiler and Bell, 1965). In practice, the rotation of the satellite during data accumulation modifies the response to a parallel beam. This response, as measured during detector calibration, is described below. The actual photopeak sensitivity of the detector for a point source in the center of the field of view of the detector at several energies is shown in Figure II-2 (Higbie et al., 1973).

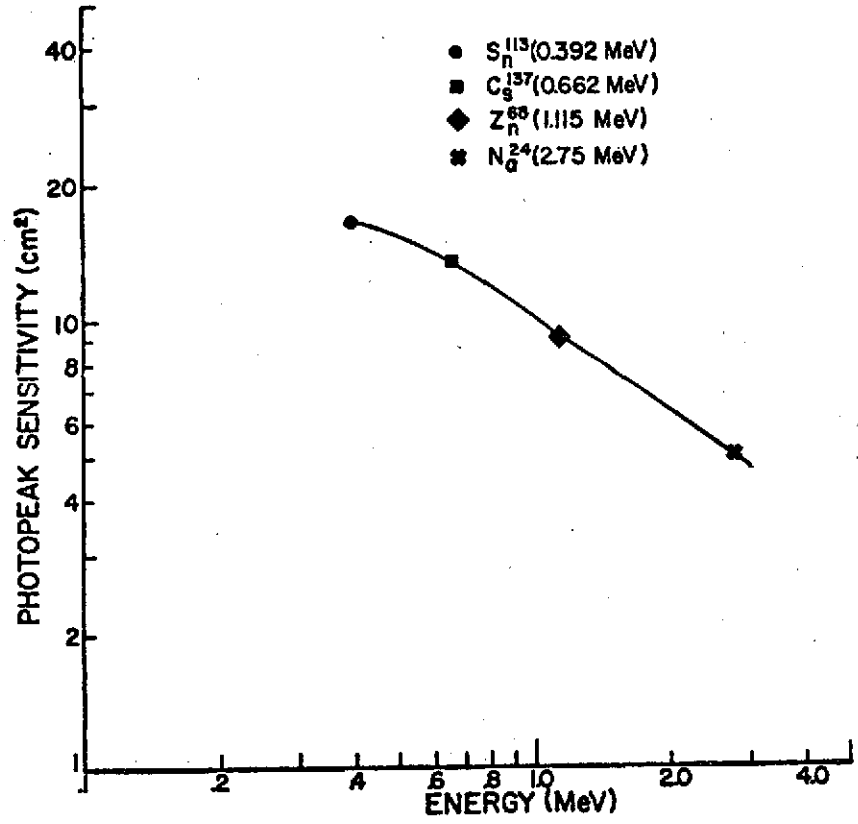

Figure II-2. Energy dependence of the detector sensitivity (cm^2) for an axial parallel beam for four line sources.

TABLE II-1

EFFICIENCY PARAMETERS FOR 7.6 cm x 7.6 cm NaI(Tl) CRYSTAL

Total Sensitivity (S_T)	42 cm^2
Photopeak Sensitivity (S_p)	25 cm^2
Efficiency (ε)	0.92
Photofraction (f)	0.64

References: Heath (1964) and Neiler and Bell (1965).

3. Angular Response

A response function for the OSO-7 detector which includes the variation of detection sensitivity with angle of photon incidence has been measured experimentally for several energies (Higbie et al., 1973). Gamma-ray energies of 0.393, 0.662, 1.12, and 2.75 MeV were obtained from the radioactive isotopes Sn^{113}, Cs^{137}, Zn^{65}, and Na^{24}, respectively. Measurement of such response functions permit the unfolding of continuum spectra and the calculation of average sensitivities to point sources. These functions are used in the present analysis. The angular response of the present detector includes the variation in look direction due to rotation of the satellite (2-second period) while the detector is accumulating data. Figure II-3 illustrates the variation of the sensitivity for a point source of energy 0.662 MeV (Cs^{137}), where the azimuth angle is the angle in the wheel plane between the look direction and the source, and the elevation angle is the angle between the source direction and the wheel plane.

4. Time resolution

There are three modes of data readout giving three possible accumulation times. In the normal mode, data is accumulated when the detector is pointed within $\pm 45^{\circ}$ of the Sun. Because of the satellite orientation, this solar scan always contains the Sun at its center (Figure II-4). Data is also accumulated separately when the detector is pointed within $\pm 45^{\circ}$ of the antisolar direction. The data accumulation thus defines a solar quadrant and an antisolar quadrant.

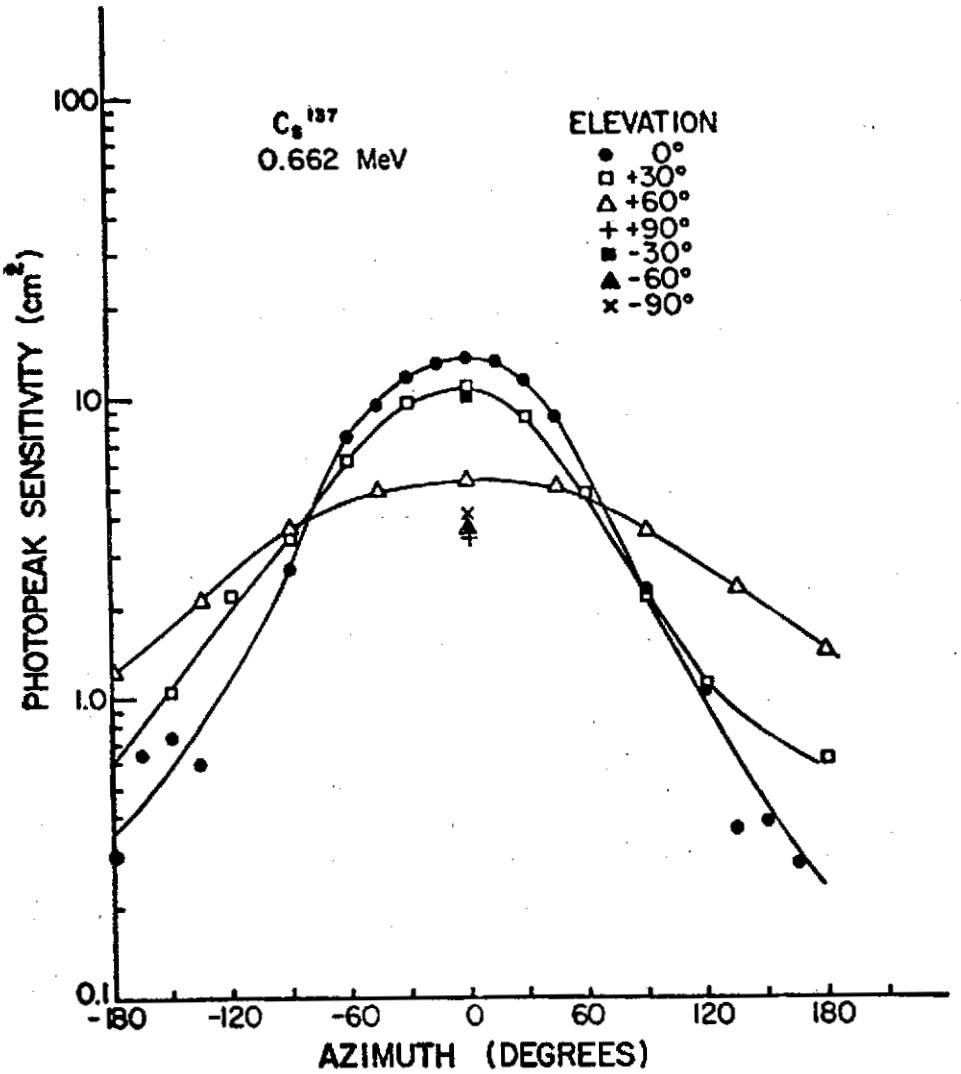

Figure II-3. Variation of detector sensitivity (cm^2) with azimuth and elevation for a 0.662 MeV (Cs^{137}) point source.

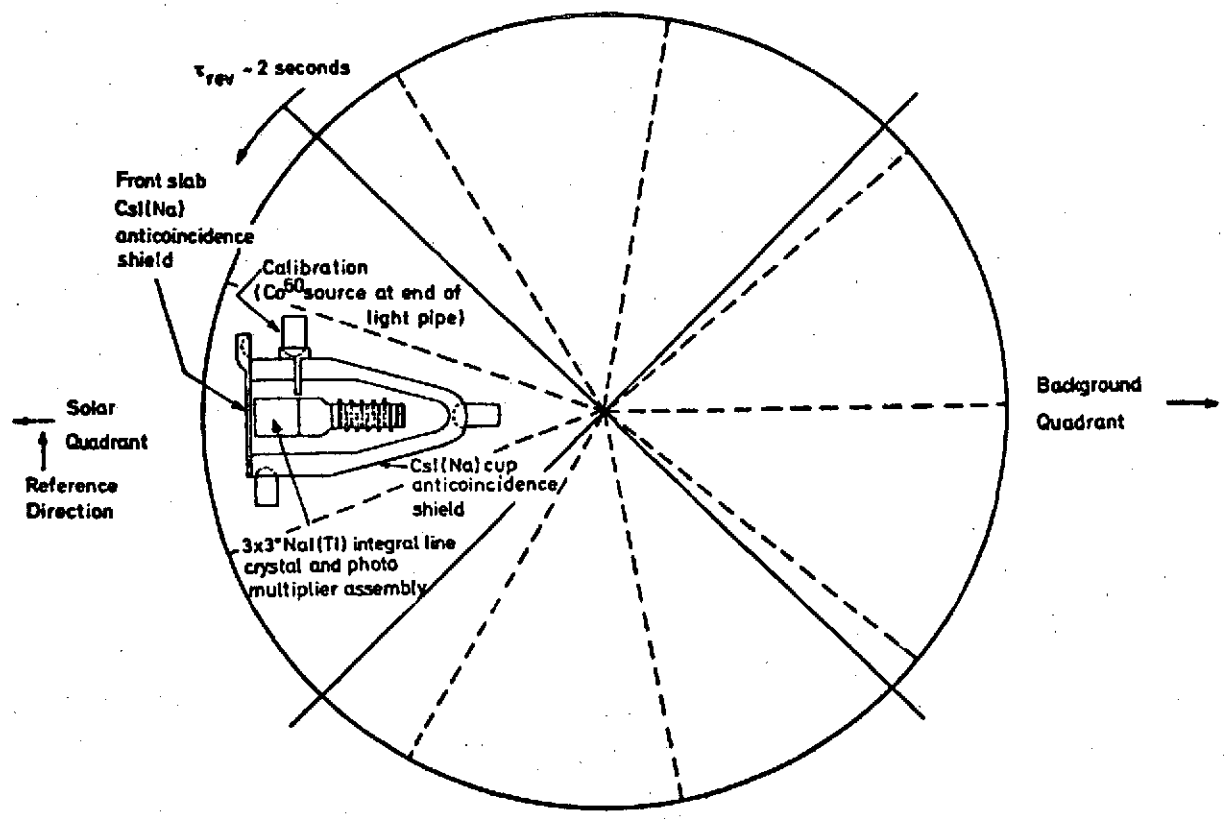

Figure II-4. Schematic of OSO-7 wheel section at the instant that the detector axis points at the Sun.

The accumulation time for each quadrant during one spacecraft rotation is about 0.5 seconds because of the 2-second rotation period. Data for each quadrant is summed separately for 3 minutes of real time before being read out.

In addition to this 3-minute time resolution, fast scans of 30 seconds and intermediate scans of 61 seconds are available on command. These faster scan modes are permitted by lowering the number of pulse height channels used. With proper gain adjustment, the fast scan mode reads out only channels covering lines at 0.511 and 2.2 MeV and calibration lines of Co^{60} (see section on calibration). The intermediate scan also covers channels for lines at 4.43 and 6.13 MeV.

The detector can also be switched by command from the normal quadrant mode (solar-antisolar quadrants) to an alternate quadrant mode in which data is collected when the detector is pointed at right angles to the solar direction. The section of the celestial sphere seen in the alternate quadrant mode depends on the solar direction and on the orientation of the spin axis of the spacecraft.

5. Housekeeping data

Information on the status of the experiment is telemetered from the spacecraft during every scan. This information includes: scan mode, quadrant mode, high and low voltage, detector and electronics temperature, slab and cup counting rates, integral counting rates for energies between 0.3 and 9.1 MeV and greater than 9.1 MeV, automatic calibration mode and magnetometer reference mode. Further housekeeping

data is included in the main frame cycle which is sent back every 3 minutes. This includes: Day/night signal, status of electronic calibration and radiation source calibration, and live time and dead time information.

C. Calibration and Gain Stability

When the detector is in the calibration mode, an entire scan is used to accumulate a spectrum from a Co^{60} calibration source located next to the central detector (Figure II-1). This calibration method has been described by Forrest et al. (1972). Briefly, it consists of a small plastic scintillator button doped with Co^{60} and mounted on the end of a light pipe viewed by a photomultiplier tube. The Co^{60} emits beta particles in conjunction with prompt gamma rays, more than 99 percent of which are cascade lines at 1.17 and 1.33 MeV. In the calibration mode, the pulses due to beta particle energy loss in the plastic are seen by the photomultiplier and are used to gate on the main detector and a calibration spectrum is accumulated. In the noncalibration (normal) mode, the detector is gated off by these pulses and the calibration interactions are excluded from the data. Since the efficiency for detecting the beta particles is not 100 percent, being somewhat greater than 95 percent, there is some leakage of the Co^{60} radiation into all the data. A sample calibration spectrum is shown in Figure II-5.

In the automatic calibration mode the Co^{60} spectra are accumulated at every satellite day/night and night/day transition. This mode can be inhibited and initiated by command from the ground.

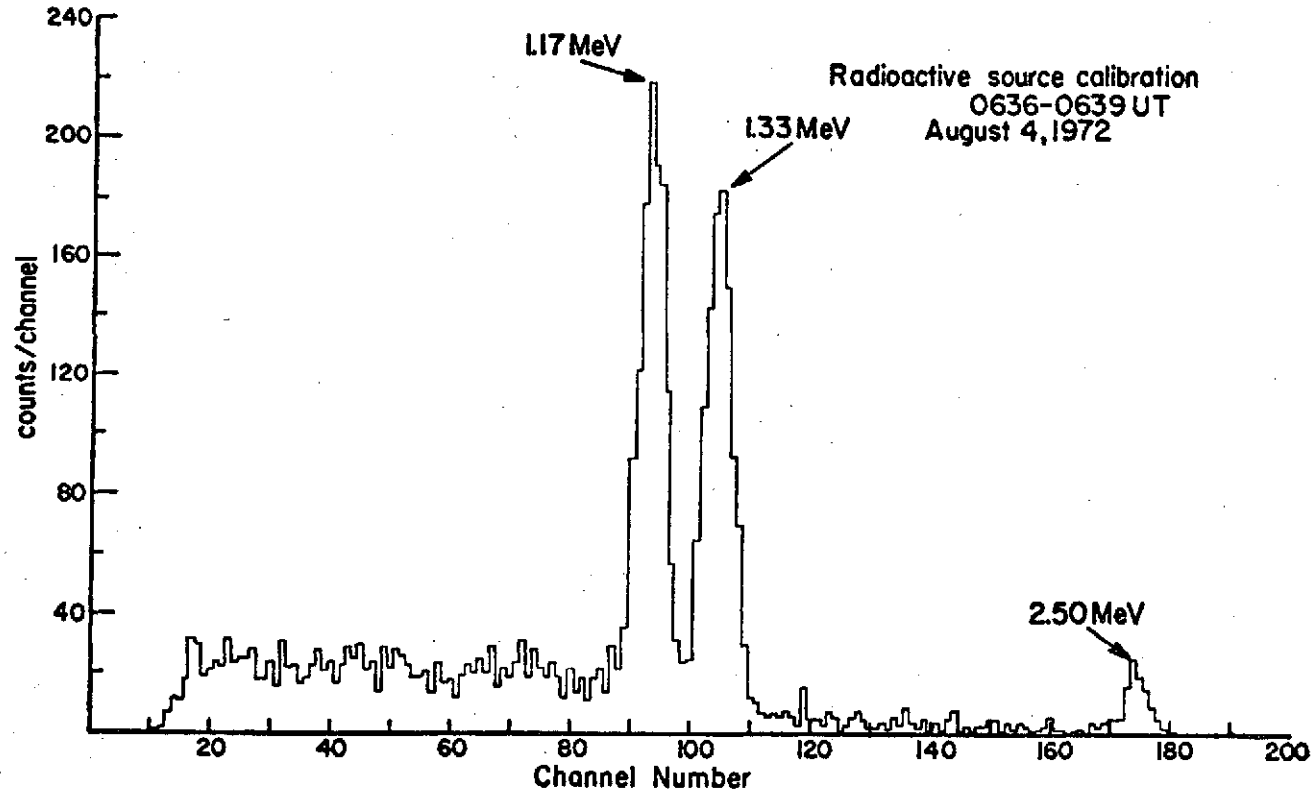

Figure II-5. Sample Co^{60} calibration spectrum obtained in orbit.

Amplifiers and thresholds are also checked electronically by the manual calibration command.

The gain of the central detector is adjustable through the variation of phototube high voltage which has two coarse adjustment steps of 150 volts each, and 64 fine adjustment steps within each coarse range. Gain control allows for correction of gain loss due to phototube aging and gives the option of changing the overall energy range of the detector.

The stability of the gain can be checked by monitoring the channel positions of the calibration peaks (1.17, 1.33, and 2.50 MeV sum peak). The satellite dawn and dusk calibration verify the stability of the gain over the characteristic time of an orbit period (about 93 minutes) or longer. Gain stability for times between calibrations can only be estimated by the position and width of peaks of known energy (such as the Co^{60} leakage peaks) in spectra summed over those times.

D. Description of Satellite Orbit, Aspect, and On-times

The Orbiting Solar Observatory (OSO-7) was launched on September 29, 1971. The orbit had the parameters listed in Table II-2. An error in Delta injection produced an anomalous eccentric orbit causing a periodic variation in the latitude of the apogee. The UNH gamma-ray monitor was turned on at 0352UT, October 3, 1971 and was fully operational at 2315 of the same day.

It was discovered soon after turn-on that the detector gain was severely degraded during and after passage through the South Atlantic anomaly region of the radiation belts. This problem was dealt with by turning off the detector during orbits that passed

TABLE II-2

OSO - 7 ORBIT PARAMETERS

Inclination	33.14°
Period	93.5 min
Perigee	330.7 km
Apogee	574.5 km
Ascending Node	310.06°
Argument of Perigee	57.48°
Semi-major Axis	6830.8 km
Eccentricity	0.01785
Mean Anomaly	201.93°
Epoch time	12:00:00 UT 29 September 1971

through the anomaly region. Using this technique, the gain was held stable, though at a lower value than at the initial turn-on. The channels containing the 0.5 MeV region remained below the detector threshold until 1006 UT April 25, 1972. At this time, the gain was raised until the threshold was at about 0.3 MeV.

The detector usually operated in the normal quadrant mode; that is, data was gathered in the solar quadrant and antisolar (background) quadrant. For about 4 hours every day the detector was switched to the alternate quadrant mode. For the next 8 hours the detector was off for passages through the anomaly, after which time it was turned on for about 12 hours of operation in the normal quadrant mode.

III. METHODS OF DATA ANALYSIS

A. Selection of Data Scans

The main limit on the data coverage in the time domain is the requirement that the detector be off during orbits that include passage through the South Atlantic anomaly. The detector is off for this reason about 25 percent of the time. Additionally, data from a given source cannot be gathered continuously because of the changes of quadrant and aspect and eclipse by the Earth. For example, data from the Sun is excluded in the alternate quadrant mode and during satellite "night." The best aspect for viewing the Earth's atmosphere is near satellite "noon" and "midnight" when the detector look direction is along an Earth radius vector.

The best time for measuring the contribution to the counting rate from sources other than local production in the spacecraft is when this local production is at a minimum. This minimum has been found to occur soon after the apogee of the orbit reaches its northernmost excursion (Figure III-1). This is because local background is at its greatest when the spacecraft passes deep into the radiation belts, which happens when the apogee is in the southern latitides (in the vicinity of the South Atlantic anomaly).

Measurement of the atmospheric contribution should be done when the contribution from the Sun is negligible. For example, during the period of solar activity from August 4 to August 11, 1972, a contribution from the Sun could be seen in the solar quadrant

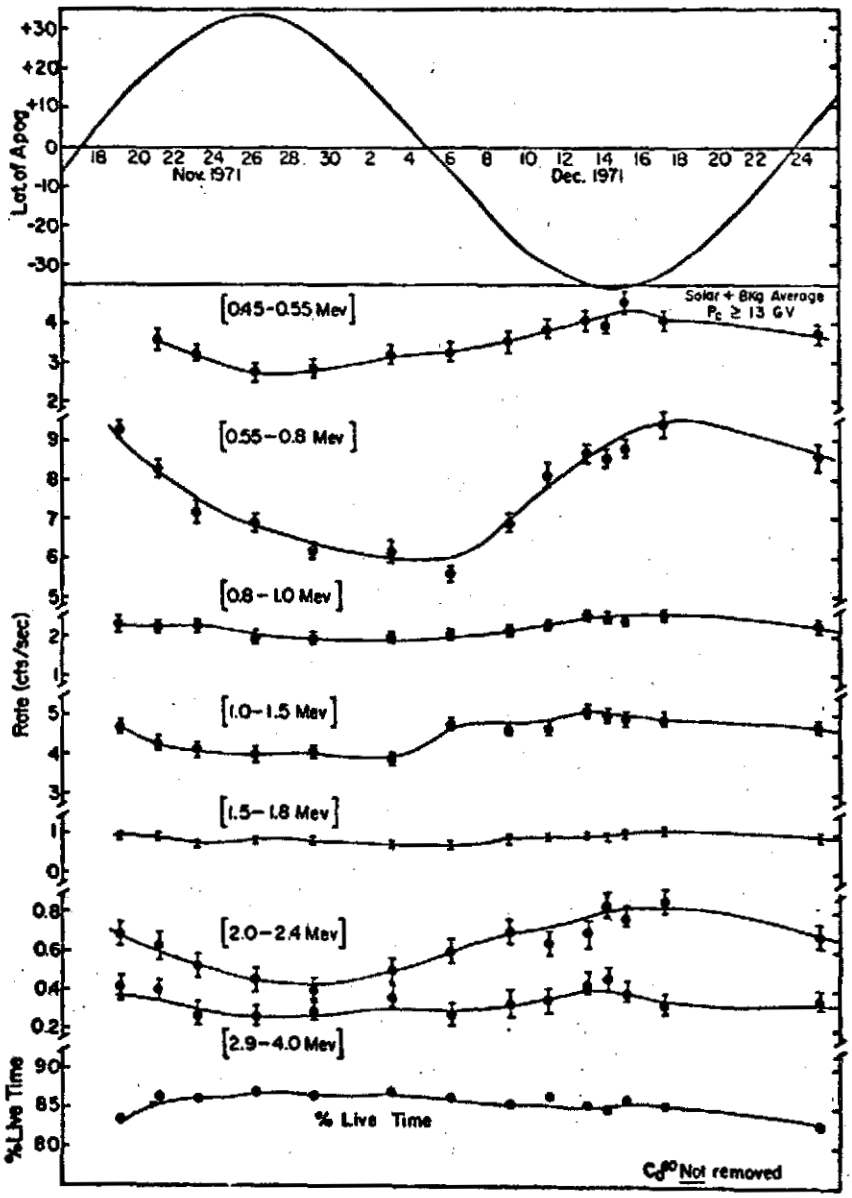

Figure III-1. Long-term variations in gamma-ray counting rate for various energy ranges. Variations are correlated with the latitude of satellite apogee.

(Section IV, D). Furthermore, there was an apparent enhancement of the flux from the atmosphere on August 4 about 8 hours after flare maximum.

In addition to data lost for the above reasons, some data must be rejected because of noise picked up during telemetry transmission. Improper data can be recognized by warnings in the data analysis chain and by nonstatistical fluctuations in one or more adjoining pulse-height channels.

B. Selection of the Peak Region

Because of the energy calibration which is done twice during each orbit, the pulse height region where the 0.511 MeV peak is expected to occur can be located with some confidence. The calibration spectra contain three peaks (Section II, C) which are used to calculate values for c and n_0 in the equation

$$E = c(n+n_0)^2.$$

From these values the channel number in which the center of a 0.511 MeV peak would fall can be calculated.

Typical values for c are shown in Figure III-2, which also shows the time variation of c. The value of n_0 is taken to be constant throughout (n_0=80.2). For this example, the center of the peak is calculated to vary between channel 43.8 and channel 45.6 for a 7 hour time span on April 27, 1972.

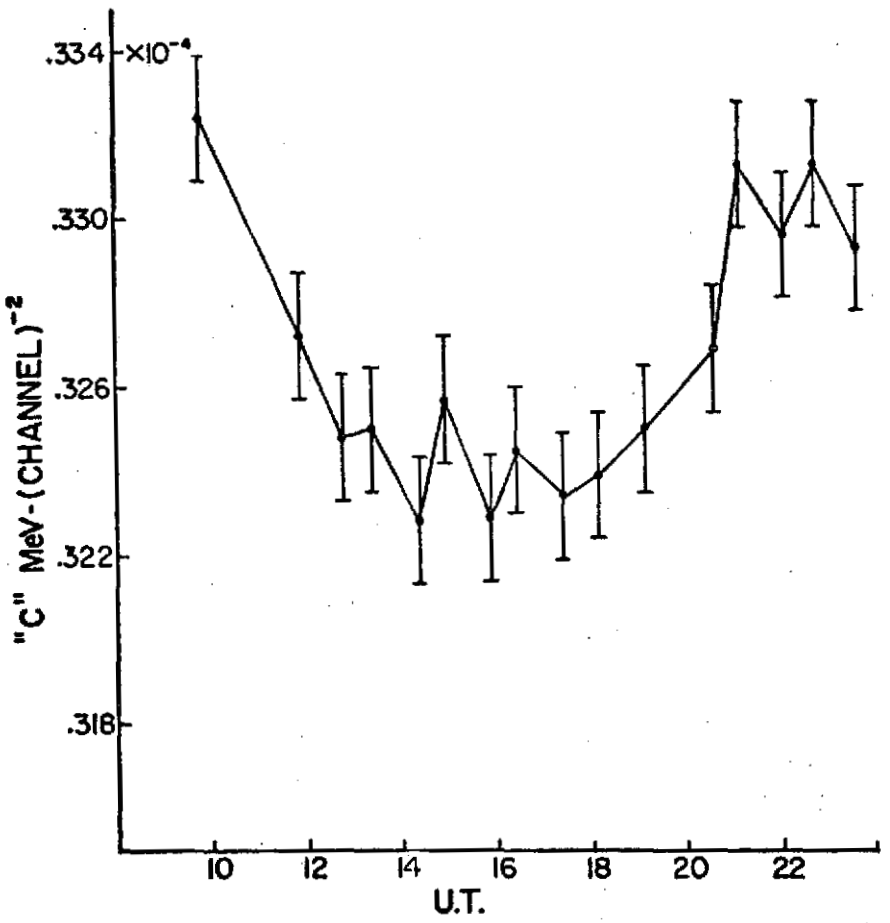

Figure III-2. Time variation of "c" on April 27, 1972.

C. Fitting the Continuum Background beneath Peak

1. Linear fit

A first attempt at determining the counting rate due to a 0.511 MeV line consists of determining the excess of counts in the peak region above an assumed "background". The qualitative behavior of the 0.511 MeV flux can be seen merely by assuming that the background is a linear interpolation between regions on each side of the peak. This fit to the data is shown in Figure III-3. The background is taken to be the average of 7-channel wide regions immediately above and below a 7-channel wide region centered on the peak. Figure III-4 shows the result of such a fit for a series of scans. Each point represents a scan for which the average altitude, rigidity and detector live time is given. A positive value for the excess at 0.5 MeV above the linear background implies the existence of a peak near that energy. A consistent excess in the 0.5 MeV region above the background exists. This shows that there is a peak at this energy indicated in the data, even for individual scans.

2. Exponential Fit

Examination of a sum of many scans reveals strong lines on both sides of the 0.5 MeV region. This indicates that the localized linear fit described above is not the most reasonable fit to the background. Figure III-5 shows a plot of data gathered while viewing the Earth. This spectrum is a summation of scans gathered over a live time of 1701 seconds. Also shown is the corresponding sum

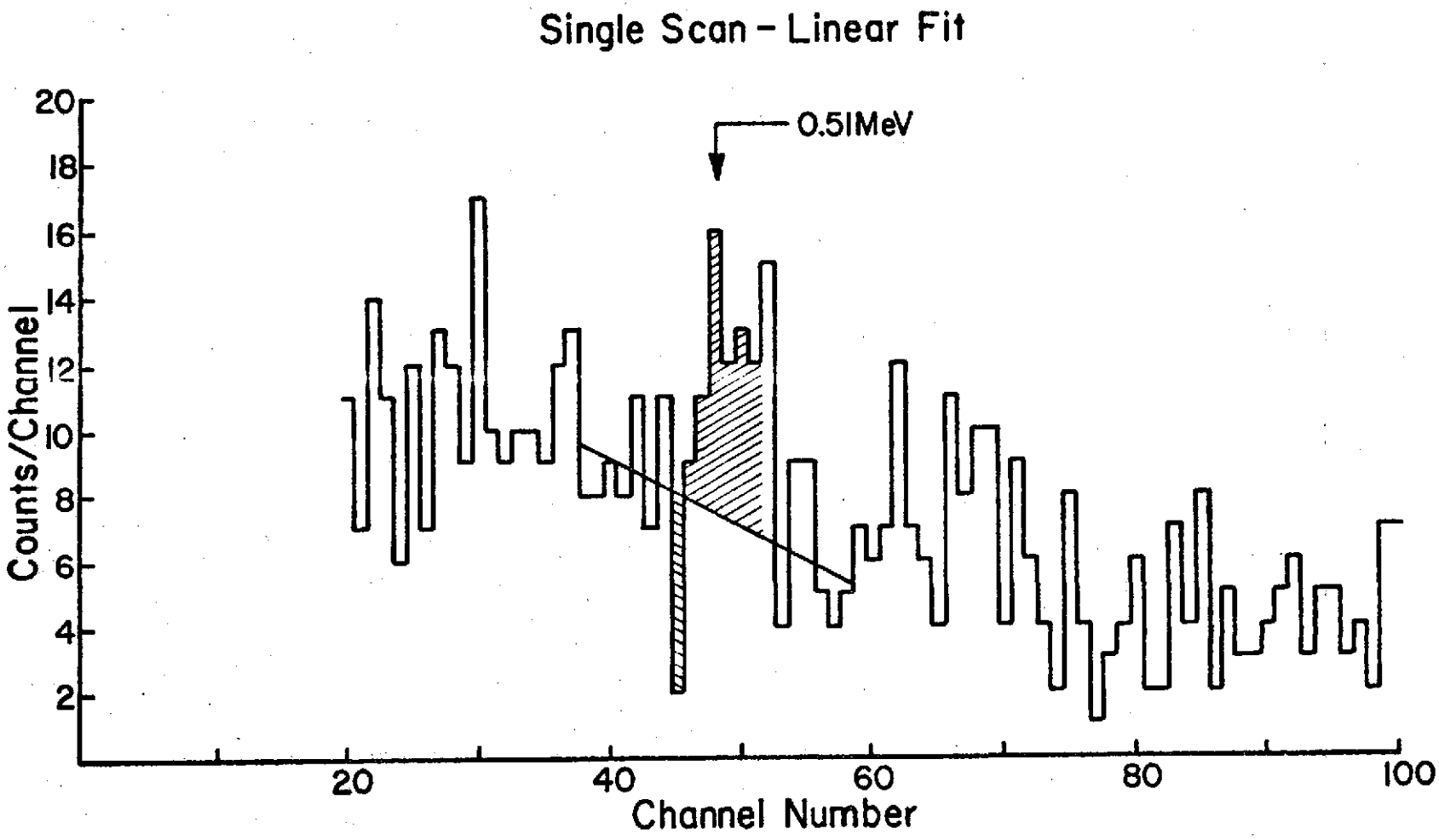

Figure III-3. Sample of a linear fit to the background for the 0.5 MeV region for a single scan.

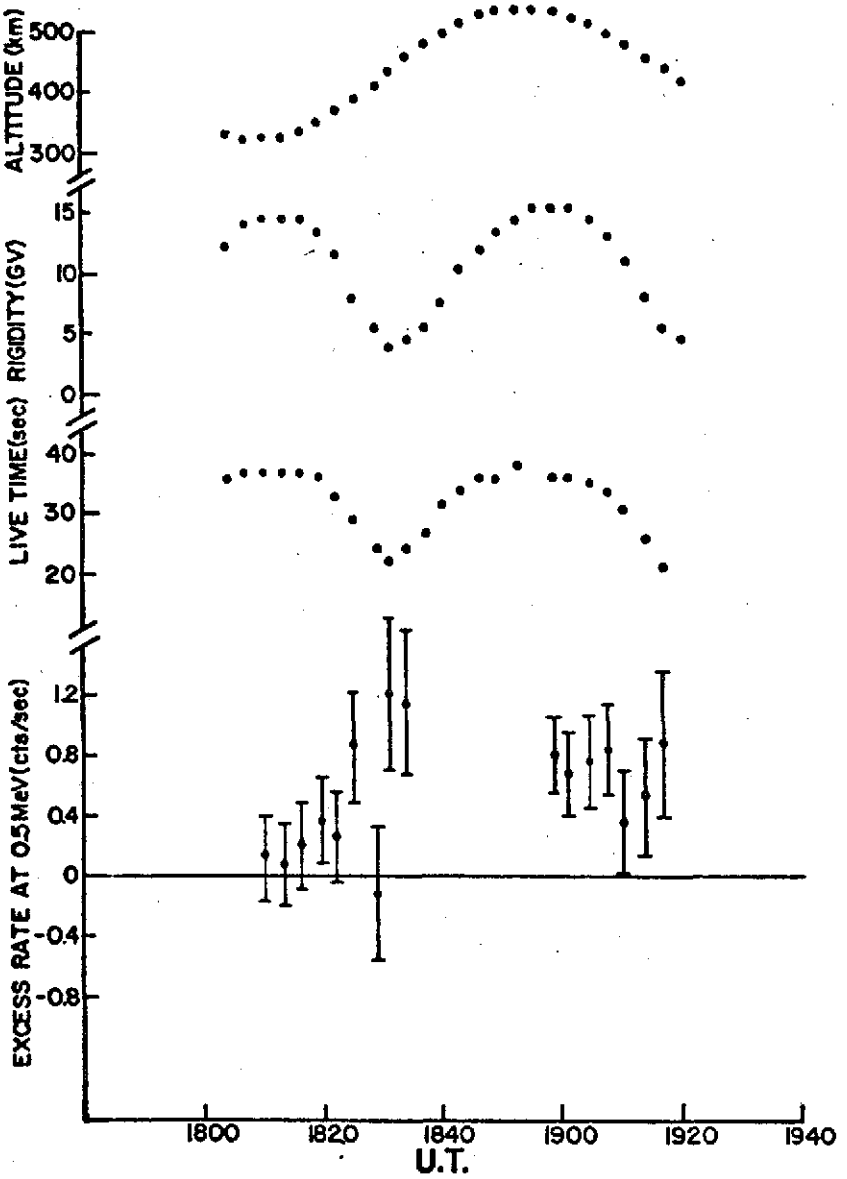

Figure III-4. Excess counts over the linear background in the 0.5 MeV region (7 channels) for a series of individual 3-minute scans. Also shown are the variations in altitude, rigidity, and live time.

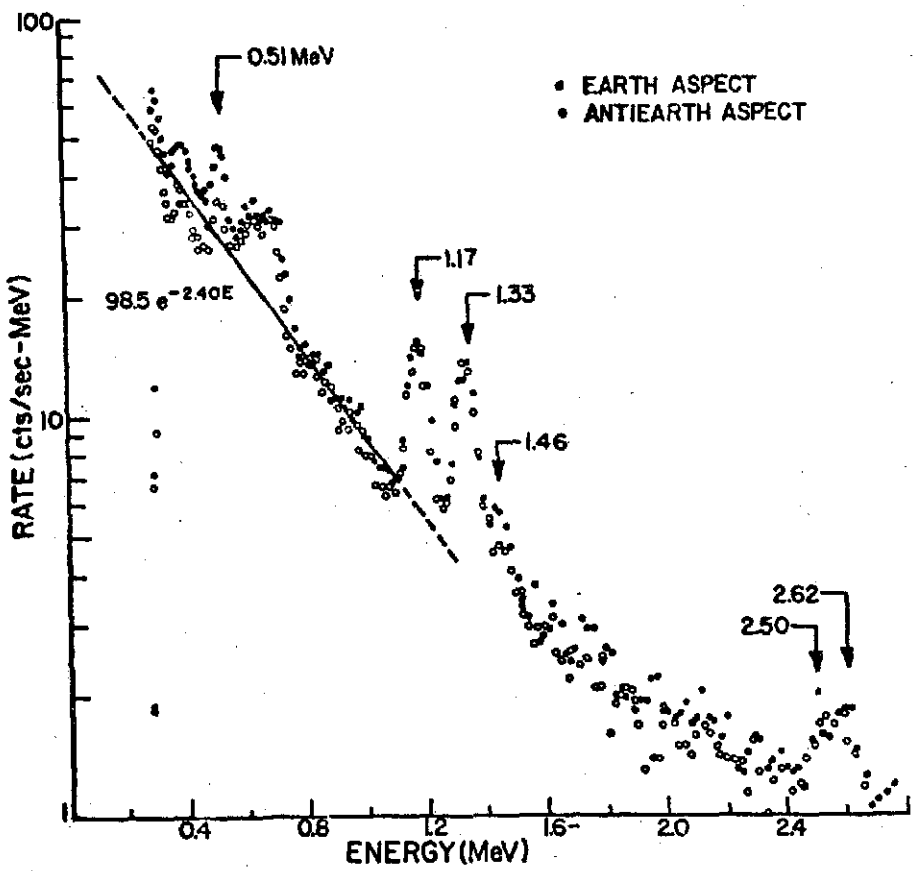

Figure III-5. Sum spectra for Earth (•) and antiearth (○) aspects, altitude < 430 km, and rigidity between 8 and 12 GV. A peak at 0.51 MeV is apparent. Some other peaks are identified by energy (MeV). Peaks at 1.17, 1.33, and 2.50 are calibration source leakage; peaks at 1.46 and 2.62 are presumably due to local K^{40} and Th decays; other peaks are due to local production.

spectrum for the antiearth direction. The data shows numerous peaks and a continuum which is fit to an exponential law of the form

$$R = Ne^{-kE} \text{ counts-sec}^{-1}\text{-MeV}^{-1}$$

where R is differential counting rate and E is energy in MeV. Figure III-5 shows this fit for the Earth aspect. The fitting is done for energies between .78 and 1.11 MeV where there appears to be a minimum contribution from strong lines. This energy region was also selected because of its proximity to the annihilation peak. An exponential which fits the continuum well at a much higher energy will not do so in this region because of the energy dependence of the e-folding energy. The region in the immediate vicinity of the annihilation line cannot be used to fit the continuum because of the existence of lines which can be attributed to local production in the satellite. This attribution is made because the strength of the lines, unlike the 0.511 MeV line, is independent of the look direction of the detector. Lines in this energy range are expected due to spallation interactions in the detector and shield (Appendix II), as well as in the rest of the spacecraft. These same interactions are also expected to give rise to an exponential continuum (Fishman, Appendix II).

The sum spectrum shown in Figure III-5 is from the 4-day period 25-28 April 1972 with scans characterized by the detector viewing the Earth with satellite altitude less than 430 km and cutoff rigidity between 8 and 12 GV. The effects of these parameters are discussed in subsequent sections. The least-squares fit spectrum shown in the figure gives the constants in the exponential law to be

$$N = 98.5 \text{ and } k = 2.40 \pm 0.09 \text{ (MeV)}^{-1}$$

A fit to the corresponding data obtained while looking away from the earth gives the values

$$N = 8\ 1.5 \text{ and } k = 2.27 \pm 0.11\ (\text{MeV})^{-1}$$

The corresponding e-folding energy of 0.4 MeV can be compared with the value of 1 MeV for laboratory produced spallation continua (Dyer and Morfill, 1971; Fishman, 1972) and the value 0.7 MeV in the post-flight analysis of the Apollo 17 detector (Peterson and Trombka, 1973).

D. Determination of Rigidity Values

A parameter which has been found to be important in the behavior of the atmospheric annihilation line flux is the value of the vertical cutoff rigidity P_c at the point of origin in the atmosphere (Kasturirangan et al., 1969; Golenetskii et al., 1971). The rigidity of a particle in volts is numerically equal to its momentum in eV/c divided by its charge number Z. The characteristic cutoff rigidity of a point near the Earth is the smallest rigidity which a cosmic ray can have, and yet reach that point by penetrating the Earth's magnetic field. Rigidity values in this paper have been obtained from the publication by Shea et al. (1968) where trajectory-traced P_c values at the Earth's surface are tabulated by geographic latitude between 85°N and 85°S in increments of 5 degrees and by geographic longitude in increments of 15 degrees. Comparison between actual proton cutoff rigidity measurements by Bingham et al. (1967) with somewhat less precise earlier calculations by Shea and Smart (1967) show that calculated values are within 10 percent of the measured values for rigidities greater than $\gtrsim$ 4 GV.

The rigidity applied to each scan is the value tabulated for the point on the Earth which marks the midpoint of the 3-minute scan time. This average rigidity is interpolated where necessary from the values tabulated by Shea et al. (1968).

IV. RESULTS OF DATA ANALYSIS

A. Plan of Analysis

Previous satellite-borne gamma-ray experiments have shown that their counting rates are a contribution from several sources, namely, local production from particle interactions, the active Sun, a cosmic flux, and a flux from the Earth's atmosphere (for a satellite in Earth orbit). The separation of the total rate into these component parts can be done, at least partially, by investigating its dependence on various parameters. This is the approach taken in the following analysis.

Since the local production rate is not of direct interest, it is minimized (but not eliminated) by appropriate data selection. The important variables of aspect, vertical cutoff rigidity, altitude, gamma-ray continuum rate, and charged-particle rate are then investigated with respect to the counting rate due to the positron annihilation line. These lead to the above-mentioned separation into components. Included in these components is a contribution from the Sun which yields only an upper limit flux for the quiet Sun. During the solar activity of August 4 to August 7, 1972, however, a positive contribution was measured. The significance of this line flux, its width, and its energy are also discussed in the following presentation.

B. Parameters Affecting 0.511 MeV Flux

1. Vertical Cutoff Rigidity

Preliminary analysis of the data indicated that rigidity (Section III, D) is an important factor affecting the gamma ray flux at satellite altitudes. This was to be expected from previous satellite and balloon measurements (Section I, B). It can be assumed *a priori* that the flux can also depend on various other parameters including: altitude, aspect or look direction, time after exposure to the radiation belt, exposure to the Sun, and changes in the cosmic ray flux, among others. The difficulty in assessing the importance of various parameters lies in holding all parameters, except the one of interest, constant, while obtaining enough data to give a statistically significant measurement.

For an investigation of the rigidity dependence, the remaining parameters were treated as follows:

1. Altitude was not constrained in the analysis. A scatter diagram reveals that the average altitude is not correlated with rigidity over the analysis period of four days so the rigidity variation is averaged over altitude.
2. Aspect was limited to orientations of the spacecraft such that the intersection point of the center of the look direction and the surface of the Earth did not differ by more than 5° in arc distance or about 1 GV in rigidity from the value in rigidity calculated as in

Section III, D. This is less than the average change in rigidity over a 3-minute scan.

3. Data was limited to that taken $\gtrsim$150 min. after passage through the South Atlantic anomaly to minimize the contribution from short-lived spallation products which could mask the rigidity dependence. Also, data was only analyzed for a 4-day period of minimum background; that is, for times when the apogee was in northern latitudes (Section III, A).

4. The quiet-time solar contribution to the 0.511 MeV flux is negligible (Section I, B) and data obtained during periods of solar activity have been omitted from the rigidity analysis.

5. Large changes in the charged-particle flux in the spacecraft environment can be monitored by observation of the counting rates in the charged-particle shield slab and cup. Times when these rates differed from quiet-time rates (such as periods of strong solar activity) were omitted from the analysis.

After choosing the scans by the above criteria, they were grouped according to rigidity (1 GV resolution), day/night status, and solar/antisolar quadrant. The counting rate in the 0.511 MeV peak was determined for each individual scan using a linear fit to the background as described in Section III, C. It can be noted here that Golenetskii, et al. (1971) used a similar approach with "Cosmos" data, since the background is apparently taken as smoothly joining the spectrum on both sides of the peak.

Data combined according to Earth aspect, with solar/day data added to antisolar/night data (antiearth data) and solar/night data added to antisolar/day data (Earth data), is shown in Figures IV-1

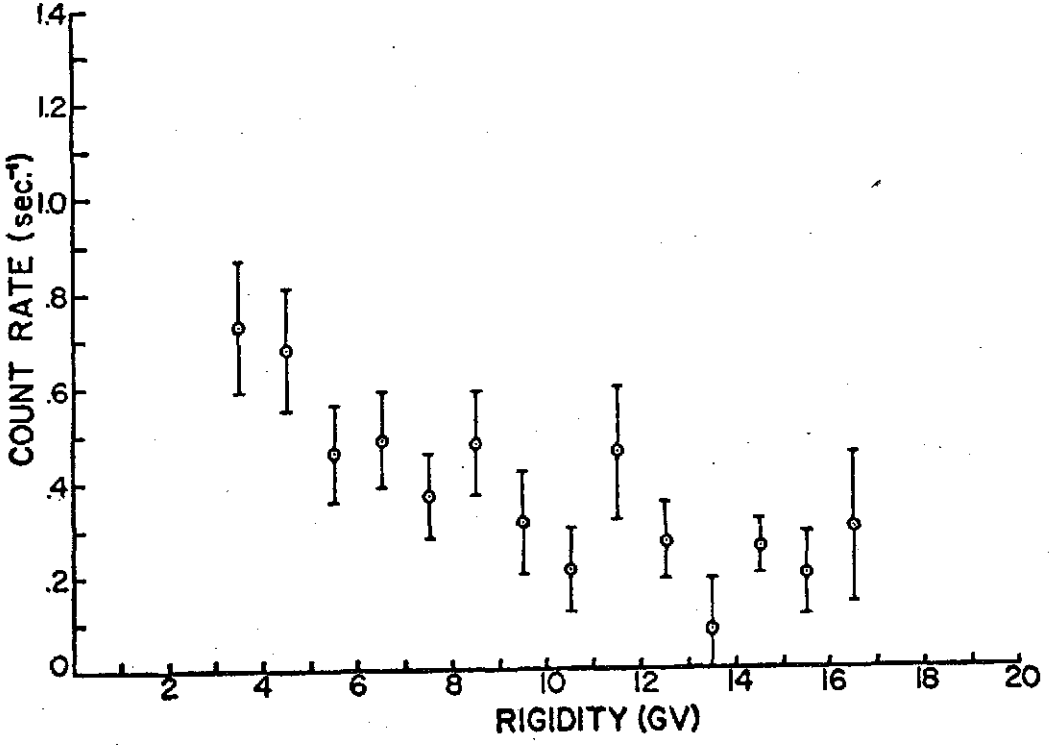

Figure IV-1. Rigidity dependence of the 0.51 MeV counting rate for anti-earth aspect. A linear fit to the background was used. Error bars are statistical 1σ.

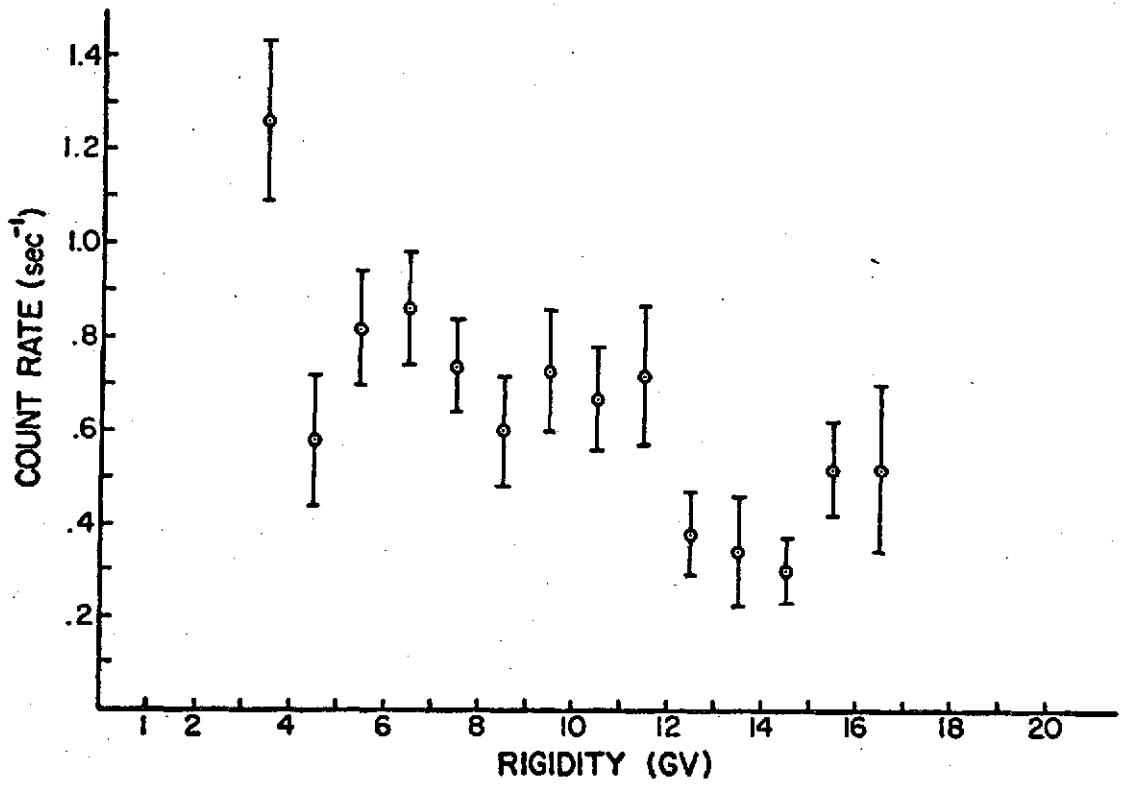

Figure IV-2. Rigidity dependence of the 0.51 MeV counting rate for Earth aspect.

and IV-2. Again, this plot is comparable to "Cosmos" data which had similar time (2-minute scans) and rigidity resolution although the essentially isotropic Cosmos detectors had no aspect criteria. Both data were also averaged over altitude, with an average altitude of $\sim$ 400 km in both cases. The plotted data summarizes the 4-day minimum background period (25 April 1972 - 28 April 1972).

It was noted in Section III that an exponential continuum is a more reasonable representation of the spectrum continuum than a linear background. There is insufficient data to fit exponential backgrounds to spectra summed over the 4-day period for single rigidity values. For this reason, the sum of scans with fitted background discussed in Section III was used to scale the rigidity dependence from a linear background assumption to an exponential background. The basis of the method is illustrated in Figure IV-3. a is the counting rate obtained from a linear fit to the background in the sum spectrum; b is the background used for a linear fit; A is the total counting rate under a gaussian peak riding on the exponential background C. Once the relationship between a and A is found for the sum spectrum, it can be found for addition values of a and A merely by varying the value of A and empirically determining the corresponding value of a. This method is applicable only if the production peaks on both sides of the annihilation peak do not vary with rigidity, for then the value of b, which contributes to the peak, would not vary linearly with C. The correction is also good as long as the exponential background C does not vary radically in shape. Both of these qualifications are met in the present analysis. The functional

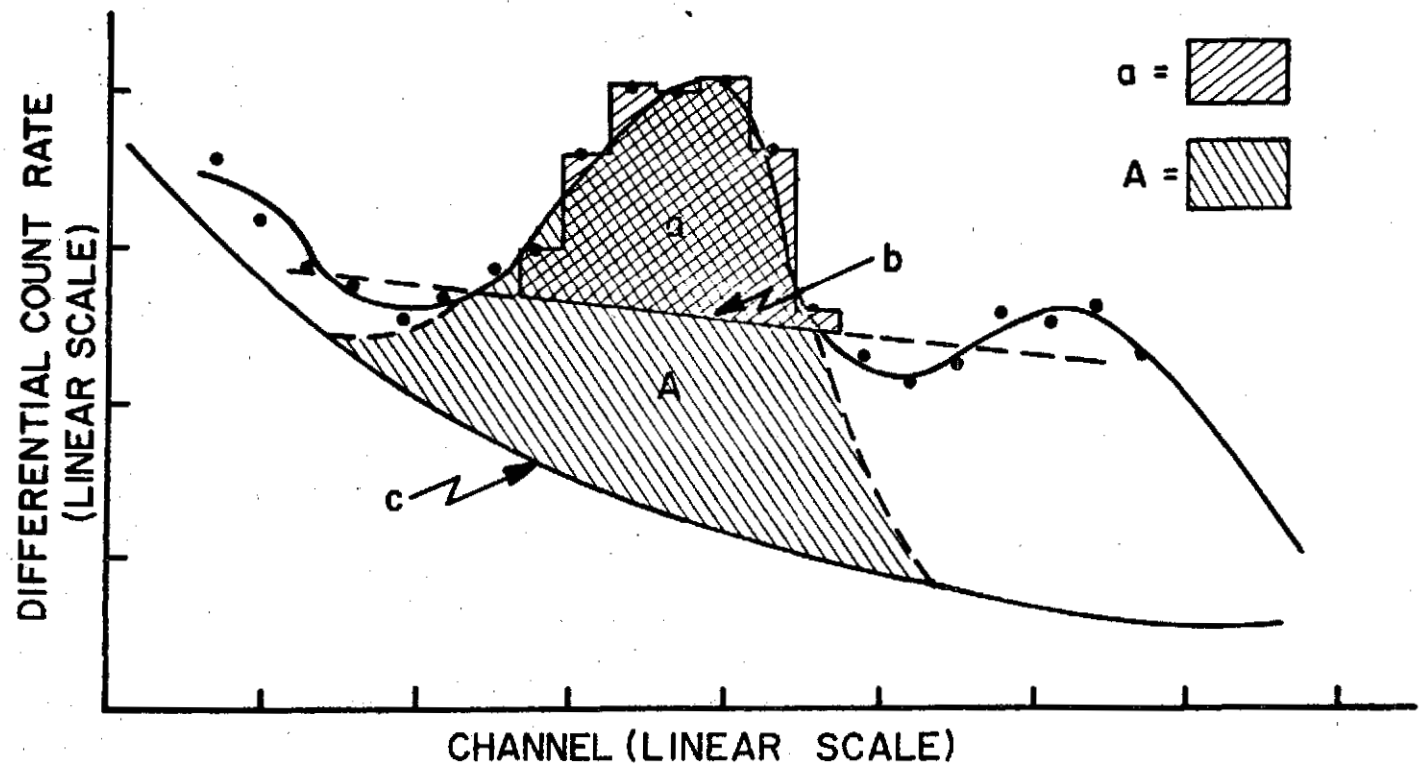

Figure IV-3. Method of correcting from linear background fit to exponential background fit. A is the total rate under the peak for an exponential background; a is the rate for seven channels using a linear background; b is the background for a linear fit; c is the background for an exponential fit.

dependence of $\underline{A}$ on $\underline{a}$ is $A = (1.21\ a + 0.26)$ counts-sec^{-1} for Earth aspect and $A = (1.21\ a + 0.12)$ counts-sec^{-1} for antiearth aspect.

Comparison of sum spectra show that the 0.511 MeV peak is in both Earth and antiearth directions with a considerable excess seen in the Earth direction (Figure III-5). The counting rate in the antiearth quadrant ($\tilde{\sim}$ 0.4 sec^{-1} or 8×10^{-3} photons cm^{-2}sec^{-1}sr^{-1}) is considerably greater than limits put on the cosmic flux for this peak determined by Metzger et al. (1964). Since positron emitters can be expected from spallation products in detector and shield materials and since Metzger and others have seen an annihilation peak associated with local background, we can tentatively identify the counting rate seen in the antiearth direction with local production. The rate seen in the Earth quadrant is therefore local production plus the Earth's contribution. In the following discussion however, the detector sensitivity will be combined with counting rates obtained in the Earth and antiearth directions to give an equivalent flux for comparison with other measurements, with the understanding that the Earth-antiearth difference flux, in which local effects cancel out, is the most physically meaningful quantity.

For a transformation from counting rate to flux for any detector, the angular dependence of the flux must be included. The most reasonable assumption for the contribution from Earth's atmosphere is an isotropic flux over the angle subtended by the atmosphere (neglecting limb effects). The relation of flux to counting rate is then obtained from

$$R = F \int S\ (\theta\ ,\ \phi) d\Omega$$

where R is the counting rate, F is the flux in photons $cm^{-2}sr^{-1}$ and $S(\theta, \phi)$ is the photopeak sensitivity discussed in Section II, B. $S(\theta, \phi)$ for 0.511 MeV photons was obtained by interpolating the experimental values obtained at 0.393 and 0.662 MeV and integrating over angle to give the values of S shown in Table IV-1.

The equivalent Earth and antiearth fluxes calculated from the above method are plotted in Figure IV-4. A similar plot of fluxes from Cosmos measurements are shown in Figure IV-4. The original data was plotted by the authors (Konstantinov et al., 1970) using the formula $F = N/S_0 \varepsilon_p$ where F is the transformed counting rate ($cm^{-2}sec^{-1}$), N is the detector counting rate, ε_p is the photopeak efficiency, and S_0 is the geometric factor of their detector for an isotropic flux. For comparison purposes, this has been transformed to an equivalent flux by assuming the Earth to be an isotropic source, subtending a solid angle $\Omega_E \cong 1.3\,\pi$ at the average altitude 400 km for the Cosmos satellite.

The above standard method of calculating the isotropic sensitivity and flux by combining the geometric factor and the efficiency for a parallel flux appears to underestimate the flux by up to 50% as is shown in the work of Forrest (1969) and of Puskin (1970). The same method has been used in most of the balloon experiments, the results of which are discussed below. No correction for this effect is included in either the Cosmos 135 results in Figure IV-4 or the balloon results in Figure IV-5.

TABLE IV-1

DETECTOR SENSITIVITY AT 0.511 MeV FOR VARIOUS ASPECTS

Time	Aspect	Source	Sensitivity
Day-night	Earth	Earth	37 cm^2sr
Day-night	Earth	Cosmic-Isotropic	16 cm^2sr
Day-night	Antiearth	Earth	3 cm^2sr
Day-night	Antiearth	Cosmic-Isotropic	50 cm^2sr
Day	Antiearth	Sun	15 cm^2

Sensitivity to an isotropic flux not screened by the Earth is 53 cm^2sr.

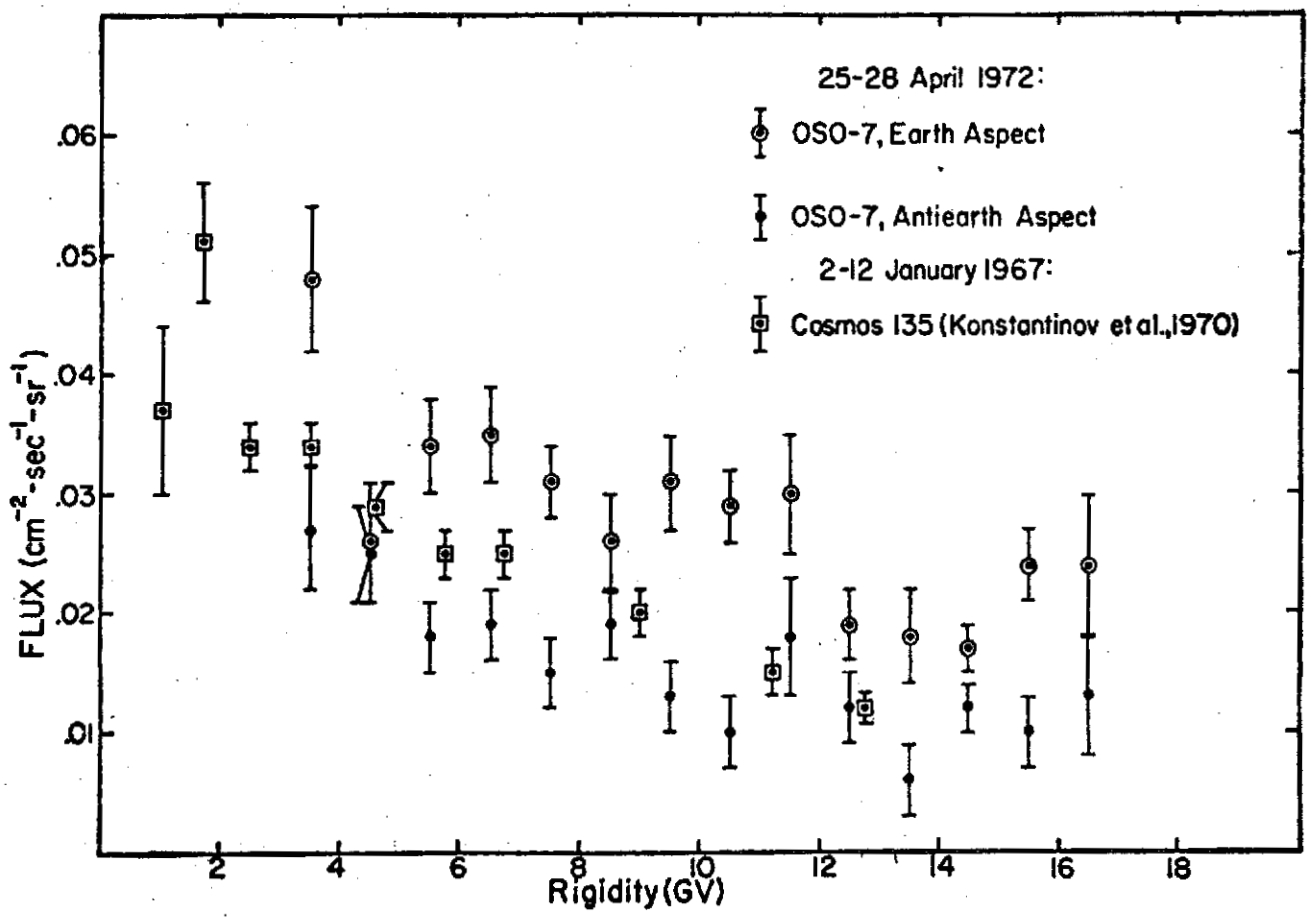

Figure IV-4. Equivalent fluxes for Earth and antiearth aspects for exponential background. Also shown are results from Cosmos 135 (Konstantinov et al., 1970).

The rigidity dependence and flux indicated here can be compared with a summary of results from balloon-borne detectors given by Kasturirangan et al. (1972). The data plotted by Kasturirangan et al. as a function of magnetic latitude is transformed to a rigidity dependence as shown in Figure IV-5. Again this flux, derived from balloon experiments, is divided by 3.8π, the effective solid angle due to the atmosphere at balloon altitudes near 1 MeV (Peterson, 1967). This gives the flux per unit solid angle which is compared with the flux coming from the Earth measured by the OSO-7 detector. The OSO-7 flux is obtained by taking the difference between the total "fluxes" seen while looking toward and away from the Earth shown in Figure IV-4. This removes the apparent flux due to local production. The leakage of a fraction of the Earth flux into the antiearth quadrant is removed by a first order correction to the data. This is given by the ratio of the sensitivity of the detector to an Earth flux while pointed away from the Earth to the corresponding sensitivity while pointing toward the Earth. This amounts to $\frac{3\ cm^2sr}{37\ cm^2sr}$ or 8%. Also shown in Figure IV-5 are data points for the balloon-borne experiments from which Kasturirangan et al. obtained the rigidity dependence of the flux. Details of these experiments are discussed in the introduction of the present work.

The agreement between the balloon measurements and the present experiment is quite good except for the anomalously low point at 4.5 GV in the present experiment. The satellite data also seems to indicate a weaker rigidity dependence than the balloon data. This may be due to the large opening angle of the satellite detector

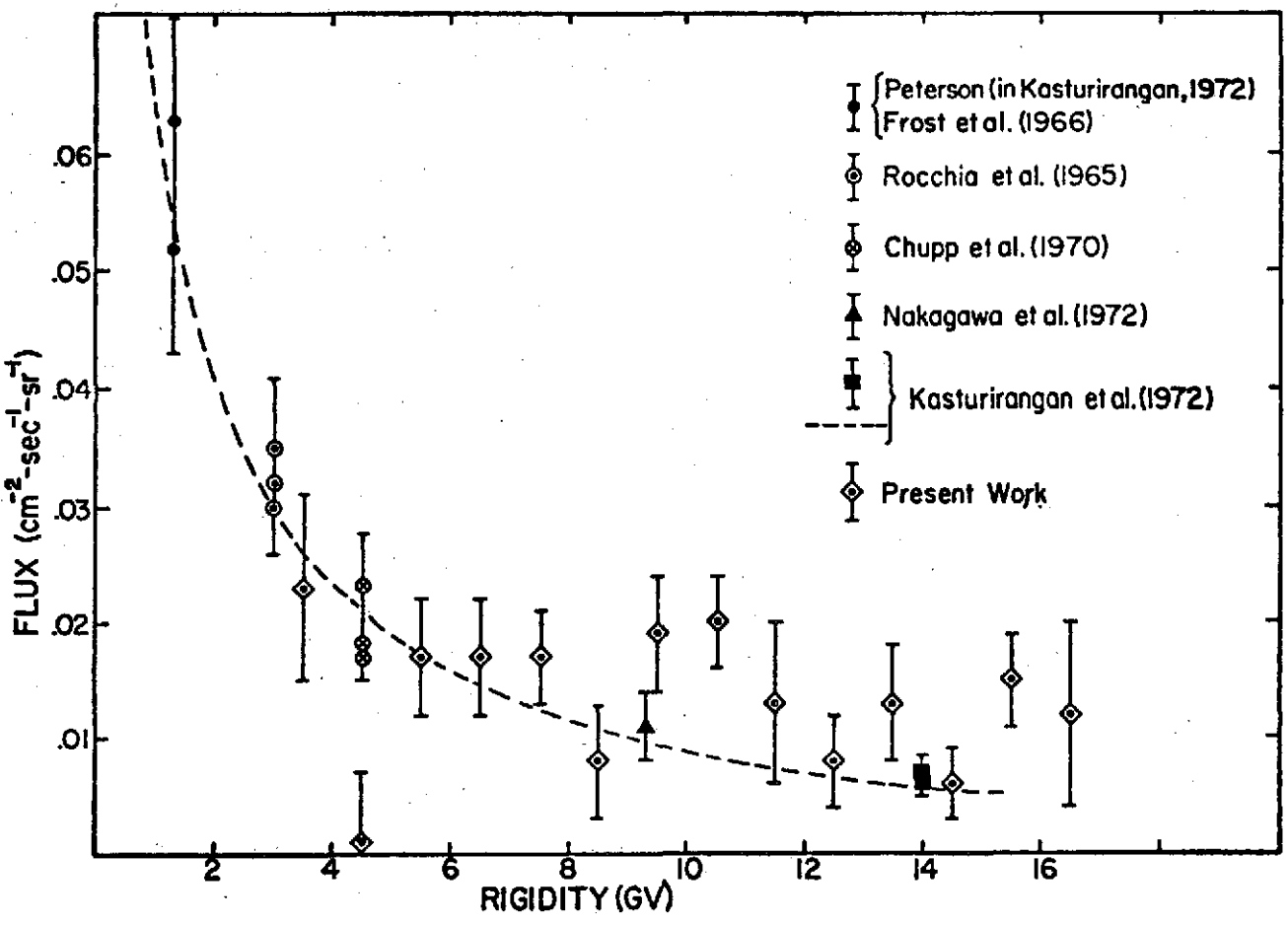

Figure IV-5. Comparison of 0.51 MeV Earth flux seen by the OSO-7 detector with a summary of balloon results given by Kasturirangan et al. (1972).

which samples a larger range of rigidity than does a balloon experiment. Since details of efficiency, angular response, and atmospheric depth corrections are not clear-cut in the compilations of balloon data, it appears to be more meaningful to compare the present experiment with a balloon experiment that is as similar to the present experiment as possible. This is done in Section IV B 3.

2. Altitude Dependence

Another satellite parameter which might be considered a priori as being of importance to the detector counting rate is the satellite altitude. Specifically, the counting rate due to radiation from the Earth in a detector with isotropic response above the Earth's atmosphere should decrease as the Earth's solid angle for isotropically produced low-energy gamma rays (Peterson, 1967). It will be shown below that the counting rate variation due to altitude changes is small and is consistent with the above model.

Figure III-5 shows a sum spectrum accumulated while looking toward the Earth over a period of four days with the satellite altitude less than 430 km during each scan, a mean altitude of 375 km, and an average cutoff rigidity below the satellite of 10.2 GV. A similar sum spectrum was accumulated for the same period at altitudes greater than 430 km, a mean altitude of 472 km, and an average rigidity of 10.1 GV. The difference between these spectra is shown in Figure IV-6 for 25-channel-wide energy bins. Also shown is the measured difference rate for the 0.51 MeV peak.

The expected or calculated rate for the 0.51 MeV peak is also shown in the same figure. This was obtained by calculating the change

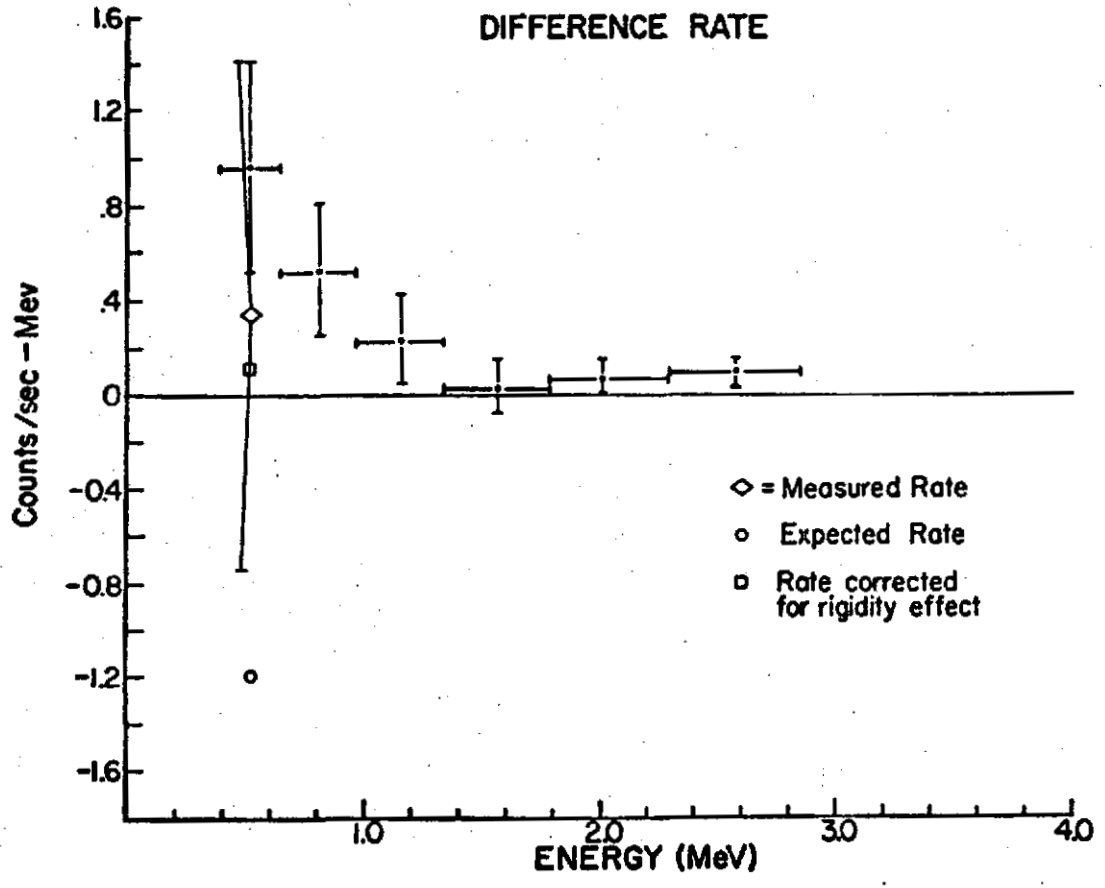

Figure IV-6. Difference rate between low-altitude (Mean Altitude = 375 km) and high-altitude (Mean Altitude = 472 km) scans. Open data points are for the 0.51 MeV peak only.

in the counting rate from the Earth that would be caused by the change in solid angle in moving from the lower altitude (375 km) to the higher altitude (472 km). There is an expected decrease at 0.51 MeV of 1.2 counts/sec-MeV as compared to a measured increase of 0.4 counts/sec-MeV. When correction is made for the difference in rigidity between the two altitudes however, the expected rate becomes +0.1 counts/ sec-MeV which is within the statistical error of measurement. In any case, the altitude dependence which is $\sim$3 percent is appreciably smaller than the rigidity dependence which causes a counting rate variation of $\sim$7 percent per GV at 10 GV and $\sim$200 percent variation over the entire rigidity range.

3. Aspect

The Earth's atmosphere is known to be a source of continuum gamma rays and an annihilation line (Appendix I). As a result, the look direction of the detector with respect to the Earth is an important paramameter affecting the counting rate in the 0.51 MeV region. The extent of this contribution is analyzed in Part B of this section. Only the active Sun is an additional source of annihilation radiation (Section IV, D) in the data analyzed for this work.

C. Variation of 0.511 MeV Flux with Cutoff Rigidity

1. Correlation with Continuum Variation

Puskin (1970) has calculated that 85 percent of the 0.3 to 10 MeV photon flux at balloon altitudes (3.5 mb) is due to electron bremsstrahlung. Most of the remaining flux is due to the 0.511 MeV line (10%) and scattered radiation from that line (5%). Since the electrons causing this radiation are produced in reactions similar to those yielding positrons, we can expect the gamma-ray continuum to depend on the same parameters as the line flux.

Figure IV-7 shows the variation of satellite cutoff rigidity, anticoincidence cup rate, and the integral gamma-ray rate (0.3 to 1.0 MeV) as a function of time for a 4-hour period on April 26, 1972. The data points cover times of good Earth aspect only. The integral rate data is plotted versus rigidity for this period in Figure IV-8, with both Earth and antiearth aspect indicated. Each data point corresponds to single scans and the counting rate is for the integral rate over the energy range 0.3 to 1.0 MeV. This data can be compared with the rigidity dependence of the calculated 0.511 MeV flux shown in Figure IV-4. Comparing the rigidity dependence of the line and the continuum in the antiearth direction, for example, indicates a stronger rigidity-independent component in the continuum. If the line rate is plotted versus the continuum rate, the resultant curve can be fitted with a linear regression giving a residual continuum rate of 13 ± 4 cts/sec for zero line flux. This residual rate is local production rather than cosmic in origin because the cosmic flux seen by Apollo 15 (Peterson and Trombka, 1973) would contribute 2.5 cts/sec at most. The existence of rigidity independent local background is not unexpected

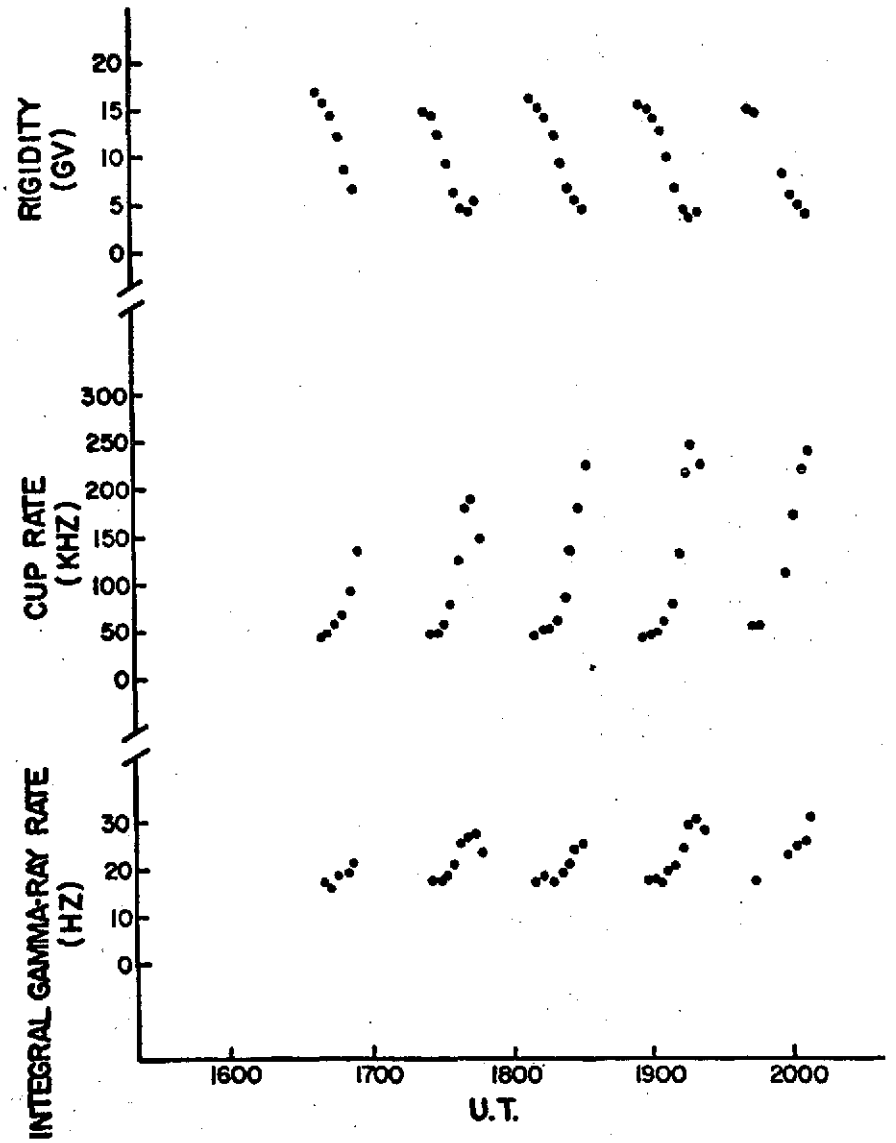

Figure IV-7. .Typical variation of satellite cutoff rigidity, anticoincidence cup rate, and integral gamma-ray rate (0.3 to 1.0 MeV) with time (April 26, 1972).

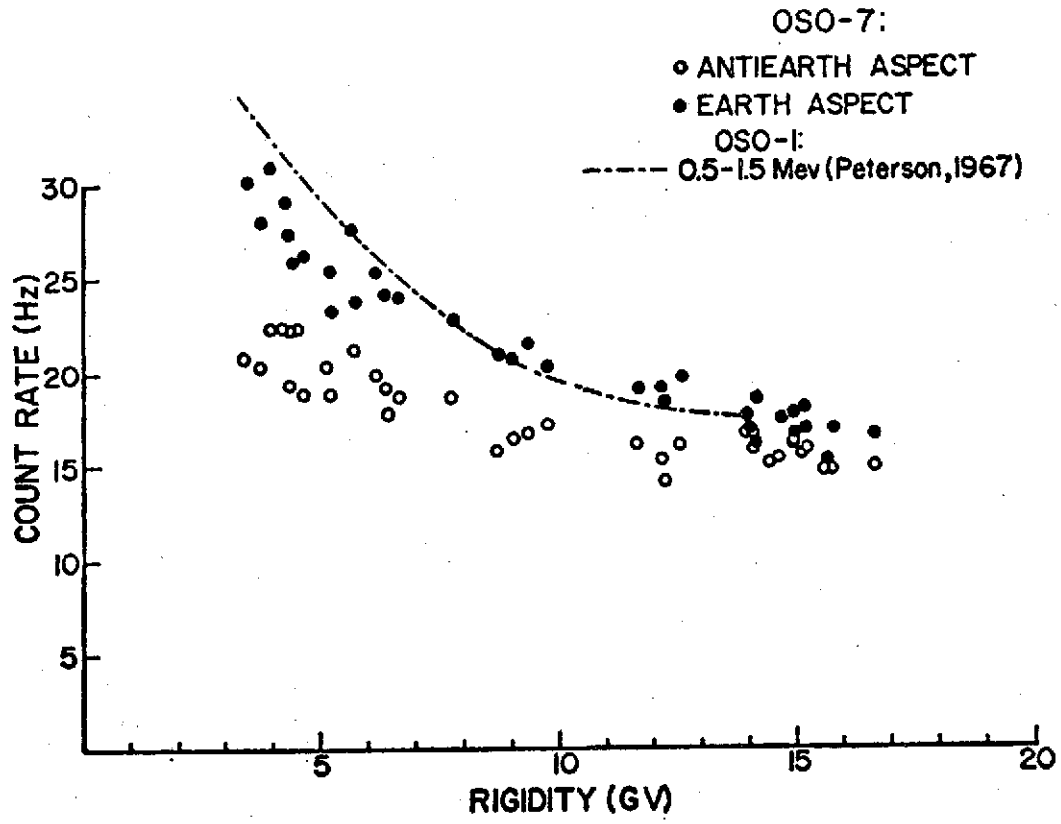

Figure IV-8. Integral gamma-ray rates (0.3 to 1.0 MeV) for Earth and antiearth aspects as a function of rigidity (April 26, 1972). Also shown are results of Peterson (1967) for 0.5 - 1.5 MeV normalized to OSO-7 at 8.3 GV.

since Figure III-1 indicates that the long-term (and therefore rigidity-independent) variation of the gamma-ray counting rate depends on energy. The combination of such long-term production effects with prompt rigidity-dependent effects make the interpretation of such procedures as extrapolation to zero rigidity difficult.

Also shown for comparison in Figure IV-8 is the rigidity dependence for 0.5 to 1.5 MeV gamma rays for the OSO-1 detector (Peterson, 1967). The OSO-1 counting rate is normalized to equal the OSO-7 counting rate at 8.3 GV. The obviously weaker rigidity dependence in the OSO-7 probably indicates a somewhat larger rigidity independent component in the present experiment.

2. Correlation with Charged-Particle Flux Variation

Figure IV-9 is a plot of cup rate versus cutoff rigidity for the same scans used in the previous plot of the gamma-ray continuum variation. It should be noted that this charged-particle shield is also sensitive to gamma rays giving an energy loss of 100 keV or more in the cup. Therefore, the plot incorporates the variation of locally produced gamma rays as well as charged particles. This plot shows a stronger rigidity dependence than either the annihilation line or the 0.3 - 1.0 MeV continuum. This is consistent with the existence of a substantial rigidity-independent local production contribution to both the annihilation line and the gamma-ray continuum.

The figure also shows the calculated rigidity dependence for the OSO-1 detector rate on cosmic ray singles events and on 0.5-1.5MeV gamma-rays (Peterson, 1967). Also included is the latitude dependence

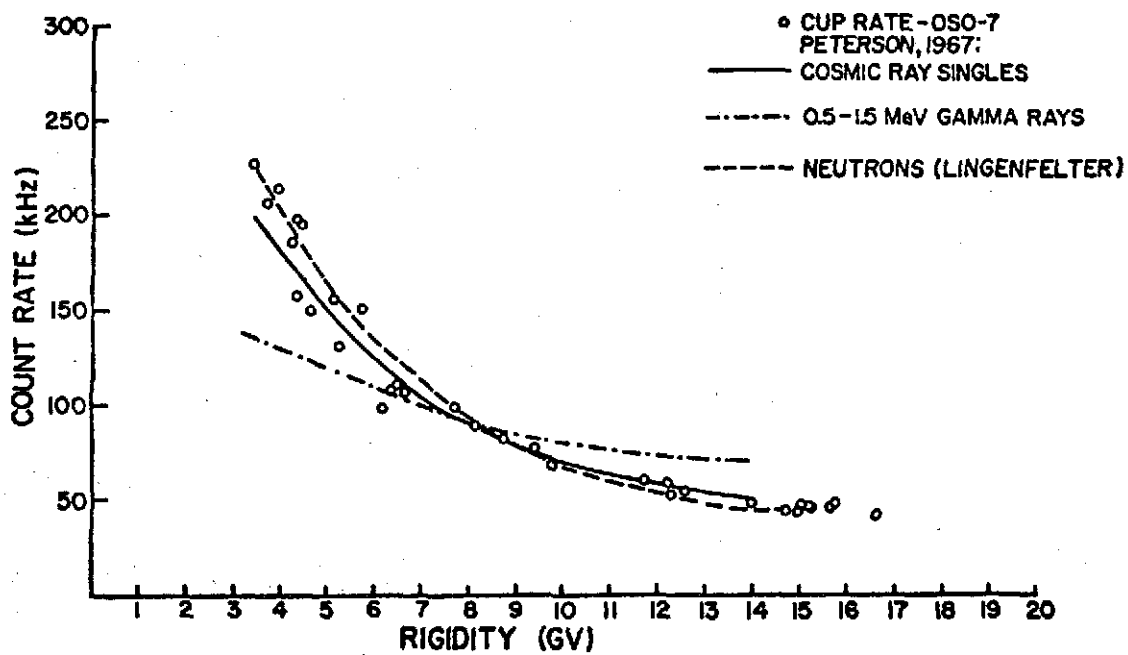

Figure IV-9. Cup rate dependence on rigidity (April 26, 1972). Also shown are the rigidity dependence for the OSO-1 detector of cosmic-ray singles events and 0.5 - 1.5 MeV gamma rays, and the calculated albedo neutron rigidity dependence of Lingenfelter (Peterson, 1967).

of the equilibrium albedo neutron flux calculated for solar minimum by R. E. Lingenfelter (Peterson, 1967). All rates are normalized to equal the OSO-7 cup rate at 8.3 GV.

3. Rigidity Variation and Components of the Flux

a. Contribution of Atmospheric Flux

The measurement of different counting rates in the 0.51 MeV region of the photon spectrum when looking toward and away from the Earth indicates that there are comparable contributions to the counting rate from local production and from gamma rays from the Earth's atmosphere. Section IV, B shows the variation with rigidity of the local production rate (antiearth direction) and the sum of local production and the Earth's contribution (Earth direction). The contribution to the annihilation line from a cosmic background is expected to be small (see below). The correctness of assuming that the difference in counting rates is indeed due to a contribution from the Earth's atmosphere can be substantiated by calculating this difference rate and comparing it with measurements of the atmospheric gamma-ray flux made with balloon-borne detectors.

The difference spectrum shown in Figure IV-10 was obtained from scans accumulated between April 25 and April 28, 1972, that is, it is the difference between the earth and antiearth spectra shown in Figure III-5. The spectra were gathered at cutoff rigidities between 8 and 12 GV and at altitudes between 320 and 430 km. Only scans for which there was good Earth aspect were chosen. The spectra obtained looking in the Earth direction and those obtained looking in the antiearth direction were summed separately. The total live time for these sum spectra is about 30 minutes, representing a real time of about 40

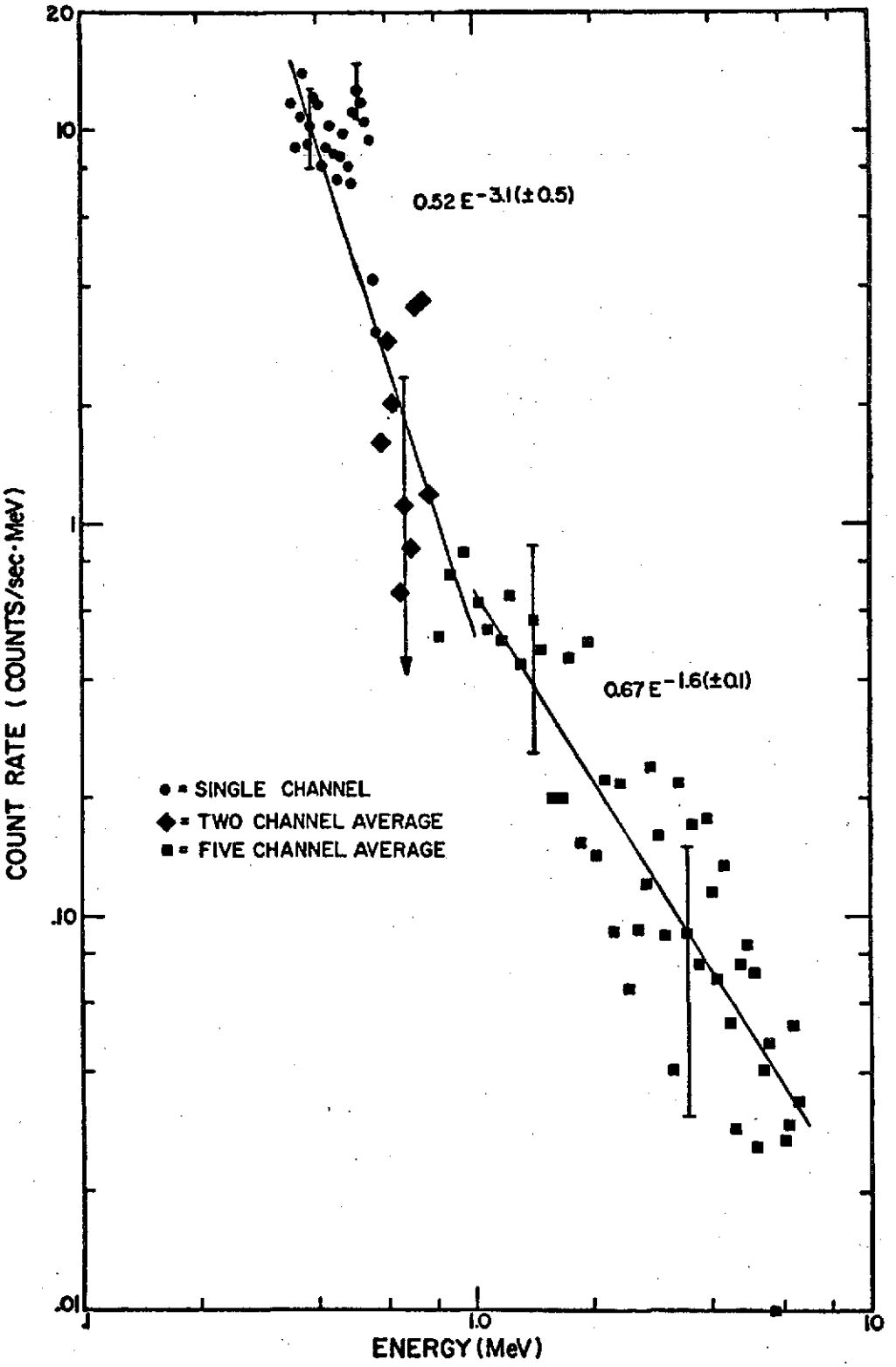

Figure IV-10. Difference between the Earth and antiearth spectra shown in Figure III-5. The only significant feature is a peak at 0.51 MeV.

minutes. Figure IV-10 is the difference between the Earth sum spectrum and the antiearth sum spectrum with each point in the differential counting rate spectrum representing an average over the number of pulse-height channels indicated. The difference spectrum shows a consistent excess in the Earth direction over the entire range of energies.

The only significant feature in the difference spectrum is the peak at 0.51 MeV. This peak is well fit by a Gaussian curve with a mean energy of .516 MeV and a full width at half maximum ($\frac{\Delta E}{E}$) of 8.8 percent. This is in good agreement with the annihilation line energy of 0.511 MeV and detector resolution of 8.8 percent at this energy. The counting rate for this line amounts to 0.41 ± 0.06 counts/sec and is about six standard deviations above the continuum background. This implies a contribution from the Earth of 0.44 ± 0.06 counts/sec when the leakage of 8 percent of the Earth flux into the antiearth quadrant is accounted for (cf. Section IV B1.). The continuum can be fit below 1 MeV by a power law of the form

$$0.52E^{-3.1(\pm 0.5)} \text{ counts/sec - MeV}$$

and above 1 MeV by a power law of the form

$$0.67E^{-1.6(\pm 0.1)} \text{ counts/sec - MeV}$$

A similar difference spectrum for altitudes between 430 and 530 km shows a power law dependence of $E^{-2.1(\pm 0.3)}$ below 1 MeV and $E^{-1.7(\pm 0.2)}$ above 1 MeV.

The gamma-ray continuum, unlike the annihilation line rate, receives an appreciable contribution from the diffuse cosmic gamma rays. In obtaining the difference spectrum in Figure IV-10, the cosmic contribution is, in effect, subtracted from Earth's contribution. In

order to obtain the actual Earth contribution, the effect of the cosmic contribution must be calculated and added on to the difference spectrum. The measurement of the cosmic flux by Apollo 15 (Peterson and Trombka, 1973) has been used for this calculation. The result is a counting rate from the Earth of

$$1.3\ E^{-2.6(\pm\ 0.5)}\ \text{counts/sec - MeV}$$

below 1 MeV and

$$1.3\ E^{-1.8(\pm\ 0.2)}\ \text{counts/sec - MeV}$$

above 1 MeV. Since measurements of the c osmic flux by different groups differ by as much a factor of 2 in this energy range, the above result cannot be considered exact.

To compare these line and continuum counting rates to measurements made in the atmosphere, it is easiest to use data from a detector with isotropic response and the same size and material as the UNH detector. The counting rate for such a 3" by 3" NaI scintillator flown in the atmosphere by L. Peterson has been published in the literature (Gorenstein and Gursky, 1970). This spectrum is similar in many respects to the difference spectrum described above. It consists of a continuum which can be described below 1 MeV by a power law of the form

$$0.4\ E^{-2}\ \text{counts/cm}^2\text{-sec-MeV}$$

and above 1 MeV by

$$0.4\ E^{-1.5}\ \text{counts/cm}^2\text{-sec-MeV}$$

The only feature is a clearly resolved peak which was assumed for energy calibration to be the annihilation peak at 0.511 MeV. The value given for the counting rate in the peak is 0.060 ± 0.003 counts/cm^{2}sec. Using the geometric factor of the isotropic detector of 67 cm^2, this is

equivalent to

$$0.060 \times 67 = 4.0 \text{ counts/sec}$$

In order to compare this to a measurement at satellite altitude, a correction must be made for the different solid angles seen by each detector. At balloon altitudes, the effective solid angle which the atmosphere subtends at an isotropic detector is about 3.8π steradians (Peterson, 1967). The effective solid angle for the UNH detector at 0.51 MeV is about 1π steradians (corresponding to a cone of 60° half angle). A further correction must be made for the change in rigidity between the balloon position (4.5 GV) and the average satellite position (10 GV). This corresponds to a decrease in counting rate of approximately a factor of 2 (Figure IV-5). There is also a small correction for the attenuation of the flux due to the front slab on the UNH detector. This amounts to a factor of 0.8. The balloon measurement as corrected to the satellite position becomes

$$4.0 \text{ counts/sec} \times \frac{1.0\pi}{3.8\pi} \times \frac{1}{2} \times 0.8 = 0.4 \text{ counts/sec}$$

This agrees very well with the measured value of 0.44 ± 0.06 cts/sec.

The energy dependence of the continuum also agrees well for both measurements -- a power law dependence with a break at 1 MeV. A comparison of the absolute rates for the continuum at 0.51 MeV gives 11 cts/sec-MeV for the corrected balloon rate compared to a measured rate of 6.8 cts/sec-MeV. The greater rate at balloon altitudes could be due partly to a lack of the Compton suppression capability which the UNH detector has. There may also be appreciable local production in the balloon experiment.

b. Contribution of Local Production

It will be shown in the section following this one that the 0.511 MeV counting rate observed while looking away from the Earth is much greater than that expected from the upper limit for an isotropic cosmic flux obtained by Metzger et al. (1964). The observed rate can therefore be identified with local production. If we consider the annihilation line counting rate averaged for 8-12 GV using the exponential continuum background calculated in Section III,C, the rate for the Earth quadrant is 1.08 cts/sec, while the rate for the antiearth is 0.56 cts/sec. We can identify the difference of 0.52 ± 0.10 cts/sec with the atmospheric flux from the Earth. This last value agrees fairly well with the value of 0.44 ± 0.06 cts/sec obtained in the previous section by fitting the continuum in the difference spectrum where no correction from linear background assumption to exponential background assumption had to be made. The agreement between the two methods gives us confidence that no significant errors are introduced in the transition to the exponential background assumption.

It should be noted that the local production (or antiearth) counting rate varies with rigidity. This rigidity-dependent part can be identified with prompt production. However, the long-term variations seen in the data imply a contribution that will remain essentially constant over the period of analysis. It is reasonable to identify this contribution with the value obtained by extrapolating the antiearth counting rate to the rate which would be associated with a null charged-particle cup rate. Using a linear extrapolation, of the 0.511 MeV rate

vs. cup rate to zero cup rate, we get a value of 0.25 cts/sec for the rigidity-independent production background. Local production therefore appears to be divisible into a rigidity-dependent portion associated with prompt production and a non-negligible rigidity independent portion probably caused by long lived isotopes. This component will, of course, depend on the epoch of satellite history in which the data is analyzed.

c. Contribution of Cosmic Flux

The possibility of a measurable flux of annihilation radiation being produced in the galaxy is discussed in Appendix I. An isotropic flux cannot be differentiated from local production in the present detector because neither will show a directional dependence. Prompt production due to cosmic rays should show a dependence on the cutoff rigidity which characterizes the point in the satellite orbit at which a spectrum is accumulated. Long-lived isotopes produced by cosmic rays or trapped particles should reach a quasi-equilibrium condition, however, which will be independent of the short-term rigidity changes. For this reason, only an upper limit can be placed on an isotropic cosmic flux.

Perhaps the most conservative value for an upper limit counting rate due to a cosmic flux is the rate measured at high rigidity when the detector is pointed away from the Earth. It is at this time that the contributions from the Earth and from prompt production are at a minimum. From the rigidity variation of the 0.511 MeV counting rate as presented in Section IV, B, the rate at high rigidities (14-17 GV) in the anti-earth direction is about 0.4 counts/sec. The sensitivity for an isotropic flux from the solid angle excluding the earth is 50 cm^2

steradians. This gives an upper limit value for an isotropic cosmic flux of 8×10^{-3} photons cm^{-2} $sec^{-1}sr^{-1}$. The limit placed on this flux from the Ranger 3 gamma-ray detector was (Metzger et al., 1964) 0.014 photons cm^{-2} sec^{-1} or 1.1×10^{-3} photons cm^{-2} sec^{-1} sr^{-1} for an isotropic flux. The OSO-7 limit is also consistent with the Apollo 15 measurement of $(3.0 \pm 1.5) \times 10^{-2}$ photons cm^{-2} sec^{-1} or $(2.4 \pm 1.2) \times 10^{-3}$ photons cm^{-2} sec^{-1} sr^{-1} (Trombka et al., 1973). Here we note that the Ranger 3 limit implies a maximum contribution to the OSO-7 counting rate of 0.055 counts/sec which is small compared to the contribution from the Earth's atmosphere of about 0.4 counts/sec.

D. Solar 0.511 MeV Flux

1. Limit for the Quiet Sun

The UNH detector gathers data in opposite quadrants virtually simultaneously. This provides the possibility of analyzing the data for a difference in counting rates in the two directions. The Earth proves to be a gamma-ray source using this method. In a search for other sources, the difficulty presents itself of choosing "background" data which can be subtracted from "signal" data. Typical pairs of scans contain one which views the Earth, either in the background quadrant during the day or in the solar quadrant during the night. Any counting rate from an extraterrestrial source would be "washed out" in a difference spectrum by the relatively strong Earth flux in the opposite quadrant.

The above difficulty can be overcome by choosing the "signal" and "background" data to be gathered while the detector is looking tangent to a surface concentric to the surface of the Earth. In this case, the Earth's contribution to the counting rate will be equal in

both directions as long as the angular response of the detector is cylindrically symmetric, which is a good approximation in the present case. The rate due to local production will also be eliminated in a difference spectrum since it will be equivalent in both directions.

The Sun is a good candidate for analysis by the above method. When the detector is operating in its normal mode, the Sun is positioned in the center of the solar quadrant, and the background quadrant views an analogous sector of the celestial sphere 180° away from the solar direction. The look direction is tangent to a sphere containing the orbit twice every orbit, and data obtained at these times can be evaluated for a solar contribution.

In general, the look direction for such scans is not perfectly tangent to the orbit. If we define $\hat{L}$ to be a unit vector in the look direction and $\hat{R}$ to be a unit vector pointing from the satellite to the center of the Earth, then the angle which defines a scan to be tangent to a sphere containing the orbit is

$$\Theta = \cos^{-1}(\hat{L} \cdot \hat{R}) = 90^{\circ}$$

This can be called a "limb" scan. Since a scan is accumulated over a period of three minutes, we can guarantee that two such "limb" scans will be accumulated each orbit if the range in Θ is taken to be about 10°. In practice, a limb scan was defined as one for which $84^{\circ} \leq \Theta \leq 96^{\circ}$. On the average, the Earth will contribute equally to a sum of solar "limb" scans and to a sum of background "limb" scans if the average value of Θ for the sum is $\approx 90^{\circ}$.

Limb spectra were obtained for the 5-day period between 14:51 UT on April 25, 1972 and 14:14 UT on April 29, 1972. The solar and anti-solar scans were summed separately and the difference between these sum

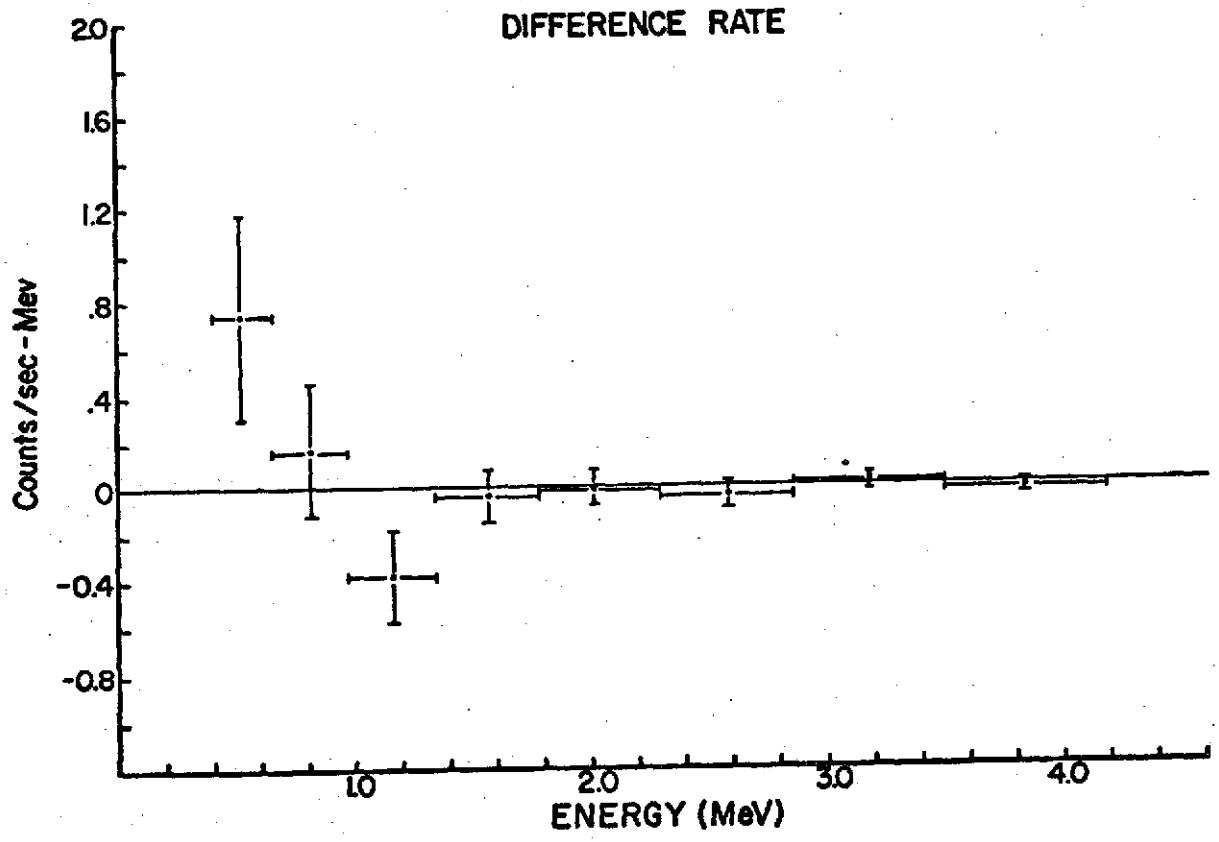

Figure IV-11. Difference between solar and antisolar sum spectra covering a live time of ≈ 1300 sec (April 25-29, 1972). No significant excess is seen in the solar direction.

spectra was taken as shown in Figure IV-11. This shows the solar sum spectrum minus the antisolar sum spectrum and comprises a live time of ≈1300 sec. The data is collected into 25-channel-wide bins and the errors shown are the 1σ errors due to counting statistics. The mean value of θ for these scans is 89.6°. No significant excess is seen in the solar direction. This null result allows an upper limit to be put on the gamma ray flux from the Sun at this time. In order to get an upper limit for the 0.511 MeV line contribution from the Sun, we can take a 5-channel region centered on this energy. This would include about 85% of the counts from a hypothetical solar line flux. The excess rate in the solar direction in this energy region is 0.015 counts per second. Using the detector sensitivity of 15 cm^2 for a point source at 0.511 MeV, this gives an excess of 1.0×10^{-3} photons/ cm^2 sec from the Sun with a 1σ error of 3.8×10^{-3} photons/ cm^2 sec.

A similar analysis can be performed for the energy region centered at 2.23 MeV, the position of a possible deuterium formation line from the Sun. In this case an excess flux of 2.1×10^{-3} photons/ cm^2 sec is seen in the antisolar direction with a 1σ error of 2×10^{-3} photons/ cm^2 sec. These limits are compared with previous searches for line radiation in Tables IV-2 and IV-3 (Chupp, 1971). The limits for this experiment are taken to be the 2σ statistical error which implies a null result at the 95% confidence level. It can also be noted that the limits in this experiment are somewhat stronger, since they include both line and continuum radiation at the respective energies. Possible contributions from known discrete gamma ray sources, the Crab Nebula and the galactic center, are negligible at these energies, being less than 1×10^{-3} photons/sec-cm^2 in both cases.

TABLE IV - 2

SOLAR UPPER LIMITS (0.511 MeV)

Date	Flux ($cm^{-2}sec^{-1}$)	Experimenters
5-2-61	1×10^{-1}	Peterson
6-10-62	1.3×10^{-2}	Frost et al
11-2-67	$(7.5 - 26) \times 10^{-3}$	Chupp et al
-68	8.4×10^{-4}	Haymes et al
-68	7×10^{-3}	Womack and Overbeck
4-24-68	$(1.1 - 4.8) \times 10^{-2}$	Chupp et al
4-72	7.6×10^{-3}	Present work

Reference: Chupp (1971).

TABLE IV - 3

SOLAR UPPER LIMITS (2.23 MeV)

Flux ($cm^{-2}sec^{-1}$)	Experimenters
5×10^{-3}	Chupp et al
4.5×10^{-3}	Womack and Overbeck
4.2×10^{-3}	Present work

Reference: Chupp (1971).

2. The Active Sun (August 2 to August 11, 1972)

On August 4, 1972 a 3B solar flare occurred while the UNH detector was in normal quadrant mode and during satellite "day". The H_α flare began at $\sim$0621 UT, reached a maximum at 0638 UT, and ended $\sim$ 0852 UT. Gamma ray line and continuum radiation were observed in the solar quadrant between the beginning of the flare and the passage of the satellite behind the Earth at $\sim$ 0633 UT (Chupp et al., 1973).

Spectra in the 0.5 MeV region obtained prior to the flare and after eclipse by the Earth can be compared with the flare-time spectrum (0623 to 0632 UT) in Figure IV-12. A peak at 0.5 MeV is evident in the flare data along with an energy-dependent continuum. Similar spectra at higher energies show a strong line at 2.2 MeV and weaker lines at 4.4 MeV and 6.1 MeV. The production of features seen at this time have been predicted to occur during solar flares from theoretical calculations (Appendix I,C). These features include a continuum produced by electron bremsstrahlung, a line at 0.511 MeV due to positron annihilation, a line at 2.23 MeV due to deuterium formation, and lines at various energies due to inelastic proton scattering on light nuclei (including lines at 4.43 MeV and 6.14 MeV from excited C^{12} and O^{16}).

Another 3B flare occurred on August 7, 1972, commencing at $\sim$ 1500 UT during satellite night. Enhancements at 0.5 MeV (Figure IV-13) and 2.2 MeV were seen in the solar quadrant at the beginning of satellite day (1538 UT) and lasted until about 1547 UT. Fluxes obtained during these flare times are summarized in Table IV-4.

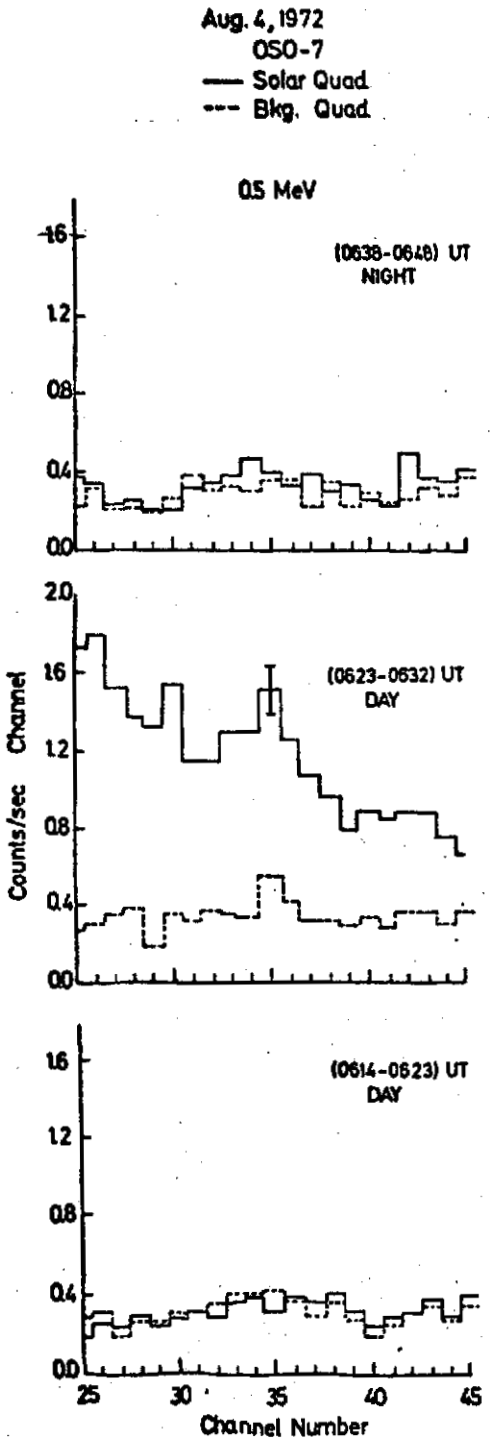

Figure IV-12. The gamma-ray pulse height spectrum for the energy region 435 - 615 keV on August 4, 1972. The H_α flare began about 0621 UT and the satellite was occulted by the Earth at about 0633 UT.

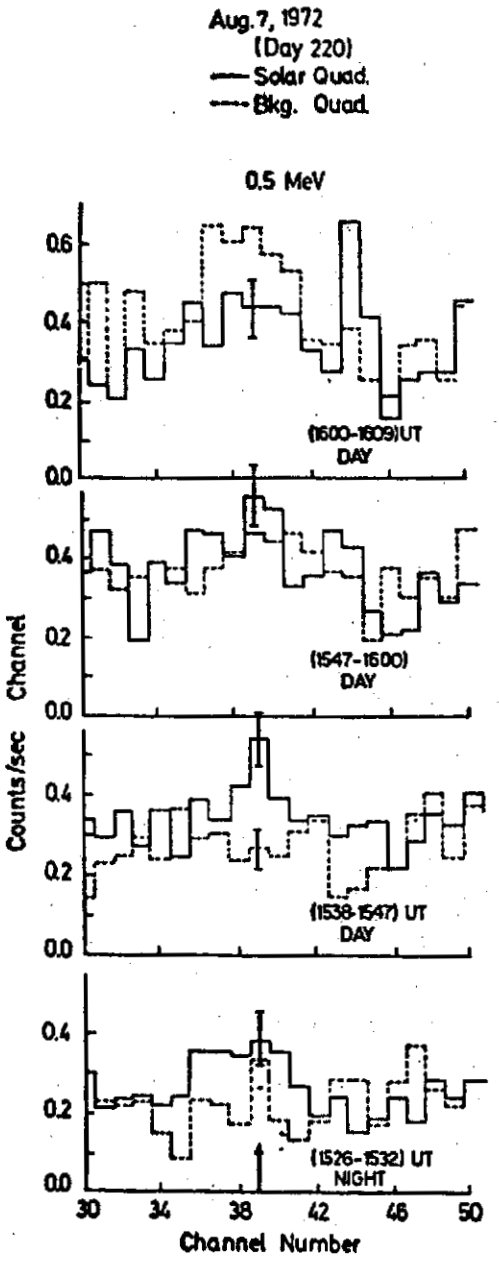

Figure IV-13. The gamma-ray pulse height spectrum for the energy region 435 - 610 keV on August 7, 1972. The H_α flare began about 1500 UT during satellite night. Satellite sunrise occurred at 1538 UT.

TABLE IV-4

MEASURED ENERGIES AND FLUXES OF LINES
AT 0.51 AND 2.2 MeV AT 1 AU

Time of Flare Observations	Energy	Flux (photons $cm^{-2}sec^{-1}$)
August 4, 1972 (0623:49-0633:02)UT	510.7 ± 6.4 keV	(6.3 ± 2.0) x 10^{-2}
	2.24 ± 0.02 MeV	(2.80 ± 0.22) x 10^{-1}
August 7, 1972 (1538:20-1547:33)UT	508.1 ± 5.8 keV	(3.0 ± 1.2) x 10^{-2}
	2.22 ± 0.02 MeV	(6.9 ± 1.1) x 10^{-2}

The possibility of observing thermal Doppler broadening in gamma-ray lines produced during solar flares has been discussed by Kuzhevskii (1969) and Cheng (1972). The observation of these lines by the OSO-7 satellite allows a limit to be put on thermal broadening and, therefore, on the temperature of the plasma in which these lines are produced.

Line broadening at 0.511 MeV due to the thermal velocities of annihilation of positrons and electrons is approximately (Aller, 1963; Stecker, 1969)

$$\left(\frac{\Delta E_\gamma}{E_\gamma}\right)_{TH} \approx 2 \left[\frac{2kT(\ln 2)}{mc^2}\right]^{1/2}$$

where $k = 8.6 \times 10^{-5}$ eV/°K is Boltzmann's constant, T is the temperature of the plasma, and mc^2 is the rest energy of the electron. In addition to the widening of the line at its source, a further broadening is introduced by the statistical nature of the detection and amplification process. Figure IV-14 shows the dependence of the resolution on the gamma ray line energy for various radioactive sources during prelaunch tests. The data are fit by the function

$$\left(\frac{\Delta E_\gamma}{E_\gamma}\right)_{DR} = 0.063\ E_{MeV}^{-0.5}$$

where $\left(\frac{\Delta E_\gamma}{E_\gamma}\right)_{DR}$ is the full width at half maximum (FWHM) of the line data.

Figure IV-14 shows the FWHM of the lines at 0.5 and 2.2 MeV observed during the August 4 flare as well as the FWHM of Co^{60} calibration lines observed before and after the flare. The FWHM's were obtained by subtracting the background quadrant data from solar quadrant data, and then subtracting a fitted continuum from the data

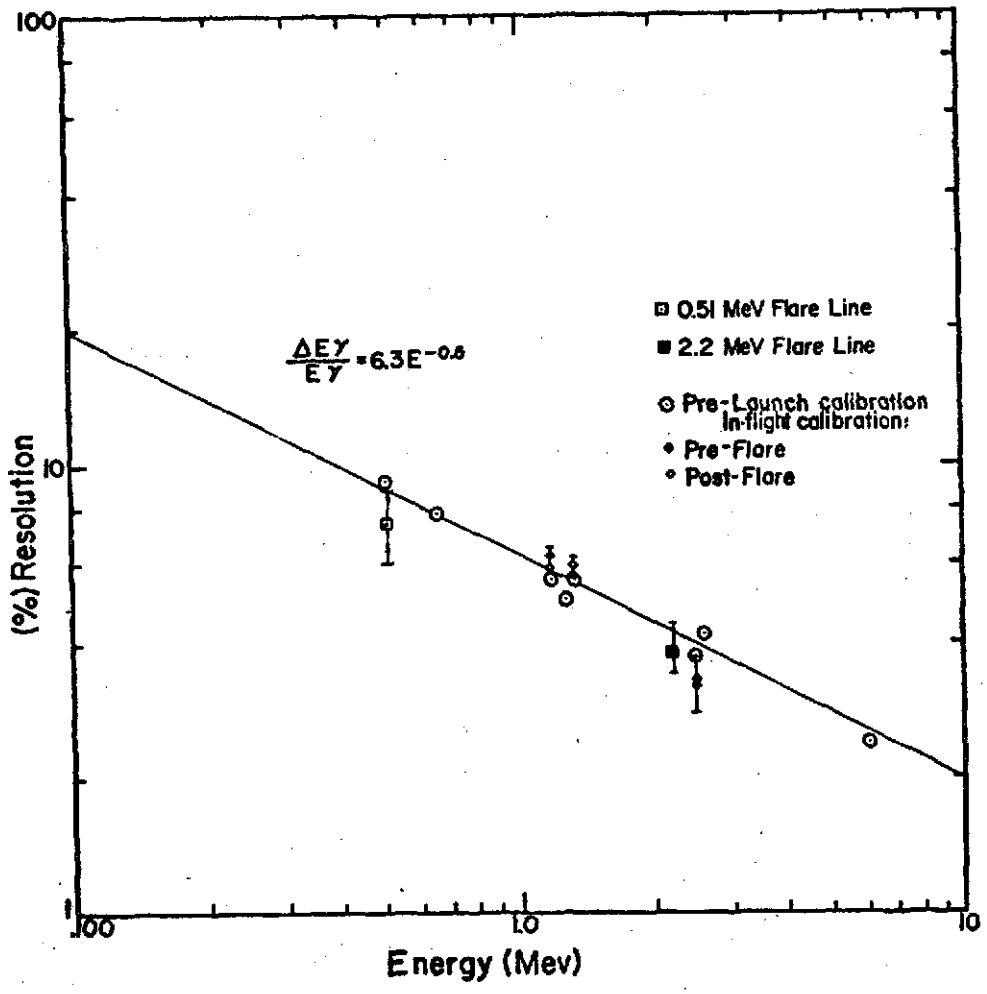

Figure IV-14. The dependence of energy resolution on energy for the UNH detector as obtained from prelaunch calibration data (⊙). Pre-flare (♦) and post-flare (◊) values for resolution come from Co^{60} calibration spectra. The measured line widths for the 0.51 and 2.2 MeV flare lines are also shown.

and fitting the remaining peaks with Gaussian curves. The exact form of the continuum was not critical to the results, but a power law below the 0.5 MeV peak fit the data best. The fit to the flare 0.5 MeV peak with a Gaussian of width 0.074 is shown in Figure IV-15. The agreement of the inflight calibration data with the prelaunch tests indicate that the detector resolution was normal at the time of the flare. Within the uncertainty of the line width determination (1_σ = 0.014), there is no additional broadening due to thermal effects at 0.5 MeV. The fact that the measured width (0.074) is less than the expected width (0.088) seems to be consistent with the uncertainty of the measurement.

We can calculate an upper limit to the thermal broadening from the resolutions which should be combined in quadrature.

$$\left(\frac{\Delta E}{E}\right)^2_{TOTAL} = \left(\frac{\Delta E}{E}\right)^2_{TH} + \left(\frac{\Delta E}{E}\right)^2_{DR}$$

A null contribution from $\left(\frac{\Delta E}{E}\right)_{TH}$ is indicated by the data, so the upper limit to the temperature is obtained from the above equation if the maximum or upper limit value of $\left(\frac{\Delta E}{E}\right)_{TOTAL}$ is used. At the 95 percent confidence level, this value is

$$\left(\frac{\Delta E}{E}\right)_{TOTAL\ MAX} = 0.088 + 0.028 = 0.116$$

where 0.028 is the 2σ uncertainty in the measurement. The Gaussian fit to the data for this confidence level is shown in Figure IV-15. At the 99 percent confidence level

$$\left(\frac{\Delta E}{E}\right)_{TOTAL\ MAX} = 0.088 + 0.042 = 0.130$$

where 0.042 is the 3_σ uncertainty in the measurement.

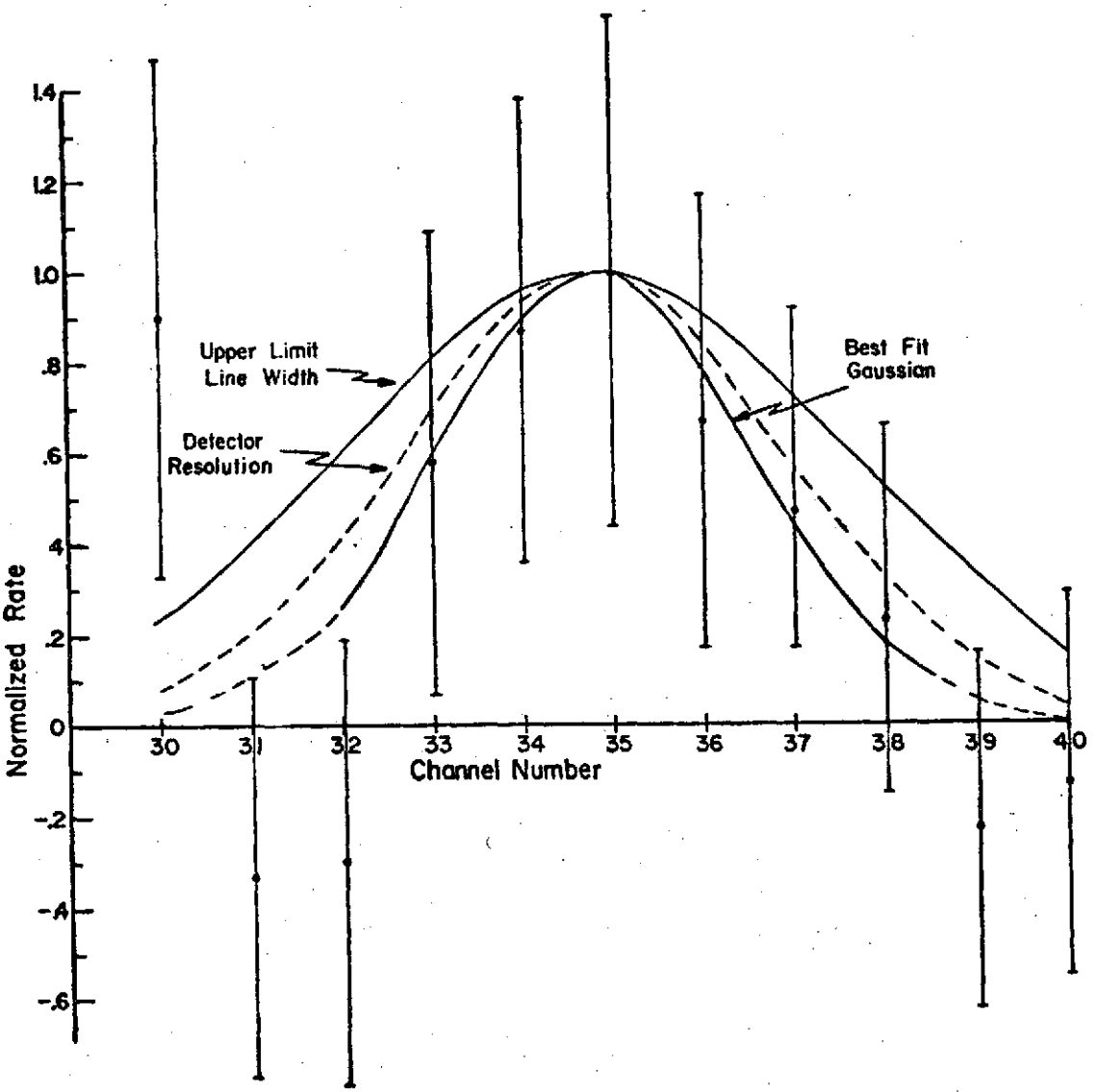

Figure IV-15. The flare peak at 0.51 MeV and the best fit Gaussian curve with a FWHM of 7.4%. Also shown are peaks with widths corresponding to the detector resolution and to the (2σ) upper limit linewidth.

Then taking $(\frac{\Delta E}{E})_{DR}$ to be 0.088 (with an error which is negligible compared to 0.014), $(\frac{\Delta E}{E})_{TH} \leq 0.076$ at the 95 percent confidence level, and $(\frac{\Delta E}{E})_{TH} \leq 0.096$ at the 99 percent confidence level. This gives upper limit temperatures in the annihilation region of 6.2×10^6 °K and 9.9×10^6 °K. Because of the large magnetic fields in the flare, it is reasonable to suppose that the positrons are produced and annihilate in the flare region and that the above temperatures are upper limits for the flare region.

A similar calculation for the 2.2 MeV line gives an upper limit temperature of $\approx 10^9$ °K. The reason for this much higher value is that the electron mass in the formula for thermal broadening must be replaced by the proton mass for deuterium formation. No analysis was done for other lines seen in this flare or for the lines seen on August 7 because of the poorer statistics due to lower fluxes. It should be noted that the 6×10^6 °K upper limit is meaningful since temperatures of $\gtrsim 10^8$ °K have been calculated by Chubb et al. (1966) to account for hard X-rays greater than 30 keV from solar flares.

Thermal broadening is not the only process which can affect the annihilation line shape. Leventhal (1973) has shown that the measured energy of an annihilation peak can be red-shifted and the peak can be broadened if it is caused by annihilation through the positronium mode. This shift and broadening are due to the folding of the three-quantum continuum and the two-quantum peak through the finite instrumental resolution. For a detector with the resolution of the present instrument (8.8% or 45 keV) at 511 keV, the apparent position of such a shifted peak would be 505 keV for annihilation totally through the postronium mode. A small fraction of bound-state annihilation

would cause a smaller shift from 511 keV. Since the presence of positronium depends on the density and temperature of the gas in which the positrons annihilate (Leventhal, 1973), the determination of the exact position of the peaks detected during the flares of August 4 and August 7, 1972 is of interest. Limits on energy shift and broadening in the present experiment lead to a limit on positronium formation in the flare.

The good energy resolution of the gamma ray detector together with the on-board calibration source allow the determination of the energy of measured line radiation with good accuracy. It will be shown here that the energy of radiation near 0.5 MeV can be determined to within $\sim$ 1 percent. The energy of a feature in the detected spectrum is determined from the formula

$$E = c \quad (n + n_0)^2$$

where n is the number of the channel in which the feature falls and c and n_0 are constants. The constant n_0 was determined by fitting ground calibration data to the above quadratic formula. This gives a value of 80.2 for n_0. The value of c is constant for a given spectrum but can vary with time due to gain changes in the detector.

Any calculation of energy from this formula involves the compounding of errors of the measured quantities c and n. The statistical error in determining the center channel n of a gamma-ray peak is taken to be σ_n. For a peak of FWHM equal to 2.35 σ_p, the error in determining its center channel is given by $\sigma_n = \sigma_p/\sqrt{N_p}$, where N_p is the number of counts in the peak. If there is a background N_B which must be subtracted, this formula must be multiplied by the factor $\sqrt{1 + x/1 - x}$, where $x = N_B/(N_p + N_B)$. For our purposes, the

random error σ_c in determining the dependence of energy on channel number for a given spectrum is taken to be an error in the factor c only. This is consistent with the ability to fit variations in gain with corresponding variations in c, while holding n_0 constant. c and σ_c can be determined for any time by appropriately fitting the time variation of c.

In practice, the value of c is determined from the position and known energy of the Co^{60} calibration peaks obtained twice every orbit while the detector is in the calibration mode. c can be determined for times between calibrations from the presence of leakage counts from the Co^{60} in normal data. Calculated values of c for times around the solar flares of August 4 and August 7, 1972 are shown in Figures IV-16 and IV-17. The c value for the flare times can be determined by assuming a linear variation of c with time near the flare period. This yields the values

$$c = (0.3930 \pm 0.0007) \times 10^{-4} \text{ MeV/(channel)}^2$$

for the August 4 flare and

$$c = (0.3619 \pm 0.0009) \times 10^{-4} \text{ MeV/(channel)}^2$$

for the August 7 flare.

The center channel of the flare peak which occurs near 0.5 MeV on August 4 is determined from a least squares fit to the data. Data obtained in the background quadrant is firs t subtracted from the solar quadrant data to eliminate local effects. The remaining spectrum can be fit with a continuum plus a Gaussian-shaped peak using several models for the continuum. The center channel does not depend strongly on the shape of the continuum. A similar technique can be used on the August 7 data, except that the continuum is negligible. For August 4

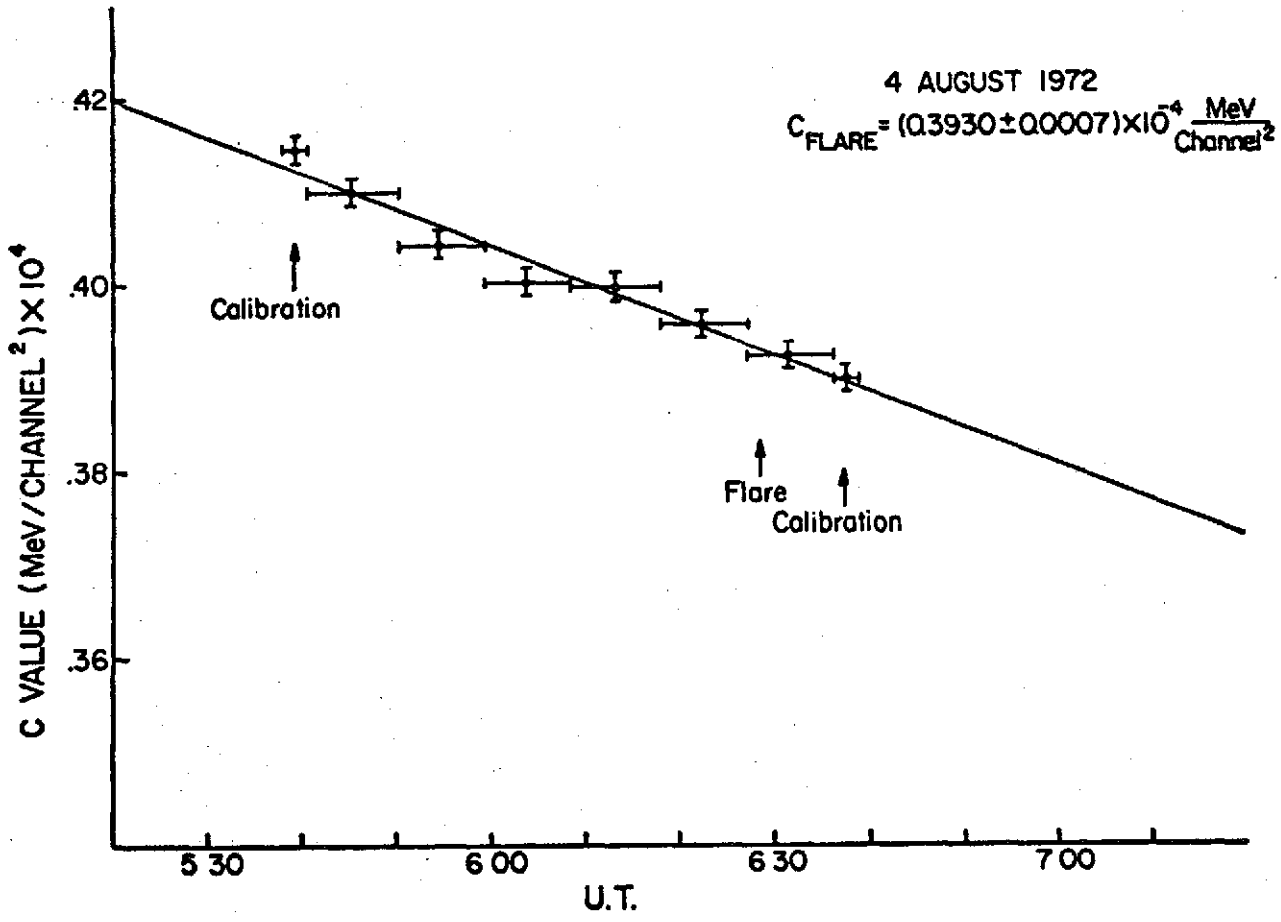

Figure IV-16. The variation of "c" with time around the flare period of August 4, 1972. The variation is fit with a straight line.

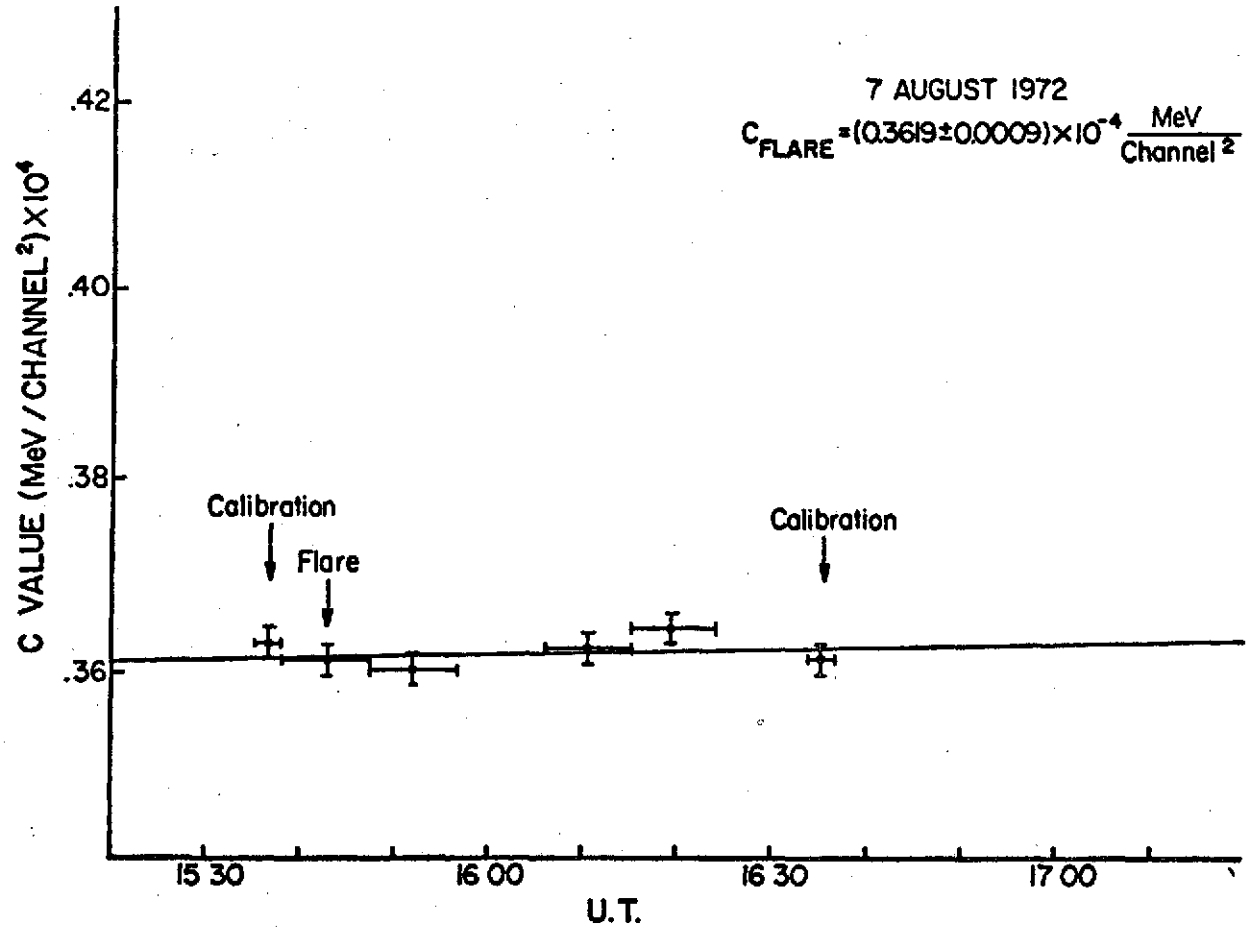

Figure IV-17. The variation of "c" with time around the flare period of August 7, 1972. The variation is fit with a straight line.

we get the value n = 34.8 ± .64 ch; and for August 7 the value n = 39.0 ± .65 ch.

The apparent energies of the flare peaks obtained using our values for c and n are

$$E = 519.9 \pm 5.8 \text{ keV for August 4}$$

and $$E = 514.2 \pm 5.8 \text{ keV for August 7.}$$

So far, only random errors in measurements have been taken into account. Nonlinearites in the detection system can cause a systematic deviation between pulse height spectrum and actual energy loss in the crystal. Such nonlinearities are a property of the pulse height analyzer as well as of inorganic scintillators themselves (Heath, 1964). The determination of n_0 by fitting calibration data minimizes the systematic error due to the nonlinearity but does not eliminate it. For example, the apparent energy of the .511 MeV ground calibration peak is .520 MeV.

A correction can be applied for such a systematic error if we use the local production annihilation peak as a calibration line. Since both flares occur while the satellite is in a region of high rigidity (> 13 GV) the contribution to the locally detected peak from the atmosphere, which may be affected by positronium production, can be neglected. A correction factor "k" which is the ratio of the apparent annihilation line energy to the true energy for the local peak is

$$k = E/E_t = 1.018 \pm 0.0057 \text{ for August 4}$$

$$k = 1.012 \pm .0022 \text{ for August 7.}$$

Using this correction factor on the apparent flare energies, we get the calculated energies

$$E_c = E/k = 510.7 \pm 6.4 \text{ keV for August 4}$$

$$E_c = 508.1 \pm 5.8 \text{ keV for August 7.}$$

where the error is due mainly to uncertainty in the center channel of the flare peaks because of random counting statistic errors. This result shows that the peaks detected during the flares of August 4 and August 7, 1972 are consistent in energy with free annihilation lines at 511 keV within the experimental errors.

As was mentioned previously, the positronium mode also causes an increase in the apparent line width of the annihilation line. The spectra for free annihilation and for bound annihilation are shown in Figure IV-18. The equivalent width of a Gaussian curve fitted to the positronium spectrum over the energy range of the data is 11.2 percent.

From the analysis of thermal broadening we have seen that width of the August 4 peak is 7.4 ± 1.4 percent, which is to be compared with 8.8 percent for free annihilations and 11.2 percent for bound annihilation. If we combine the measurements of energy and line width, the likelihood that the apparent peak energy is as low or lower than that required by totally bound annihilation and the width is as great or greater than that required by totally bound annihilation is $\approx$ 1 percent. Although it is probably better not to combine the data of two different flares, the peak of August 7 shows a similar lack of broadening and large energy shift, but at a lower confidence level. Implications of the positronium limit are given below.

The energy limits also put a limit on a Doppler shift of the line due to bulk motion of the plasma. For a bulk velocity much less than the speed of light

$$\left(\frac{\Delta E}{E}\right)_{DOPPLER} \approx \frac{V_r}{c}$$

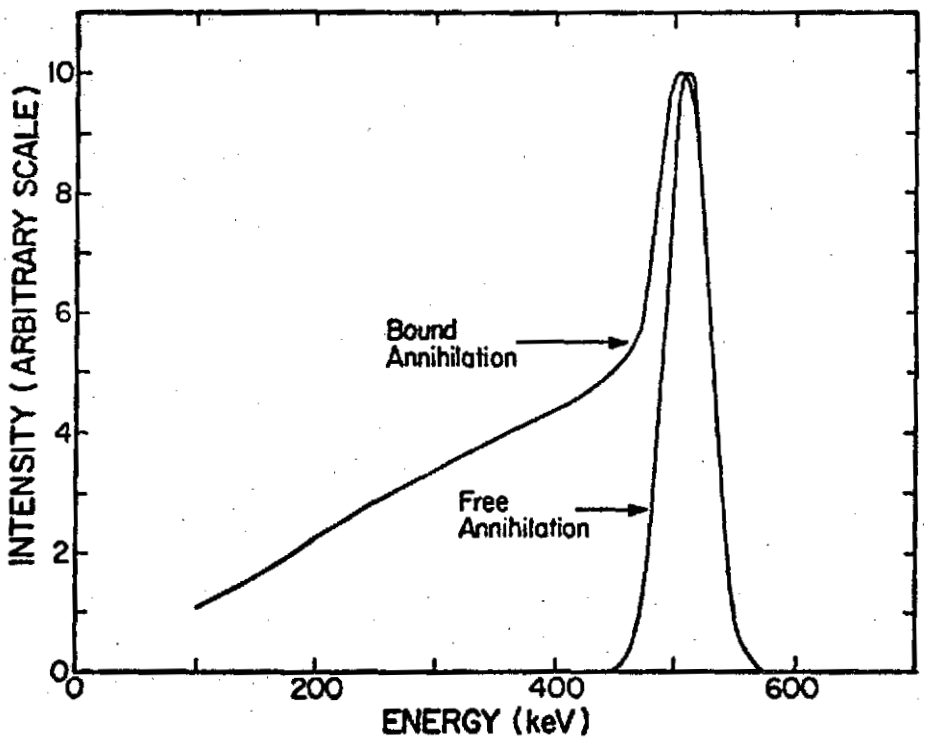

Figure IV-18. Spectra for free annihilation and bound annihilation after folding through the detector resolution of 8.8% (45 keV) at 511 keV.

where $(\frac{\Delta E}{E})_{DOPPLER}$ is the fractional energy shift due to the Doppler effect, V_r is the velocity along the line of sight and c is the speed of light. At the 95 percent confidence level, the uncertainty in E is

$$\Delta E = 2\sigma \approx 12 \text{ keV},$$

so $V_r / c \leq 12 \text{ keV}/511 \text{ keV} = 0.02$

and $V_r \leq 6 \times 10^3$ km/sec.

For purposes of comparison, the velocity of the solar wind near the Earth is $\approx 5 \times 10^2$ km/sec.

E. Discussion of Results

The UNH detector on OSO-7 has proved to be a useful tool in gamma-ray astronomy. Its primary goal was fulfilled by the observation of solar gamma rays during the solar activity of August 2 to August 11, 1972. The wide-angle telescopic properties which made this observation a clear-cut one also made possible a distinction between radiation from the Earth and locally produced radiation. The Earth annihilation line flux obtained in this way agrees very well with a similar Earth-based experiment. For a vertical cutoff rigidity of 10 GV this flux is 1.0×10^{-2} ($\pm 0.2 \times 10^{-2}$) photons-cm^{-2}-sec^{-1}-sr^{-1}.

The agreement between the annihilation flux from the Earth measured by OSO-7 with that measured from balloon experiments in the atmosphere (Figure IV-5) encourages us that there are no large scale systematic errors in the present data analysis. However, we cannot rule out systematic errors of the size of the error bars in Figure IV-5 on the grounds of the difference technique alone. It appears that spallation produced β^+ emitters with half-lives less than one-half the rotation period of the satellite could produce a "pseudo-Earth"

counting rate if the proton flux > 300 MeV has an anisotropy of the proper magnitude and direction. Because of the thick active shielding, the bulk of local production observed in the detector is that which is produced in the detector and in the shield itself. This is supported by the analysis of the line contributions to the sum spectra. As indicated in Appendix II, the strong lines are due to spallation products in the shield and detector.

A survey of the spallation cross-sections for isotopes produced in the shield and detector shows that the cross-sections for the production of the proper short-lived (10μ sec-1 sec) β^+ emitters by incident protons (0.3-3 GeV) at least an order of magnitude below the corresponding cross-sections for the production of long half-life β^+ emitters and the isotopes which contribute an observable rate to the local production spectrum (e.g. I^{126} and I^{124}) (Fishman, 1972). Specifically, the products Na^{20} (0.4 sec), Ne^{18} (1.46 sec) and Ne^{17} (0.10 sec) are the only important short-lived β^+ emitters in the detector and shield materials. Their cross-sections are < 10 mb compared to $\tilde{>}100$ mb for the observed lines. Furthermore, neglecting surface effects, the positrons emitted in such decays have a continuum kinetic energy distribution (E_{max} of 2.57 MeV or greater) yielding a continuum of energy loss in the detector rather than an annihilation peak. This would reduce any apparent anisotropic component by at least another order of magnitude.

Therefore, anisotropies of the order of 100/1 would be necessary to cause the observable excess from the Earth. But even here, the longer lived isotopes would be produced at a rate only 50% reduced.

from the isotropic case. Therefore, the anisotropic local production would be $\tilde{\sim}$ 2/100 or about 2% rather than the $\tilde{\sim}$ 50% effect seen.

The method of measuring the difference between "limb" spectra has given an upper-limit quiet Sun flux of 7×10^{-3} photons-cm^{-2}-sec^{-1}. This compares favorably with upper limits measured by balloon-borne experiments. Only the upper limit of Haymes et al. (1968) of 8×10^{-4} is lower. Since the present limit was calculated from data taken over a 5-day period, a significant lowering of the OSO-7 limit can be obtained by using all of the OSO-7 data in which the 0.5 MeV region is covered. This amounts to some 240 days. Since the upper limit depends on the observation time τ_0 as $1/\tau_0^{\frac{1}{2}}$, there is enough data available to confirm the limit of Haymes provided that systematic errors do not become important.

The previous arguments regarding anisotropic local production apply to the solar quiet-time limit also, except the particle anisotropy to be dealt with is the East-West anisotropy of high-energy protons. Balloon flights by Webber and Ormes (1967) show that the East-West effect is of the order of 50% or less for proton energies between 60 and 300 MeV. This anisotropy appears to extrapolate to higher energies.

Heckman and Nakano (1963) have found an East-West asymmetry for protons of E > 57 MeV in the South Atlantic anomaly region at about 400 km. The magnitude of this effect gives a factor of 2.3 more protons incident from the west than from the east. Even if the proton anisotropy is this large at OSO-7, anisotropic production is calculated to be about an order of magnitude smaller than the error used to calculate the quiet-time solar upper limit at 0.511 MeV. Analysis of

all of the OSO-7 data may reveal whether such systematic effects become important as the statistical errors are decreased. The absence of a significant excess or defect in the difference spectrum given in Figure IV-11 also argues against the presence of systematic errors as large as the statistical errors presented.

Upper limits similar to those given above can be put on any celestial point sources which are positioned near the center of the detector field of view during "limb" scans. Such regions sweep the sky through the year due to the apparent motion of the Sun across the celestial sphere. Such objects as x-ray sources, supernovae and the Galactic Center are likely candidates for a search. For example, the flux from the Crab Nebula (Haymes et al., 1968) should reach the 99 percent confidence level for the first energy interval shown in Figure IV-11 for data taken over a period of about 2 weeks. Unfortunately, the Crab Nebula and the Galactic Center lie almost opposite one another on the celestial sphere, therefore a positive excess in one of the opposing quadrants might not lend itself to a straightforward interpretation.

The present detector is not well designed for a measurement of an isotropic gamma-ray background at 0.511 MeV. Since there is no configuration in which the detector is screened from this source, except by the Earth, which is a strong source itself, no difference spectrum can be obtained by which the local production contribution (which is considerable) can be removed. These difficulties could be overcome partially by separation of the detector from the spacecraft and by avoiding the trapped radiation belts either by low-lying orbits or in cislunar space as in the Ranger experiments. This would minimize

the magnitude of charged-particle effects. The addition of an active shutter which could be inserted before and removed from the aperture of a collimator would allow a calculation and subsequent subtraction of the remaining local contribution.

With regard to the calculation of the Doppler broadening of the flare annihilation line, the upper limit temperature of $\approx 6 \times 10^6$ °K cannot be used to determine the region on the Sun in which solar flares occur. The temperature of the solar atmosphere varies from $\approx 4 \times 10^3$ °K at the base of the chromosphere to $\approx 10^6$ °K in the corona. However, high energy solar x-rays (> 30 keV) have sometimes been explained as thermal bremsstrahlung of hot plasmas at temperatures of 10^7 °K and greater (Chubb et al., 1966). In fact, temperatures of the order of 10^{10} °K would be required to explain the gamma ray continuum observed by the UNH detector in the August 4, 1972 flare. Although temperatures of 10^7 °K and higher are not indicated in the present analysis, the existence of such high temperature regions cannot be ruled out. The line from positrons annihilating there would be greatly broadened and could be lost in the statistical fluctuations of the continuum.

Analysis of the annihilation line width and energy shows that the fraction of annihilations in the bound state is less than 100 percent at the 99 percent confidence level and less than 75 percent at the 95 percent confidence level. This result can be caused by high temperature or strong magnetic fields in the annihilation region.

In a neutral medium, positronium is formed by energetic positrons via charge exchange. At energies above the ionization potential, I, of the ambient gas, elastic collisions and free annihilation dominate over positronium formation although only a few percent or

less of the positrons annihilate above this energy. For positron energies between I and (I-6.8 eV), where 6.8 eV is the binding energy of positronium, the positronium formation cross-section dominates the free annihilation cross-section by many orders of magnitude. Below the energy I, positrons annihilate only in the free state. However, for ambient densities $\lesssim 10^{15}$ atoms cm^{-3} virtually all of the positrons will have been lost to positronium formation before falling below that threshold (Stecker, 1969; Leventhal, 1973). In media of sufficient density ($> 10^{15}$ atoms cm^{-3}) orthopositronium annihilation is quenched by collisional dissociation. This density is obtained approximately by setting the mean time between collisions ($\frac{1}{\sigma n v}$) equal to the orthopositronium lifetime (1.4×10^{-7}sec), where n is the density, σ is the positronium ionization cross-section, and v is the positron velocity. At higher densities the ratio of positronium annihilation to all annihilations varies between 20%-50% depending on the nature of the ambient gas (Green and Lee, 1964).

In a plasma, charge exchange is no longer important, however, and the postronium annihilation rate is determined by ionization and recombination of the positronium atom. If the recombination coefficient is taken to be the same as that of hydrogen, the recombination time is $1.5 \times 10^{9} T^{0.85}/n_e$ sec, where n_e is the electron density and T is the temperature of the plasma (Ramaty and Lingenfelter, 1973). Since the mean rate for free annihilation is $7.5 \times 10^{-15} n_e$ sec^{-1} (Deutsch, 1953), the corresponding mean time is $1.3 \times 10^{14}/n_e$ sec. Setting this equal to the recombination time we see that high temperatures can quench annihilation via positronium independent of ambient density. The temperature at which the positronium formation rate equals the free

annihilation rate is $\gtrsim 7 \times 10^5$ °K (Ramaty and Lingenfelter, 1973). This mechanism could explain the present observation that annihilation is not totally through the positronium mode. It should be noted, however, that up to one-third of the three-photon decays (those from the m=0 substates) can be quenched in magnetic fields $\gtrsim 5$ kG (Green and Lee, 1964). This is due to the mixing of those states by the perturbing magnetic field and the subsequent annihilation in the singlet state since its lifetime (1.4×10^{-7} sec) against annihilation in considerably shorter than the lifetime in the triplet state (1.3×10^{-10} sec).

The accuracy of line width measurements such as the one presented in this work is limited by the counting rate, the background, and the resolution of the detector. The relationship between line broadening and temperature is approximately

$$\left(\frac{\Delta E}{E}\right)_{TH} \gtrsim 2 \left[\frac{2kt\ (\ln\ 2)}{mc^2}\right]^{1/2}$$

In the OSO-7 experiment for the 0.511 MeV line seen during the solar flare, the calibrated resolution for the detector and the uncertainty in the width of the measured line were 0.088 and 0.028, respectively, with the uncertainty at the 95 percent (2σ) confidence level (i.e., about 30 to 35 percent of the detector resolution). The uncertainty depends on the ability to subtract background and the ability to fit the remaining peak to a Gussian. If N_B is the number of counts in the background and N_P is the number of counts in the peak, then the uncertainty in the background fit goes approximately as $\sqrt{N_B}$ and the uncertainty in the peak fit goes approximately as $\sqrt{N_P}$ where N_P is the number of counts in the peak. For our flare data the errors due to

both sources were about equal and of the order of 0.01, or about 10 percent of the resolution of the detector.

It is interesting to calculate the improvement made by using a detector of superior resolution such as a solid-state detector. Such detectors generally have lower sensitivity than the inorganic scintillator used on the OSO-7, however. For a solid-state detector, let us take a resolution a factor of ten less than OSO-7 (i.e., 1 percent at .5 MeV, or 5 keV). Let us also suppose that the sensitivity is a factor of ten down.

For the solid-state detector the channels must be packed 10 times as densely as the OSO-7 analyzer so that there are still about 5 channels under the peak. The factor of 10 change in resolution is balanced by the factor of 10 decrease in the sensitivity so the counts per channel in the peak are the same. However, the continuum has decreased by a factor of 10. Therefore, the error in fitting the continuum is down by a factor of 3 (i.e., $\sqrt{N_B/10}$ rather than $\sqrt{N_B}$) which makes it smaller than the Gaussian fitting error which should still be about 10 percent of width due to the intrinsic resolution of the detector. This is true because the counts per channel in the peak are the same as in the original case. So if an upper limit were calculated for this solid-state detector in the same way as for the OSO-7,

$$\left(\frac{\Delta E}{E}\right)_{TH} \approx 2\left[\frac{2kt\ (\ln 2)}{mc^2}\right]^{1/2} = 3 \times 10^{-5}\ T^{1/2}$$

Combining the components of line width in quadrature as in Section IV, D, for the upper limit to $\left(\frac{\Delta E}{E}\right)_{TH}$

$$\left(\frac{\Delta E}{E}\right)_{TH}^2 \leq \left(\frac{\Delta E}{E}\right)_{TOTAL}^2 - \left(\frac{\Delta E}{E}\right)_{DR}^2$$

where $\left(\frac{\Delta E}{E}\right)_{TOTAL} \cong 0.01 + 2\sigma = 0.012$, $\left(\frac{\Delta E}{E}\right)_{DR} \cong 0.01$

so $\left(\frac{\Delta E}{E}\right)_{TH} \leq 0.007$

and $T^{1/2} \leq 7 \times 10^{-3}/3 \times 10^{-5} = 233$ and $T \leq 5 \times 10^{4}\ ^{0}K$

In this case, thermal broadening should certainly be seen. All of this depends on the assumption that background effects, shielding, pointing, angular response, etc. are the same or equivalent.

APPENDIX I

GENERATION OF ANNIHILATION RADIATION

A. General Theory

The existence of a positively charged particle of mass equal to that of an electron was first postulated theoretically by P. A. M. Dirac as the physical interpretation of the negative energy solution of the Dirac equation (Dirac, 1928a; Dirac, 1928b). Tracks of the positron were discovered in cloud chamber photographs by C. D. Anderson in 1932 (Anderson, 1932; Anderson, 1933).

The cross-section for electron-positron two-photon annihilation was first deduced by Dirac (1930), while the cross-section for pair creation by gamma rays in the vicinity of a nucleus was calculated by Heitler and Sauter (1933) and by Bethe and Heitler (1934). Modern presentations of the theory are given by Heitler (1960) and by Bjorken and Drell (1964).

1. Annihilation Mechanisms

The differential cross-section for two-photon annihilation is given by (Heitler, 1960)

$$d\sigma = \frac{e^4}{4p_0}\left[\frac{E_o^2+p_o^2+p_o^2\sin^2\theta}{E_o^2-p_o^2\cos^2\theta} - \frac{2p_o^4\sin^2\theta}{(E_o^2-p_o^2\cos^2\theta)^2}\right]\sin\theta\, d\theta\, d\phi$$

in the center-of-momentum frame for unpolarized quanta and particles, where p_0 is the electron momentum in the c.m. frame, E_0 is the electron energy in the c.m. frame, θ is the angel between p_0 and the direction of one photon, and ϕ is the azimuth of the direction of that photon.

Transforming to the lab frame in which the electron is at rest, and integrating over both angles, the cross-section for the annihilation of a positron of energy E_+ is

$$\sigma = \pi r_o^2 \frac{1}{\gamma+1}\left[\frac{\gamma^2+4\gamma+1}{\gamma^2-1}\ln(\gamma+\sqrt{\gamma^2-1}) - \frac{\gamma+3}{\sqrt{\gamma^2-1}}\right]$$

where $\gamma = E_+/mc^2$ and $r_0 = e^2/mc^2$.

An approximate form for $\gamma \sim 1$ ("non-relativistic" case) valid for positron kinetic energies such that $e^2/hc << T_+ << mc^2$ is

$$\sigma \approx \pi r_o^2 \, c/v_+$$

where v_+ is the positron velocity and T_+ is the positron kinetic energy. An approximate form for $\gamma >> 1$ (extreme relativistic case) is

$$\sigma \approx \frac{\pi r_o^2 mc^2}{E_+}\left(\ln\frac{2E_+}{m} - 1\right)$$

Although two-photon annihilation is the predominant channel for free positron decay, there are several competing processes. Single-photon annihilation can take place when the electron is strongly bound to a nucleus of charge Ze. (The nucleus is necessary to conserve energy and momentum). However, the cross-section for single-photon annihilation is, at most, about 20 percent that of two-photon annihilation even for the heaviest nuclei (Heitler, 1960). For example (Hayakawa, 1969), for $\gamma >> 1$

$$\frac{\sigma_1}{\sigma_2} \approx \frac{4z^5\alpha^4}{\ln(2\gamma)-1}$$

where σ_1/σ_2 is the ratio of single-photon to two-photon cross-sections, $\alpha = e^2/hc = 1/137$, and for $\beta >> 1$

$$\frac{\sigma_1}{\sigma_2} \approx 4/3 \; z^5\alpha^4\beta^2$$

where $\beta = \frac{v_+}{c}$, but $z^5\alpha^4 << 1$ so $\frac{\sigma_1}{\sigma_2} << 1$.

Another possible process is one in which no photons are emitted and the energy of annihilation is given off to a second electron in the

vicinity of the collision. The cross-section for this process is small (Heitler, 1960).

Three-photon decay will occur when two-quantum annihilation is forbidden by selection rules which are applicable. For an unbound S state, the ratio of the cross-section for three-quantum decay to that for two-quantum decay is (Ore and Powell, 1949)

$$\frac{\sigma_1}{\sigma_2} = \frac{1}{372}.$$

For states of greater angular momentum, the cross-sections decrease. The positron and electron can form a bound state (positronium) in which the three-photon decay mode becomes important. For example, if $\ell = 0$, the formation of the triplet $^3S_1$ state (orthopositronium) is 3 timesmore probable than the formation of the singlet $^1S_0$ state (parapositronium). Since the decay of positronium obeys the selection rule (Stecker, 1969)

$$(-1)^{\ell}(-1)^{S+1}(-1)^{\zeta}=(-1)$$

where ℓ is the orbital angular momentum quantum number, S is the spin quantum number, and ζ is the number of photons in the final state, three-quarters of the positronium decays go to three photons and one-quarter go to two photons. The decay rates for states $\ell = 0$ are negligible compared to the $\ell = 0$ rate (Deutsch, 1953). The astrophysical conditions under which positronium formation is important have been discussed by Stecker and by Leventhal (1973). Stecker shows that under interstellar conditions positrons generated by cosmic ray interactions annihilate from rest via positronium formation over 95 percent of the time. In most gases near atmospheric pressure, positrons will annihilate through the positronium mode between 21

percent (nitrogen) and 50 percent (oxygen) of the time (Green and Lee, 1964). Leventhal calculates that the positronium formation fraction can approach 100 percent for atomic hydrogen as the density falls below 10^{15} atoms cm^{-3}. At high enough densities or temperatures, however, triplet decay and positronium formation can be supressed by collisions. Furthermore, high magnetic fields ($\gtrsim$ 5kG) can decrease triplet decay by one-third (Green and Lee, 1964). In solids, three photon annihilation is negligible.

2. Generation of Positrons

There are three modes of positron production which dominate in interactions of astrophysical importance; these are: 1. pair production, 2. positive pion decay, and 3. decay of positron-emitting nuclei.

Pair production is the conversion of an energetic photon ($E > 2mc^2$) into a positron-electron pair. Energy and momentum conservation requires that another particle be present. The cross-sections for this interaction were first calculated by Heitler and Sauter (1933) and by Bethe and Heitler (1934). For pair creation in the vicinity of a nucleus of charge Ze the cross-section is (Heitler, 1960)

$$\sigma E_+ \, dE_+ = \bar{\sigma} \frac{p_+ p_-}{k^3} dE_+ \{ -\frac{4}{3} - 2E_+E_- - \frac{p_+^2+p_-^2}{p_+^2 p_-^2} +$$

$$+ (mc^2)^2 \left(\frac{E_+E_-}{p_-^3} + \frac{\varepsilon_+E_-}{p_+^3} - \frac{\varepsilon_+\varepsilon_-}{p_+p_-}\right) + L \left[\frac{k^2}{p_+^3 p_-^3}(E_+^2E_-^2+p_+^2p_-^2) - \right.$$

$$\left. -8/3 \frac{E_+E_-}{p_+p_-} - \frac{(mc^2)^2 k}{2p_+p_-} \left(\frac{E_+E_- - p^2}{p_-^3} \varepsilon_- + \frac{E_+E_- - p_+^2}{p_+^3} \varepsilon_+ + \frac{2kE_+E_-}{p_+^2 p_-^2}\right)\right] \}$$

where k is the momentum of the photon, $E_{+(-)}$ is the total energy of the positron (electron), $p_{+(-)}$ is the momentum of the positron

(electron), $\varepsilon_+ = 2\ell n \frac{(E_+ + p_+)}{mc^2}$ $L = 2\ell n \frac{(E_+E_- + p_+p_- + (mc^2)^2)}{mc^2 k}$,

and $\bar{\sigma} = Z^2 r_o^2/137$

This formula is valid under the conditions of the Born approximation, assuming that the screening of the nuclear Coulomb field by the outer electrons is negligible. By integrating this expression over E_+, a total pair-creation cross-section can be obtained. For the case in which all energies are large compared with mc^2,

$$\sigma = \bar{\sigma} \left(\frac{28}{9} \ln \frac{2k}{mc^2} - \frac{218}{27}\right)$$

In general, the pair production cross-section for an electron rises from a negligible value (compared to the Compton cross-section) below 1 MeV and levels off to a weak dependence on photon energy above 100 MeV.

Another mechanism important is astrophysics is the decay of the positive pion. The normal pion decays are (Segré, 1964)

$$\pi^o \rightarrow 2\gamma \left(T \simeq 2 \times 10^{-16} \text{ sec}\right), \quad \pi^+ \rightarrow \mu^+ + \nu\mu$$

and $\pi^- \rightarrow \mu^- + \bar{\nu}_\mu \quad (T_\pm \simeq 2.55 \times 10^{-8} \text{sec})$

Down in probability by a factor of 10^{-4} is

$$\pi^+ \rightarrow e^+ + \nu_e .$$

Down in probability by a factor of 10^{-8} is

$$\pi^+ \rightarrow \pi^o + e^+ + \nu_e .$$

Free muons obtained from the pions decay by the scheme (Segré, 1964)

$$\mu^- \rightarrow e^- + \bar{\nu}_e + \nu_\mu$$

$$\mu^+ \rightarrow e^+ + \nu_e + \bar{\nu}_\mu \quad (T_\mu \simeq 2.2 \times 10^{-6} \text{ sec})$$

The mean energy of the resulting electron is roughly one-quarter the energy of the original pion (Cheng, 1972).

Negative muons react weakly with nuclei (e.g., $p + \mu^- \rightarrow n + \nu$), but μ^+ decays freely as indicated above. The chain $\pi^+ \rightarrow \mu^+ \rightarrow e^+$ is

important because pions are produced by cosmic ray interactions in interstellar space by reactions such as (Ramaty and Lingenfelter, 1966)

$$p+p \rightarrow A+B+a\pi^{+}+b(\pi^{+}+\pi^{-})+c\pi^{o}$$

and

$$p+He^{4} \rightarrow A+B+C+a\pi^{+}+b(\pi^{+}+\pi^{-})+c\pi^{o}$$

where A, B, and C are nuclei and nucleons and a, b, and c are zero or positive integers. About 30 percent of the incident kinetic energy of the protons goes to pion energy (Cheng, 1972). Most of the galactic pions are produced by cosmic rays of energy 500 MeV or greater. The contribution from cosmic ray α-particle interactions with He^4 and proton interactions with heavier nuclei can be neglected because of low relative intensity and density. The contribution from kaon production and decay can be neglected because the kaon production cross-section is 10-20% of the pion cross-section and kaons carry a smaller fraction of the total energy. Similarly, the positron contribution from other strange particles is negligible.

Another source of positrons (of energies below 20 MeV) is the decay of β^{+} emitting isotopes (e.g., C^{10}, C^{11}, N^{13}, O^{14}, O^{15}). These radionuclides can be formed in the cosmic ray spallation interactions between protons and C^{12}, N^{14}, and O^{16} nuclei, as well as in similar interactions in the atmospheres of the Earth and the Sun. The role of this mechanism in the production of positrons in the galaxy has been investigated by Stecker (1969) and Ramaty, Stecker, and Misra (1970) using cross-sections published by Audouze et al. (1967).

Less important modes of pair production include the following:

1. Creation of pairs in the collision of two heavy particles. Here, $\sigma \simeq \frac{r_o^2}{137^2}(mc^2)^2 \frac{z_1^2 z_2^2}{M_2 c^2 T_2}\left(\frac{z_1 M_2 - z_2 M_1}{M_1}\right)^2$ where particle 1 is initially at rest and T_2 is the kinetic energy of

particle 2 (assuming $T_2 << M_2c^2$) (Heitler, 1960).

2. Creation of pairs by a fast electron in the field of a nucleus. Here, $\sigma \simeq \frac{r_o^2 z^2}{137^2} \frac{28}{27\pi} (\ln E_o/mc^2)$ and the electron energy $E_0 >> mc^2$.

3. Creation by collision between two electrons.

4. Creation by the annihilation of two light quanta (inverse pair annihilation).

5. Conversion of a γ quantum emitted by a nucleus into a pair in the field of that nucleus. All of these latter processes are negligible compared to the first three.

B. Production in the Earth's Atmosphere

1. Cosmic Ray Interactions

Cosmic rays which are incident on the Earth's atmosphere generate continuum and line gamma radiation, which have been measured by balloon-borne detectors (Jones, 1961; Peterson, 1963; Haymes et al., 1969; Chupp et al., 1967). The channels into which the energy of the cosmic rays goes is shown in the following table (Hayakawa, 1969):

Process	Energy dissipation ($MeV\text{-}cm^{-2}\text{-}sec^{-1}\text{-}sr^{-1}$)
Ionization in the atmosphere	730
Residual energy at sea level	40
Nuclear disintegration	150
Neutrinos	230
TOTAL	1150

where the numbers hold for latitude 50°. The incident and dissipated energies can also be analysed into the species by which they are carried (Hayakawa, 1969):

Species	Incident Energy ($MeV-cm^{-1}-sec^{-1}-sr^{-1}$)
Protons	889 ± 25
He - nuclei	200 ± 4
L - elements	6 ± 2
M - elements	47 ± 1
H - elements	40 ± 1
TOTAL	1180 ± 30

where L, M, and H refer to light, medium, and heavy cosmic ray nuclei.

Species	Dissipated Energy
Proton Ionization loss	129 ± 3
$\pi^{\pm}$	416 ± 14
π^{o}	265 ± 24
Nuclear disintegration	301 ± 68
TOTAL	1110 ± 80

where the estimates have been made for a geomagnetic latitude of 55°. The above tables illustrate the importance of pions in cosmic ray interactions in the atmosphere.

Cosmic ray components can also be characterized by their ability to penetrate matter. The so-called soft component is composed of electrons and photons (the electronic or E-component). Near sea-level the charged pions have largely decayed into μ mesons (the penetrating component) which interact with matter even less strongly than the N-component. The genetic relationships among the cosmic ray

secondaries are illustrated by Hayakawa (1969) in the following diagrams:

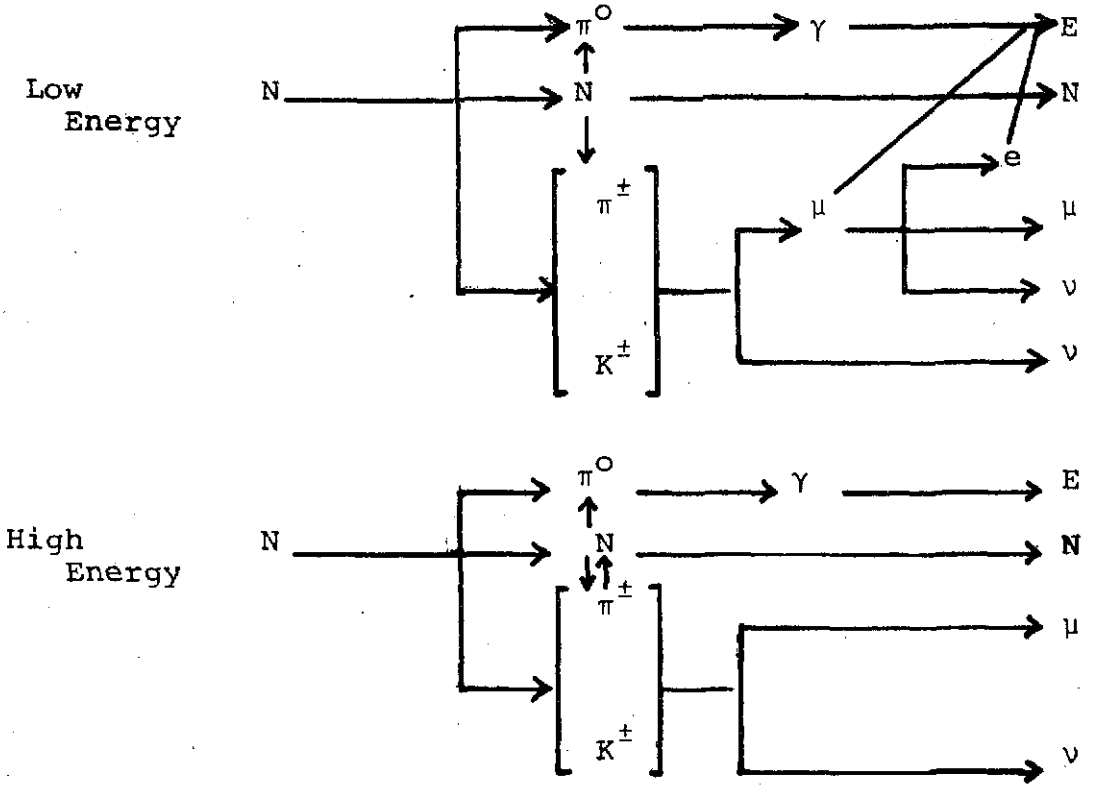

Although these diagrams are only rough schematics, they indicate that the main contribution to the electronic component (and, hence, to the positron annihilation radiation and the gamma-ray continuum) is π^o production. This can be seen quantitatively in the graphs of the intensity versus atmospheric depth in Figure A-1 and Figure A-2 (Hayakawa, 1969) where the electron (positon plus negaton) fluxes from π^o interactions and from μ decays are compared. Only at large depths ($> 600 g/cm^2$) does the $\mu \rightarrow e$ source become important. Since balloon-borne gamma-ray detector measurements have shown that the flux of annihilation radiation increases with decreasing atmospheric depth

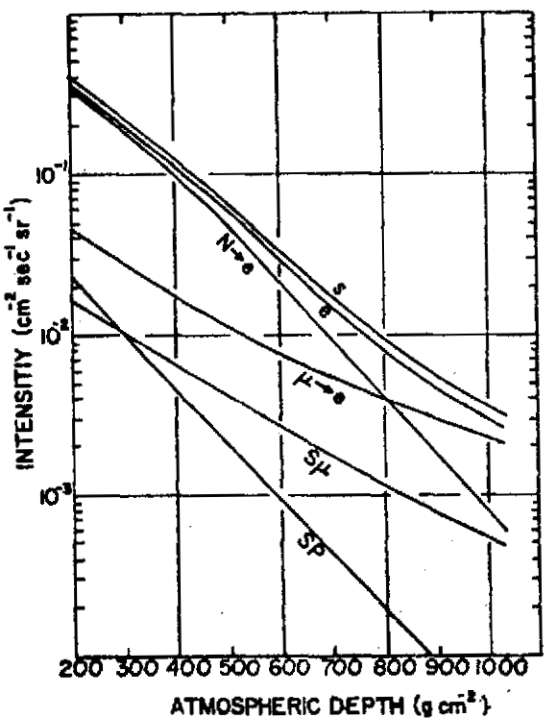

Figure A-1. Vertical intensities versus atmospheric depth of the soft component (S) and its subcomponents; S = e + sμ + sp, e (electrons) = N → e (electrons from π^0) + μ → e (electrons from the knock-on and decay processes of muons),(Hayakawa, 1969).

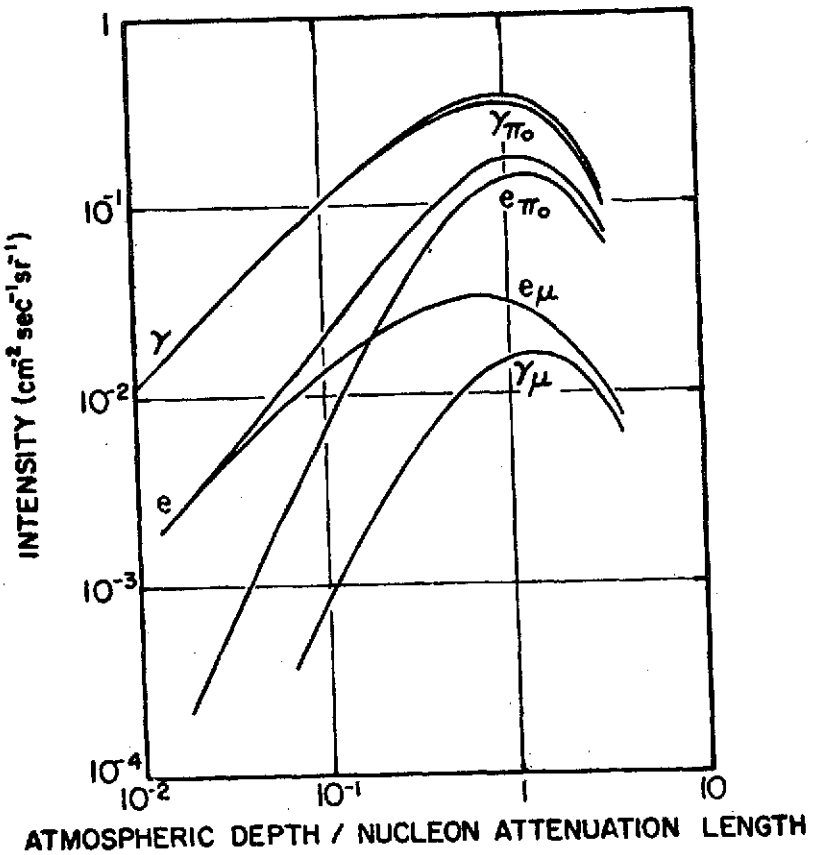

Figure A-2. Intensities of electrons (e) and gamma rays (γ) of energies above 100 MeV versus atmospheric depth, in units of the nucleon attenuation length, 110 g- cm^{-2}. The contributions of $\pi^0 - 2\gamma$ decays ($\gamma_{\pi 0}$, $e_{\pi 0}$) and $\pi - \mu - e$ decays (γ_μ, e_μ) to gamma rays and electrons are shown separately. (Hayakawa, 1969).

in a manner similar to the E-component (Kasturirangan, 1972), we can conclude that the positrons which produce this radiation come mainly from the channel

$$N \rightarrow \pi^{o} \rightarrow \gamma \overset{\rightarrow}{\leftarrow} e^{+}$$

where the positron is produced by pair production and loses energy by bremsstrahlung radiation ($E_e > 100MeV$) and ionizing collisions ($E_e < 100MeV$).

The generation of low energy gamma rays in the atmosphere has been investigated by Puskin (1970). Using electron flux measurements of Verma (1967) and Brini et al. (1967), he has calculated that 84% of the photon flux at 3.5 mb residual pressure from 0.3 to 10 MeV can be explained by electron bremsstrahlung in the atmosphere. Less important processes are annihilation line and scattered radiation, nuclear de-excitation radiation, and gamma rays directly from π^{o} decay. Calculations and observations by Kasturirangan et al. (1972) and Haymes et al. (1969) also show that the low energy photons largely originate from the electronic component of the secondary cosmic radiation. The positron portion of the electronic component also gives rise to the 0.511 MeV radiation.

2. Antimatter in Meteor Showers

The distribution of antimatter in the universe is a phenomenon in cosmology that may be amenable to study by gamma-ray astronomy. Konstantinov (1966) has hypothesized the existence of meteor-like bodies exchanged between matter and antimatter stellar systems. Positive evidence for this idea has been claimed through a correlation between the intensity of high energy gamma-ray flux and neutron

measurements in the upper tropopause with the time of entry of individual meteors into the Earth's atmosphere (Konstantinov et al., 1966; Konstantinov et al., 1967).

Konstantinov et al. (1970) have analysed gamma ray data in the range 0.3 to 2.7 MeV from the Cosmos-135 satellite and have found an enhancement during meteor showers in the 0.511 MeV radiation observed by their detector. The observations were made during the Geminide, Urside, and Quadrantide showers of 1966-1967 and amounted to a 50% effect.

The enhancement was not correlated with changes in the gamma ray continuum or with charged-particle effects. According to the hypothesis, the observed enhancement could be caused by about 20 mg. of antimatter introduced into the Earth's atmosphere during one day.

The 4-day period of 25-28 April 1972 used in Section IV of this work in an investigation of aspect and rigidity variation has also been used to investigate the time variation of the 0.511 MeV flux. In order to see daily variations which are independent of rigidity effects, scans used to obtain a daily average must be characterized by the same rigidity from day to day; that is, if two scans at 4-5 GV and three scans at 10-11 GV are used to obtain an average rate on 26 April, equivalent scans must be used to obtain the average rate for 27 April if a valid time dependence is to be seen. Other parameters need not be considered since they do not affect the rate by the factor of 50% seen by Konstantinov et al.

The variation of the average daily rate is shown in Figure A-3. The error bars shown are due only to counting statistics but include

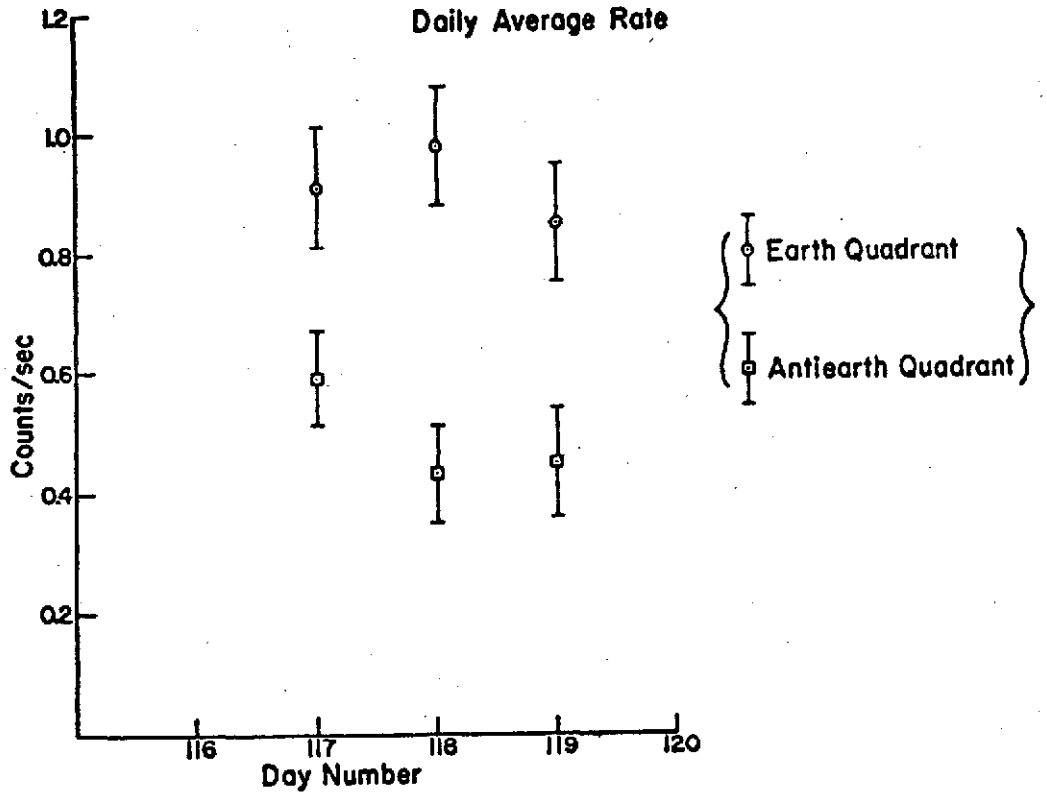

Figure A-3. Daily variation in the 0.51 MeV counting rate for a linear fit to the background. Each point is an average of 22 scans.

the uncertainty in subtracting a linear background from beneath the peak. Each point is an average of 22 scans. The 1 σ error bars are about 15% of the average rate in length. A consistent increase in the rate of 50% or more over a period of several days in coincidence with a meteor shower, as was seen by Konstantinov et al., should be apparent in this type of analysis.

At the time of the present work, only 4 days of data were available for computer analysis. In the future, however, data covering April to December 1972 will be available. This span of time includes such large showers as Aquaride, Perseid and Orionide. If the 0.511 MeV enhancement is a general property of meteor showers as the work of Konstantinov et al. implies, it should be confirmed in the OSO-7 data.

C. Production in the Solar Atmosphere

1. Quiet Sun

Although the high energy thermonuclear reactions in the Sun's core produce x- and gamma-radiation, these photons are degraded in energy in their passage through the solar material to the surface. The temperature of the surface of the photosphere is $\approx$4500°K, and the Sun's spectral distribution can be approximated by a black body at about 6000°K. This distribution peaks at about 5000Å and virtually all of the energy of the Sun's radiation is below 2000Å (Green and Wyatt, 1965). The temperature of the corona is about 10^6°K, and it radiates like a "gray body" with a distribution peaked at 29Å (0.43 keV). However, this emission rarely exceeds 10^{-3} of the solar constant (Green and Wyatt, 1965).

The average kinetic energy of gas particle is:

$$\bar{T} = 3/2\ k\ \Theta$$

for a Maxwell-Boltzmann distribution, where Θ is the kinetic temperature and k is Boltzmann's constant (8.6×10^{-5} eV/^{o}k). For a temperature of $6 \times 10^{3\,o}$K, $\bar{T}$ = 0.77 eV; and for $10^{6\,o}$K, $\bar{T}$ = 130 eV. The threshold for positron producing mechanisms are much greater than these values. For example, the threshold for the production of β^{+} emitters in nucleon-nucleon collisions in the solar atmosphere is 5 MeV or higher (Dolan and Fazio, 1965; Cheng, 1972). The thresholds for π^{+} production in p-p and p - α reactions are 290 MeV and 172 MeV, respectively. Finally, the contribution to the annihilation gamma ray flux from the thermonuclear reaction

$$H^{1} + H^{1} \rightarrow H^{2} + e^{+} + \nu$$

is expected to be small even for the hot corona and coronal condensation as compared with a flare-related contribution (Cheng, 1972).

Because of the above considerations, the gamma radiation emitted by the quiet Sun is negligible compared with emission during solar flares (Dolan and Fazio, 1965). No positive measurements of quiet-sun gamma rays have been made to date; a summary of upper limits for the gamma ray continuum has been presented by Cheng (1972) and a similar summary for the 0.51 MeV radiation has been given by Chupp (1971). The listing of Chupp is reproduced here as Table A-1.

TABLE A-1

EXTRATERRESTRIAL UPPER LIMITS (0.51 MeV)

Source	Date	Photons $cm^{-2}sec^{-1}$	Experimenters
Sun (Crab)	5-2-61	1×10^{-1}	Peterson (1963)
Cosmos	1-62	1.4×10^{-2}	Metzger et al. (1964)
Sun	6-10-62	1.3×10^{-2}	Frost et al. (1966)
Sun	11-2-67	$(7.5\text{-}26) \times 10^{-3}$	Chupp et al. (1968)
Crab (Sun)	-68	8.4×10^{-4}	Haymes et al. (1968)
Cygnus	-68	1.24×10^{-3}	Haymes et al. (1968)
Virgo	-68	2.1×10^{-3}	Haymes et al. (1968)
Cent A	-68	1.8×10^{-3}	Haymes et al. (1968)
Sun	-68	7×10^{-3}	Womack and Overbeck (1968)
Sun	4-25-68	$(1.1\text{-}4.8) \times 10^{-2}$	Chupp et al. (1970)
Sun	7-7-66	Null result	Cline et al. (1968)
	8-28-66		OGO-III
	5-23-67		

Reference: Chupp (1971)

2. Solar Flares

A review of theoretical flare mechanisms has been presented by Sweet (1969). These models include the acceleration of fast nuclei which are sometimes detected directly and which must be present for the production of annihilation radiation. In fact, high energy protons have been thought to be produced predominantly 1) before the flare (H. Elliot), 2) during the explosive phase (K. Sakurai), and 3) during the decay stage (C. de Jager) (Sweet, 1969). A review of flare models as related to gamma ray and neutron production has been done by Chupp (1971). Here the models and flux estimates are differentiated according to their geometries: A) the directed particle geometry (S. I. Syrovatskii), B) isotropic thin target geometry (R. E. Lingenfelter and R. Ramaty, acceleration phase), C) isotropic thick target geometry (Lingenfelter and Ramaty, slow down phase), and D) magnetic bottle geometry (H. Elliot and E. Schatzman) (Chupp, 1971).

The rate of generation of annihilation radiation during solar flares has been calculated by several workers. The main sources of positrons are the decay of π^+ mesons produced in p-p reactions and the β^+ decay of spallation products. Dolan and Fazio (1965) have calculated the time-averaged annihilation line flux assuming a rigidity dependent proton spectrum

$$\frac{dN}{dR} = N_0 e^{-R/R_0}.$$

Lingenfelter and Ramaty (1967) have calculated the flux for a positron production rate per g/cm^2 of flare proton range averaged over the

particle acceleration time (geometry B, above). The range of the accelerated protons is generally taken to be ~ 1 g/cm^2. A flux can also be produced during the slowing down of those particles which do not escape the Sun. For this geometry (C), the authors have assumed that 1/2 the flare particles are directed toward the Sun where they interact and slow down. Assuming the same rigidity-dependent spectrum as Dolan and Fazio, the mean gamma ray flux per unit time at Earth during acceleration is

$$\bar{\Phi}_{acc} \simeq \frac{N_T x_1}{t_1} \left(\frac{\Phi_{acc}}{x_1}\right)$$

where N_T is the number of accelerated particles >30 MeV, x_1 is the range (g/cm^2) of these particles during acceleration, t_1 is the acceleration time, and Φ_{acc}/x_1 is tabulated by Lingenfelter and Ramaty. The flux during slowdown is given by

$$\bar{\Phi}_{sd} = \frac{N_T \varepsilon \left(\Phi_{sd}\right)}{t_{sd}}$$

where ε is the fraction of particles which interact after acceleration, t_{sd} is the time over which interaction takes place, and Φ_{sd} is tabulated.

Cheng (1972) has taken into account the time-dependent energy losses of the flare-acceleration of particles followed by energy loss through various mechanisms. They may remain trapped in the flare region or a large fraction may escape and interact on the (high density) solar surface. The fluxes are calculated both for a power law in initial particle kinetic energy

$$\frac{dN}{dE} = K(E-Mc^2)^{-\alpha}$$

and for an exponential law in rigidity

$$\frac{dN}{dR} = Ke^{-R/R_0}$$

Then the initial maximum annihilation flux at Earth due to π^+ production is

$$J_{\pi,\gamma} = 7.1 \times 10^{-28} (n_H KV) Q_{\pi,+} \text{ photons cm}^{-2}\text{sec}^{-1}$$

where n_H is the ambient proton density, V is the gamma-ray emitting volume ($KV=N/R_0$, where N is the total number of accelerated protons), and $Q_{\pi,+}$ is the positron production rate tabulated by Cheng. The time dependence of the flux goes as $\exp[-(t-T_{an})/T]$ for $t \geq T_{an}$ where T is the "decay" time for π^+ production (due to proton energy losses), and T_{an} is the mean time for positron production to annihilation. The initial flux due to β^+ - decay positrons is

$$J_{\beta,\gamma} = 7.1 \times 10^{-28} q_\beta KV \quad \text{photons cm}^{-2}\text{sec}^{-1}$$

where q_β is the positron production rate which is graphed by Cheng as a function of time for various n_H and R_0. There is a fixed delay of T_{an} between positron production and annihilation where 120 sec $\leq T_{an} \leq$ 1.2 sec for electron densities between 10^{12} cm^{-3} and 10^{14} cm^{-3}.

The fluxes obtained by these models can be compared for a flare with parameters

$$N = 10^{32}$$

$$V = 10^{28} \text{cm}^3$$

$$R_0 = 200\text{MV}$$

$$n_H = 3 \times 10^{13} \text{cm}^{-3}$$

Model	0.51 MeV flux at earth		
	π^+ decay	β^+ decay	Total
Dolan and Fazio*	4.2×10^{-1}	2.1×10^{-2}	4.4×10^{-1}
Lingenfelter & Ramaty*	---	---	3×10^{-1}
Cheng**	1.2×10^{-2}	1.4×10^{-4}	1.2×10^{-2}

* average flux over 100 seconds

**initial maximum flux

D. Cosmic Sources

Stecker (1969) has calculated that there may be a detectable flux of annihilation gamma rays from the galactic disk. As in solar flares, the two main possible positron production modes are from the formation of π^+ mesons and positron emitting radionuclides. Stecker's argument shows that an annihilation gamma ray flux will be due mainly to β^+ decay of products of $p - C^{12}$, $p - N^{14}$, and $p - O^{16}$ spallation interactions rather than π^+ formation. This is because positrons from β^+ decay have a lower initial energy (less than a few MeV) than positrons which result from reactions producing π^+ mesons (greater than a few MeV). The latter positrons have a much greater probability of escaping the galaxy before annihilating.

For the π^+ decay mode, the positron spectrum can be calculated from knowledge of the galactic cosmic ray spectrum (assumed to be the same as that measured above 500 MeV near the Earth). The positron energy loss rate (via ionization, bremsstrahlung, synchrotron radiation, and Compton collisions) and trapping time in the galaxy also determines

the shape of the annihilation gamma ray spectrum. Because of the high velocity at which annihilation takes place, Doppler shifting is important in this mode and the characteristic peak is smeared between 250 and 500 keV. Only 1-2% of these positrons annihilate near rest.

The second important source of galactic positrons is spallation interactions. Stecker (1969) uses the list of interactions of Audouze et al. (1967) and the quiet-sun cosmic-ray spectrum between 20 and 1000 MeV/nucleon of Comstock et al. (1966) to estimate the positron production from β^+ emitters. Most of these positrons are emitted with energies less than 5 MeV and over 95 percent of them annihilate near rest in the galaxy. Stecker's calculations indicate that almost all of these positrons form positronium, 25 percent of which decays into 0.51 MeV gamma rays and 75 percent of which decays in a continuum of energy less than 0.51 MeV (see appendix on General Theory of Annihilation). The most optimistic estimate of the annihilation line flux which comes out of this analysis is about 10^{-3} photons $cm^{-2}sec^{-1}$ sr^{-1} from the galactic disk, with more conservative values being 4×10^{-4} $cm^{-2}sec^{-1}sr^{-1}$ or less.

A later analysis by Ramaty, Stecker, and Misra (1970) concludes that the flux for a homogeneous disk model of the galaxy would be smaller than the background continuum ($\approx 3 \times 10^{-4} cm^{-2}sec^{-1}sr^{-1}$) unless the mean cosmic ray energy density is much larger than seems probable from the general dynamics of the interstellar medium. Thus the hypothetical flux would be very difficult to detect. However these authors go on to argue that physical conditions in the galactic center could modify the energy density argument and so it might be a detectable source of 0.51 MeV gamma rays.

Johnson et al. (1972) have detected a gamma-ray continuum and a peak at 476 ± 30 keV from the galactic center region. This measurement has received several interpretations. The most interesting one, in the present context, is due to Leventhal (1973). He suggests that a line-plus-continuum spectrum, which is emitted from the galactic center by annihilating positronium, is folded through the 86 keV energy resolution of the detecting instrument. This resolution causes the apparent energy of the maximum of the peak to be shifted down to 490 keV. The observed flux for this feature is $1.8 \pm 0.5 \times 10^{-3}$ photons $cm^{-2}sec^{-1}$ for a point source (or about 3×10^{-3} photons $cm^{-2}sec^{-1}sr^{-1}$ for source extended over the 24° angular opening of the detector). It should be mentioned here that Metzger et al. (1964) have put an upper limit of 1.1×10^{-3} photons $cm^{-2}sec^{-1}sr^{-1}$ for an isotropic cosmic flux. Trombka et al. (1973) have a positive, though weak, indication of an annihilation radiation of cosmic origin, although other sources cannot be completely ruled out. Their measurement indicates a flux of $2.4 \pm 1.2 \times 10^{-3}$ photons $cm^{-2}sec^{-1}sr^{-1}$.

APPENDIX II

LOCAL PRODUCTION IN THE SATELLITE

It is reasonable to expect that charged-particle interactions with the spacecraft material would produce low energy gamma rays. Satellites are always exposed to cosmic rays and those in Earth orbit can be exposed regularly to trapped particles. The gamma ray experiment aboard the Ranger 3 Spacecraft indicated the significance of cosmic ray effects (Metzger et al., 1964). Spectra in the range 70 keV 4.4 MeV were measured with an isotropic detector both stowed on the spacecraft and extended on a 6-foot boom. Comparison of the spectra showed a decrease in counting rate of about a factor of 2 in the extended position as compared to the stowed position. The difference, due to secondary production in the spacecraft, included a peak at 0.51 MeV. This background was apparently caused by cosmic rays.

An analysis of the background produced in the OSO-1 satellite by Peterson (1967) indicated that about 50 percent of the counting rate in the energy range 1.5 to 4.5 MeV was caused by secondary production in the spacecraft, about 40 percent was due to atmospheric gamma rays and 10 percent to cosmic gamma rays. Additional background was seen after exposure to trapped protons encountered in the 500 km orbit. The mechanism was indicated as being due to the decay of 25-minute I^{128} activity induced in the NaI crystal by secondary neutrons produced by trapped protons (Peterson, 1965).

More recent analysis tends to indicate that spallation reactions in the detector and spacecraft are more important gamma ray sources

than neutron capture. Fishman (1972) has calculated the spallation yields for 100 MeV protons interacting with NaI scintillator material. These calculations were checked experimentally by irradiating NaI with 600 MeV protons and observing the spectra of the decay products as a function of time. The analysis indicated numerous lines in the spectra due to the decay by electron capture or internal transition of isotopes of iodine, tellurium, and antimony. An exponential continuum due to beta emitters and unresolved lines was also found.

Dyer and Morfill (1971) have obtained similar results for the irradiation of CsI(Tl) with 155 MeV protons. These results were used to predict production in this material by cosmic rays and trapped protons.

The recent Apollo flights have enabled Peterson and Trombka (1973) to measure the activation in a NaI scintillator directly. A 7.0 cm x 7.0 cm NaI crystal was stowed in the Apollo 17 Command Module for some 300 hours and passed through the Van Allen belts twice before it was examined on the ground about 1 1/2 hours after re-entry into the atmosphere. The crystal was examined by viewing it with a photomultiplier tube and by exposing it to Ge(Li) detectors and a large 4π scintillation counter. Radioactive nuclides in the crystal were identified by the characteristic energies of the gamma rays emitted by them and by their half lives. Qualitative identification was obtained for the following nuclides: Na^{22} (2.6 yrs), Na^{24} (15 hrs), I^{123} (13 hrs), I^{124} (4 days), I^{126} (13 days), I^{128} (25 min) and Xe^{127} (34 days). The Na^{24} and I^{128} are evidently produced from neutron capture by Na^{23} and I^{127}, respectively. Na^{22} is produced by spallation from Na^{23}, and the

other products result from the spallation of I^{127}. The lines at 1.46 MeV and 2.62 MeV due to K^{40} and Th were also observed.

Several of the lines seen by the UNH detector are consistent with these sources. In Figure III-5 we see a peak near 0.40 MeV and a broad feature between 0.59 and 0.78 MeV. The feature at 0.40 MeV may be due to the 0.39 MeV line from I^{124} together with the 0.44 MeV line from I^{128}. A feature similar to the one between 0.59 and 0.78 MeV was seen by Peterson and Trombka. This was caused by the following lines: 0.60 MeV (I^{124}), 0.67 MeV (I^{126}), 0.72 MeV (I^{123}) and 0.75 MeV (I^{126}).

The local source of annihilation radiation is a large number of positron emitters that can be produced by spallation. When these radionuclides are produced in the scintillator itself, they produce an energy loss continuum spectrum rather than an annihilation line. This is because the positrons release energy by ionization losses as they slow down in the scintillator, prior to annihilation. The CsI shield, however, should be an important source of 0.51 MeV gamma rays because of its massiveness and because it surrounds the central detector.

The theoretical and laboratory analysis of Dyer and Morfill (1971) indicate that numerous positron emitters can be produced by spallation in CsI. The most important are: Cs^{130}(30 min), Cs^{128}(3 min), Cs^{126}(1.6 min), Xe^{125}(120 min), I^{122}(4 min), I^{121}(96 min), $Sb^{m\ 118}$(3.5 min) and Sb^{116}(15 min). Positron emitters produced in the photomultiplier tube and in the rest of the spacecraft may also contribute to the detected background. The multiplicity of positron emitters makes the analysis of the background rate into various

contributors prohibitively difficult in this experiment. Instead, the telescopic properties of the detector are used to distinguish local production from external sources.

BIBLOGRAPHY

Aller, L. H., Astrophysics, 2nd ed., Ronald Co., New York, 1963.

Anderson, C. D., The Positive Electron, Science, 76, 238, 1932.

Anderson, C. D., The Positive Electron, Phys. Rev., 43, 491, 1933.

Anderson, K. A., Cosmic Ray Photons Below Cascade Energy, Phys. Rev., 123, 1435, 1961.

Audouze, J., M. Epherre, and H. Reeves, Survey of Experimental Cross Sections for Proton Induced Spallation Reactions in He^4, C^{12}, N^{14}, and O^{16}, in High-Energy Nuclear Interactions in Astrophysics, edited by B. S. P. Shen, W. A. Benjamin, Inc., New York, 1967.

Bethe, H. and W. Heitler, Stopping of Fast Particles and Creation of Electron Pairs, Proc. Roy. Soc., 146, 83, 1934.

Bingham, R. G., W. R. Webber, D. M. Sawyer, and J. F. Ormes, Direct Measurements of Geomagnetic Cutoffs for Cosmic Ray Particles in the Latitude Range 45° to 70° Using Balloons and Satellites, Proc. Int. Conf. Cosmic Rays, Calgary, Canada, S1078, 1968.

Bjorken, J. D. and S. D. Drell, Relativistic Quantum Mechanics, McGraw-Hill Book Co., New York, 1964.

Brini, D., V. Ciriegi, F. Fuligni, and E. Moretti, Low-Energy Cosmic-Ray Photons in Atmosphere, J. Geophys. Res., 72, 903, 1967.

Burtis, D. W., D. Aalami, R. H. Evelyn-Veere, and A. A. Sarkady, A Quadratic Pulse Height Analyzer for Space Applications, IEEE Trans. Nuc. Sci. NS-19, 613, 1972.

Cheng, C., Theoretical Studies of the Flux and Energy Spectrum of Gamma Radiation from the Sun, Space Sci. Rev., 13, 3, 1972.

Chubb, T. A., R. W. Kreplin, and H. Friedman, Observations of Hard X-Ray Emission from Solar Flares, J. Geophys. Res., 71, 3611, 1966.

Chupp, E. L., Gamma Ray and Neutron Emissions from the Sun, Space Sci. Rev., 12, 486, 1971.

Chupp, E. L., and D. J. Forrest, Discussion of Paper by R. C. Haymes, S. W. Glenn, G. J. Fishman, and F. R. Harnden, Jr., J. Geophys. Res., 75, 871, 1970.

Chupp, E. L., A. A. Sarkady, and H. P. Gilman, The 0.5 MeV Gamma-Ray Flux and the Energy Loss Spectrum in CsI(Tl) at 4 g/cm^2, Planet. Space Sci., 15, 881, 1967.

Chupp, E. L., D. J. Forrest, A. A. Sarkady, and P. J. Lavakare, Low Energy Gamma Radiation in the Atmosphere During Active and Quiet Periods on the Sun, Planet. Space Sci., 18, 939, 1970.

Chupp, E. L., D. J. Forrest, P. R. Higbie, A. N. Suri, C. Tsai, and P. P. Dunphy, Solar Gamma Ray Lines Observed During the Solar Activity of August 2 to August 11, 1972, Nature, 241, 333, 1973.

Deutsch, M., Annihilation of Positrons, in Progress in Nuclear Physics, Vol. 3, edited by O. Frisch, Pergamon Press, London, 1953.

Dirac, P. A. M., Quantum Theory of the Electron, Proc. Roy. Soc., A117, 610, 1928a.

Dirac, P. A. M. Quantum Theory of the Electron. Part II, Proc. Roy. Soc., A118, 351, 1928b.

Dirac, P. A. M., Annihilation of Electrons and Protons, Proc. Cambridge Phil. Soc., 26, 361, 1930.

Dolan, J. F. and G. G. Fazio, The Gamma-Ray Spectrum of the Sun, Rev. of Geophys., 3, 319, 1965.

Dyer, C. S. and G. E. Morfill, Contribution to the Background Rate of a Satellite X-ray Detector by Spallation Products in a Caesium Iodide Crystal, Astrophys. and Space Sci., 14, 243, 1971.

Fishman, G. J., Proton-Induced Radioactivity and NaI(Tl) Scintillation Detectors, Teledyne Brown Engineering, Huntsville, Alabama, Report SE-SSL-1497, 1972.

Forrest, D. J., unpublished thesis, University of New Hampshire, 1969,

Forrest, D. J., P. R. Higbie, L. E. Orwig, and E. L. Chupp, An Electronically Gated Gamma and X-Ray Calibration Scheme, Nucl. Instr. and Methods, 101, 567, 1972.

Frost, K. J., E. D. Rothe, and L. E. Peterson, A Search for the Quiet-Time Solar Gamma Rays from Balloon Altitudes, J. Geophys. Res., 71, 4079, 1966.

Green, J. and J. Lee, Positronium Chemistry, Academic Press, New York, N. Y., 1964.

Green, A. E., and P. J. Wyatt, Atomic and Space Science, Addison-Wesley Publishing Co., Inc., Reading, Mass., 1965.

Golenetskii, S. V., E. P. Mazets, V. N. Il'inskii, M. M. Bredov, Yu. A. Gur'yan, and V. N. Panov, Cosmic Gamma-Ray Measurements in the Range 0.3-3.7 MeV, Astrophys. Lett., 9, 69, 1971.

Gorenstein, P. and H. Gursky, Characteristic γ and X-Radiation in the Planetary System, Space Sci. Rev., 10, 770, 1970.

Hayakawa, S., Cosmic Ray Physics, John Wiley & Sons, Inc., New York, 1969.

Haymes, R. C., D. V. Ellis, G. J. Fishman, J. D. Kurfess, and W. H. Tucker, Observation of Gamma Radiation from the Crab Nebula, Astropys. J. Letters, 151, L9, 1968.

Haymes, R. C., S. W. Glenn, G. J. Fishman, and F. R. Harnden, Jr., Low Energy Gamma Radiation in the Atmosphere at Midlatitudes, J. Geophys. Res., 74, 5792, 1969.

Haymes, R. C., S. W. Glenn, G. J. Fishman, and F. R. Harnden, Jr., Reply, J. Geophys. Res., 75, 873, 1970.

Heath, R. L., Scintillation Spectrometry, Gamma Ray Spectrum Catalogue, AEC Research and Development Report-Physics TID-4500, 1964.

Heckman, H. H. and G. H. Nakano, East-West Asymmetry in the Flux of Mirroring Geomagnetically Trapped Protons, J. Geophys. Res., 68, 2117, 1963.

Heitler, W., The Quantum Theory of Radiation, Oxford University Press, London, 1936, 1960.

Heitler, W. and F. Sauter, Stopping of Fast Particles with Emission of Radiation and the Birth of Positive Electrons, Nature, 132, 892, 1933.

Higbie, P. R., E. L. Chupp, D. J. Forrest, and I. U. Gleske, A Gamma Ray Monitor for the OSO-7 Spacecraft, IEEE Trans. Nuc. Sci. NS-19, 606, 1972.

Higbie, P. R., D. Forrest, I. Gleske, E. L. Chupp, and D. Burtis, Experimental Gamma Ray Response Function for the OSO-7 Spacecraft, Nucl. Instr. and Methods, 108, 167, 1973.

Jones, F. C., Cosmic Ray Production of Low-Energy Gamma Rays, J. Geophys. Res., 66, 2029, 1961.

Kasturirangan, K, U. R. Rao, and P. D. Bhavsar, Low Energy Atmospheric Gamma Rays Near Geomagnetic Equator, Planet. Space Sci., 20, 1961, 1972.

Konstantinov, B. P., M. M. Bredov, A. I. Belyaevskii, and I. A. Sokolov, The Possible Antimatter Nature of Micrometeorites, Cosmic Res., 4, 58, 1966.

Konstantinov, B. P., M. M. Bredov, A. I. Belyaevskii, I. A. Sokolov, Yu. A. Gur'yan, L. P. Pakhomov, V. K. Bocharkin, L. F. Alekseev, N. I. Orlov, and V. I. Chesnokov, An Experiment to Test the Hypothesis of the Antimatter Nature of Meteoric Swarms, Soviet Phys. Tech. Phys., 12, 531, 1967.

Konstantinov, B. P., S. V. Golentskii, E. P. Mazets, V. N. Il'inskii, R. L. Aptekar', M. M. Bredov, Yu. A Gur'yan, and V. N. Panov, Investigation of the Variations of Annihilation Gamma Radiation by the Artificial Earth Satellite "Cosmos-135" in Connection with the Possible Antimatter Nature of Meteor Streams, Cosmic Res., 8, 879, 1970.

Kuzhevskii, B. M., Nuclear Reactions and the Line Spectrum of Solar-Flare Gamma Rays, Sov. Astron. AJ, 12, 595, 1969.

Leventhal, M., Positronium-Formation Redshift of the 511-keV Annihilation Line, Astrophys. J. Lett., 183, L 147, 1973.

Lingenfelter, R. E. and R. Ramaty, in High Energy Nuclear Reactions in Astrophysics, ed. by B. S. P. Shen, W. A. Benjamin Press, New York, N. Y., 1967.

Metzger, A. E., E. C. Anderson, M. A. Van Dilla, and J. R. Arnold, Detection of an Interstellar Flux of Gamma-Rays, Nature, 204, 766, 1964.

Nakagawa, S., M. Tsukuda, K. Okudaira, Y. Hirasima, M. Yoshimori, T. Yamagami, H. Murakami, and S. Iwama, The 0.511 MeV Gamma Rays Measured with the Ge(Li) Detector at the Balloon Altitude, in Proc. Int. Conf. Cosmic Rays, OG-26, 1971.

Neiler, J. H., and P. R. Bell, in Alpha-, Beta- and Gamma-Ray Spectroscopy, ed. by K. Siegbahn, North-Holland Publishing Company, Amsterdam, 1965.

Northrop, J. A. and R. L. Hostetler, Measurements of Gamma-Ray Fluxes in and above the Atmosphere, Bull. Amer. Phys. Soc., 6, 52, 1961.

Ore, A. and J. L. Powell, Three-photon Annihilation of an Electron, Phys. Rev., 75, 1696, 1949.

Perlow, G. J., and C. W. Kissinger, A Search for Primary Cosmic Radiation II, Low Energy Radiation Above and Within the Atmosphere, Phys. Rev., 84, 572, 1951.

Peterson, L. E., The 0.5-MeV Gamma-Ray and the Low-Energy Gamma-Ray Spectrum to 6 Grams per Square Centimeter over Minneapolis, J. Geophys. Res., 68, 979, 1963.

Peterson, L. E., Radioactivity Induced in Sodium Iodide by Trapped Protons, J. Geophys. Res., 70, 1762, 1965.

Peterson, L. E., Gamma-Ray Production by Cosmic Rays Observed on OSO-1, University of California, San Diego, Report UCSD-SP-68-1, 1967.

Peterson, L. E., and J. I. Trombka, The Measurement and Interpretation of the Cosmic Gamma-Ray Spectrum Between 0.3 and 27 MeV as Obtained During the Apollo Mission, in International Symposium and Workshop on Gamma-Ray Astrophysics, GSFC Preprint X-641-73-180, Greenbelt, MD., 1973.

Puskin, J. S., Low-Energy Gamma Rays in the Atmosphere, Smithsonian Astrophysical Observatory Special Report No. 318, 1970.

Ramaty, R., and R. E. Lingenfelter, Galactic Cosmic-Ray Electrons, J. Geophys. Res., 71, 3687, 1966.

Ramaty, R., and R. E. Lingenfelter, Nuclear Gamma Rays from Solar Flares, Proc. Int. Conf. Cosmic Rays, Denver, 1590, 1973.

Ramaty, R., F. W. Stecker, and D. Misra, Low-Energy Cosmic Ray Positrons and 0.51-MeV Gamma Rays from the Galaxy, J. Geophys. Res., 75, 1141, 1970.

Rest, F. G., L. Reiffel, and C. A. Stone, Note on Soft Gamma Component of Cosmic Rays, Phys. Rev., 81, 894, 1951.

Rocchia, R., J. Labyrie, G. Ducros, and D. Boclet, Gamma-Ray Generation in the High Atmosphere, Proc. Int. Conf. Cosmic Rays, London, 423, 1965.

Segrè, E., Nuclei and Particles, W. A. Benjamin, Inc., New York, 1965.

Shea, M. A., and D. F. Smart, Worldwide Trajectory-Derived Vertical Cutoff Rigidities and Their Application to Experimental Measurements, J. Geophys. Res., 72, 2021, 1967.

Shea, M. A., D. F. Smart, and J. R. McCall, A Five Degree by Fifteen Degree World Grid of Trajectory-Determined Vertical Cutoff Rigidities, Can. J. Phys., 46, S1098, 1968.

Stecker, F. W., Equilibrium Spectra of Secondary Cosmic Ray Positrons and the Spectrum of Cosmic Gamma Rays Resulting from Their Annihilation, Astrophys. Space Sci., 3, 579, 1969.

Sweet, P. A., Mechanisms in Solar Flares, Ann. Rev. Astron. Astrophys, 7, 149, 1969.

Trombka, J. I., A. E. Metzger, J. R. Arnold, J. L. Matteson, R. C. Reedy, and L. E. Peterson, The Cosmic γ-Ray Spectrum Between 0.3 and 27 MeV Measured on Apollo 15, Astrophys. J., 181, 737, 1973.

Verma, S. D., Measurement of the Charged Splash and Re-Entrant Albedo of the Cosmic Radiation, J. Geophys. Res., 72, 915, 1967.

Vette, J. I., Low-Energy Gamma Rays in Air and in Lead, J. Geophys. Res., 67, 1731, 1962.

Webber, W. R. and J. F. Ormes, An Upper Limit on the Quiet Time Solar Neutron Flux at Energies >60MeV, J. Geophys. Res., 72, 3387, 1967.

BIOGRAPHICAL DATA

Name Philip Patrick Dunphy

Date of Birth [redacted]

Place of Birth [redacted]

Collegiate Institutions attended

Seton Hall University, South Orange, N.J.

B. S. (Cum laude) - Physics June 1965

Honors or Awards

Academic Excellence - Physics
Seton Hall University, 1965

Cross and Crescent Honor Society
Seton Hall University, 1965

NASA Training Grant
University of New Hampshire

Associate Member, Society of the Sigma Xi
University of New Hampshire

Publications

Chupp, E.L., D.J. Forrest, P.R. Higbie, A.N. Suri, C. Tsai, and P.P. Dunphy, "Solar Gamma Ray Lines Observed During the Solar Activity of August 2 to August 11, 1972, Nature, 241, 333, 1973.